SYNERGISTIC ENHANCEMENT OF STRENGTH AND WEAR RESISTANCE OF TITANIUM ALLOYS BY TiN SURFACE NETWORK REINFORCEMENT

CHAN ON KI

M.Phil

The Hong Kong Polytechnic University

2015

THE HONG KONG POLYTECHNIC UNIVERSITY

Department of Industrial & Systems Engineering

Synergistic Enhancement of Strength and Wear Resistance of Titanium Alloys by TiN Surface Network Reinforcement

CHAN On Ki

A thesis submitted in partial fulfillment of the requirements for the Degree of Master of Philosophy

March 2013

CERTIFICATE OF ORIGINALITY

I hereby declare that this thesis is my own work and that, to the best of my knowledge and belief, it reproduces no material previously published or written, nor material that has been accepted for the award of any other degree or diploma, except where due acknowledgement has been made in the text.

________________________________ (Signed)

Chan On Ki (Name of student)

Abstract

Because of the unique properties as smart material and the biocompatibility, near-equiatomic nickel titanium (NiTi) was widely applied in making biomedical devices. Further improvements in the tribological and mechanical properties of NiTi could bring benefit in improving biocompatibility and durability of these devices. Various surface modification techniques such as PVD, CVD, plasma spraying, etc., have been developed and applied on NiTi over years but all of these techniques have different limitations such as poor interfacial bonding at the surface and long production time.

This project investigates the feasibility of applying laser gas nitriding technique to improve the tensile stiffness, wear resistance and corrosion resistance of nickel titanium (NiTi). In the present work, a continuous wave fibre laser was applied to perform laser gas nitriding process under a pure nitrogen environment on the substrate of commercial NiTi plates. A Taguchi analysis was implemented in this project to optimize the process parameters for laser gas nitriding. Optimum parameters for nitriding in terms of output power, scanning speed, beam diameter and nitrogen flow

rate were obtained. The optimum set of process parameter for laser gas nitriding was subsequently applied to fabricate titanium nitride (TiN) tracks on surface of NiTi with hardness more than 700HV.

With the optimized parameters, different thickness of TiN single track could be produced at the surface of the NiTi alloy using laser gas nitriding. Two schemes of combining single TiN tracks were investigated: a) parallel longitudinal tracks for studying the effect of laser gas nitriding on the tensile stiffness of NiTi; b) network grid for studying the effect of laser gas nitriding on wear and corrosion resistance of NiTi.

The results from scheme (a) indicate that the amount of TiN surface coverage may not be a linear relationship with the increase of the tensile stiffness of the NiTi. Sample with 40% TiN surface coverage has the highest tensile stiffness. Using scheme (b), with a 47% and 76% grid surface coverage, the average wearing volume are 0.00495 μm^2 and 0.00859 μm^2 respectively less than that of the untreated NiTi. The corrosion resistance of the NiTi is enhanced as well. The i_{corr} for untreated, 47% and 76% grid surface coverage was $0.5\mu A/cm^2$ and $0.34\mu A/cm^2$ respectively. It could be concluded that reinforcement tracks or grid of TiN by laser gas nitriding could be effective in improving the tensile stiffness, wear and corrosion properties of NiTi. These innovative surfacing schemes enable NiTi to be treated in an efficient and more economical way.

Acknowledgements

I would like to express my deep appreciation to my research supervisor, Prof. H.C. Man, for his support and guidance. He always gave me valuable advice for my project. His encouragement motivated me to have better performance. I would also like to express my gratitude to Dr. Dennis Lo, Dr. F. T. Cheng and Dr. C. W. Chan for always supporting me and discussing different issues concerning the project. Their suggestions on research direction and methodology were so helpful for me.

I would like to appreciate the help from the laboratory technicians including Mr. T. W. Chan, Mr. S. Y. Lau and Mr. Rico Cheung. I also wish to thank to my friends in my office (EF403) and my department. I am so happy to meet them during my research study. Thank you for sharing happiness and sorrow with me.

Besides, I would express my heartfelt thanks to my family members. Thank you for supporting me for my study. Thank you for their endless love to me. I also like to say thank you to my friends for accompanying me when I felt alone and confused during me study.

Table of Content

List of Figures

List of Tables

Chapter 1 Introduction

1.1 Background of Study

Biomedical materials usually have excellent mechanical properties, formability and stability. These materials are widely applied in dental and plastic surgery. Biomedical materials are often applied in force devices or implants such as artificial joints, stabling screws inside broken bones and dental implants. As a biomaterial, it should be non-poisonous to organisms, resistant to body fluid and highly biocompatible. One common biomaterial is nickel titanium (NiTi).

NiTi is an alloy composed of specific amount of Ni and Ti. Equiatomic NiTi has the properties as smart material. Its unique shape memory property is utilized for making implant fixing devices in human body. However, research showed that the biocompatibility and corrosion behavior of NiTi is dependent on the surface conditions. (Trépanier et al. 1998). Surface modification of NiTi could be one effective method to keep the bulk properties at the same time improve the clinical application performance.

In order to enhance the properties including wearing resistance, corrosion resistance and strength of NiTi, researchers have developed titanium-metal-matrix-composites

(Ti-MMCs). According to Yasmin and Bowen (2003), Ti-MMCs have higher strength to weight ratio than most common structural metals. In addition, they could perform better under severe loads and conditions when compared with their monolithic counterparts. Therefore, investigation of Ti-MMCs becomes a popular topic that many researchers are interested in it. Titanium nitride (TiN) is one commonly used Ti-MMC in engineering field. According to Liu (2009), titanium nitride has high hardness, high wear resistance and high corrosion resistance. It is widely applied for manufacturing cutting tools. Its biocompatibility is very useful and important for body implants. Previous study has also proved that titanium nitride layer covering human artificial joints could improve the wear resistance and fatigue strength of the substrate material (Mändl & Rauschenbach, 2002). In dental field, titanium nitride is widely used for strengthen dental tools and artificial dental implant.

Nitriding is proved to be one method to strengthen the surface layer of titanium and its alloys (Man et al., 2011). The high solubility of nitrogen in alpha-titanium and higher diffusion coefficients in titanium alloys make the process feasible and effective. TiN and Ti_2N may be produced by nitriding process. The surface hardness of these materials is high. It is believed that the formation of nitride compound on NiTi may improve the tribological performance of them.

Much research has investigated nitriding on NiTi by different techniques. Plasma immersion ion implantation and deposition technique was applied and TiN could be successfully formed on NiTi. However, the processing time for one small sample takes about 40 minutes, and the thickness is also small (Cheng and Zheng 2006). Other studies investigated nitriding by applying original PIRAC nitriding method. Smooth and uniform nitride film was formed on the surface of NiTi. However, the processing time (ranging from 0.5 to 5 hours) could be very long (Starosvetsky and Gotman 2001). In addition, high temperature of 1000°C is required for the process. High energy input is required. This may not be suitable for industrial production. Physical vapor deposition (PVD) and chemical vapor deposition (CVD) have also been investigated for fabricating TiN on NiTi surface. But one major problem for using these methods would be that the nitride coatings fabricated usually have structural defects (Milošev and Navinšek 1994).

Laser gas nitriding is one efficient technique for surface modification of metals. As suggested by Peter (2002), laser gas nitriding is a fast process to obtain thick layer of nitride on metal surface. In addition, it could improve several types of metal surface properties including hardness, wear resistance and corrosion resistance. One important advantage of laser gas nitriding is that a metallurgical bond between nitride and NiTi could be created. Nevertheless, laser gas nitriding may be possible to be conducted in air. Large vacuum nitriding chamber may not be necessary for the process.

Preliminary study in Department of Industrial and Systems Engineering of The Hong Kong Polytechnic University has investigated the effect of laser surface hardening on steel. Instead of treating the whole steel surface, researcher fabricated laser tracks to form a network. The experimental results showed that the yield stress and hardness of the treated samples were improved. However, the study only focused on laser hardening of steel. There is no published literature reports on the application of such network scanning method using laser gas nitriding technique on NiTi.

It is believed that network scanning using laser gas nitriding could improve the hardness as well as the tensile stiffness of metal. To investigate the effects of such network scanning method, there is the need to conduct a comprehensive analytical study of the tensile stiffness, wear resistance and corrosion resistance on NiTi.

1.2 Research Objectives

With the final aim of understanding the ultimate effects by combining laser gas nitriding and network system scanning on NiTi, the project objectives are:

i. To investigate the relationship of laser processing parameters upon the geometric characteristics of the single track of TiN on NiTi.

ii. To study the microstructural characteristics of laser track after nitriding of NiTi using fibre laser, by the Taguchi method;

iii. To fabricate TiN tracks respectively on NiTi with different TiN percentage coverage. Then examine the tensile stiffness of these specimens.

iv. To fabricate network grid of TiN on NiTi with different TiN percentage coverage and examine wear properties of these specimen.

v. To study the corrosion behavior of NiTi after laser gas nitriding for different TiN coverage on the surface in sodium chloride solution with temperature of 37°C ± 1°C

1.3 Research Significance and Value

Good mechanical properties and biocompatibility of NiTi make them favorable in various areas of application. However, the scope of application in various industries can be further widened if their performance in tribological condition could be further improved. Therefore, the results of this research could contribute to the knowledge and understanding about surface modification of NiTi. The significance of this research includes:

i. Contribution to the development of an optimum laser surface nitriding process of NiTi using high brightness fibre laser.

ii. Understanding the effects of laser gas nitriding combined with surface texturing on NiTi.

iii. Improvement surface properties of NiTi for potential application such as lighter combustion engines, disk brake rotors, seals and bearings.

iv. Contribution to energy saving and increase in service life of tribological engineering components made of NiTi.

1.4 Dissertation Structure

This dissertation is divided into five sections. Chapter one is the introduction section which gives the background information, objective and significance of this project. Chapter two is the Literature Review section. The essential knowledge regarding this research and some reviews of the literature from existing research studies are presented. Chapter three is Experimental Details section. The major methodologies including Taguchi analysis, laser gas nitriding, tensile test, corrosion analysis and wear analysis are illustrated. Chapter four is the Results and Discussions section, the results concerning the analysis involved in this project would be provided and deeply discussed. The last section is the Conclusion section. It includes the summary of the research project as well as potential future development of the project.

Chapter 2 Literature Review

2.1 Titanium and its Alloys

Titanium is an important material for national defense and civilian applications. It is a transition element which is located at period 4, group IV in Periodic table. It has the structure that the outermost electrons are not completely filled. This structure leads to the ability of titanium to for solid solution with other elements with atomic radius difference within 20% (Liu, 2009). Some general properties of titanium are shown in Table 2.1.

Table 2.1 – General properties of titanium (Liu, 2009)

Atomic number	22
Atomic mass	47.90
Density (g/cm^3)	4.54
Melting point (℃)	1668
Boiling point (℃)	3260
Modulus of elasticity of α phase (GPa)	105
Yield strength of α phase (GPa)	692
Ultimate strength of α phase (GPa)	785

There are two crystallographic forms for titanium in room temperature. Normally, unalloyed titanium is in the form of hexagonal closed packed crystal structure. This is distinguished as α phase of titanium. Unalloyed titanium transforms to body centered cubic structure which is defined as β phase at the temperature of 883℃ (Kim, 2010). Both α and β phase generally has relatively high corrosion resistance. However, the strength is relatively low for α phase (Liu, 2009). It is possible to alter the properties of titanium alloys by verifying alloying and thermo-mechanical processing properly.

2.2 Biomaterials

Biomaterials are playing an important role in medical application. They are mainly materials from nature or manufactured in laboratory. These kinds of materials are usually applied for producing body implants to replace whole or part of body structure. One major reason that biomaterials could be applied in animal bodies is their biocompatibility behavior. Biocompatibility is related to the behavior of biomaterials in various environments under different chemical and physical conditions. According to Williams (1999), biocompatibility is the ability of a material to perform with an appropriate host response in a specific application. A biocompatible material could give no immune response in a given organism. Williams (2008) had also further elaborated that biocompatible materials could perform its desired function according to the medical treatment and do not result in any undesirable effects in the recipient. They could also give the best cellular or tissue response in the specific condition. Finally the performance of the medical therapy could have optimistic result. Some kind of biocompatible materials could even integrate with part of tissue in body Titanium and its alloys have good biocompatibility that makes themselves become a major metallic material for medical tools and implants. Common biomedical titanium alloys include Ti-6Al-4V, Ti-6Al-7Nb, Ti-15Mo and NiTi.

2.3 Nickel Titanium

Nickel titanium is also known as nitinol. It was developed by William J. Buehler and Frederick Wang at Naval Ordnance Laboratory in 1962. The name, nitinol was come from its composition and the laboratory, Nickel Titanium Naval Ordnance Laboratory (Kauffman and Mayo, 1997). Nickel titanium (NiTi) is a metal alloy with approximately equal atomic percentages of nickel and titanium. Researchers are keen on investigating NiTi mainly because of its unique properties. They are shape memory and superelasticity. Shape memory means that NiTi could return to the pre-deformed shape when heated above its transformation temperature. Superelasticity occurs above the transformation temperature with a narrow temperature range. The recovery of undeformed shape could happen without heating. At the moment, NiTi exhibits an enormous elasticity. This superelasticity is a response to the stress from transformation between the austenitic and martensitic phases of the crystal. Researchers call the materials having these special properties smart or active materials. NiTi could sustain high deformation in low temperature phase. At high temperature phase, it could recover their original shape. It is different from other conventional metals. The main properties of NiTi alloys are listed in Table 2.2.

Table 2.2 – Properties values of NiTi (Van Humbeeck, 2001)

	Property	**Units**	**NiTi**
Physical	Melting point	°C	1300
	Density	gcm^{-3}	6.5
	Transformation enthalpy	$J\ kg^{-1}$	20000
	Corrosion performance		Similar to 300 series stainless steel
Mechanical	Young's modulus Austenite	GPa	80
	Elongation at failure	%	30 - 50
	Yield strength		
	Austenite	MPa	195 - 690
	Martensite	MPa	70 - 140
	Poisson's ratio		0.33
	Elastic Modulus		
	Austenite	GPa	75 - 83
	Martensite	GPa	28 - 40
Shape memory	Transformation temperature	°C	-100 - 100
	Hysteresis	°C	5 - 50
	Superelastic strain	%	6 - 8

2.3.1 Mechanical Behavior

The stress-strain curve of NiTi alloy with equal atomic ratio has discontinuous yielding and large Lüders strains (Otsuka and Wayman, 1998) within the temperature from -196°C to 75°C. Lüders strain will disappear. There will be more than 15% elongation before fracture. Figure 2.1 presents a stress-strain curve of a near-equiatomic NiTi alloy wire after annealing at 400°C and tested at 30°C. Instead of increasing linearly as other metals, NiTi gives a stress-strain curve with step.

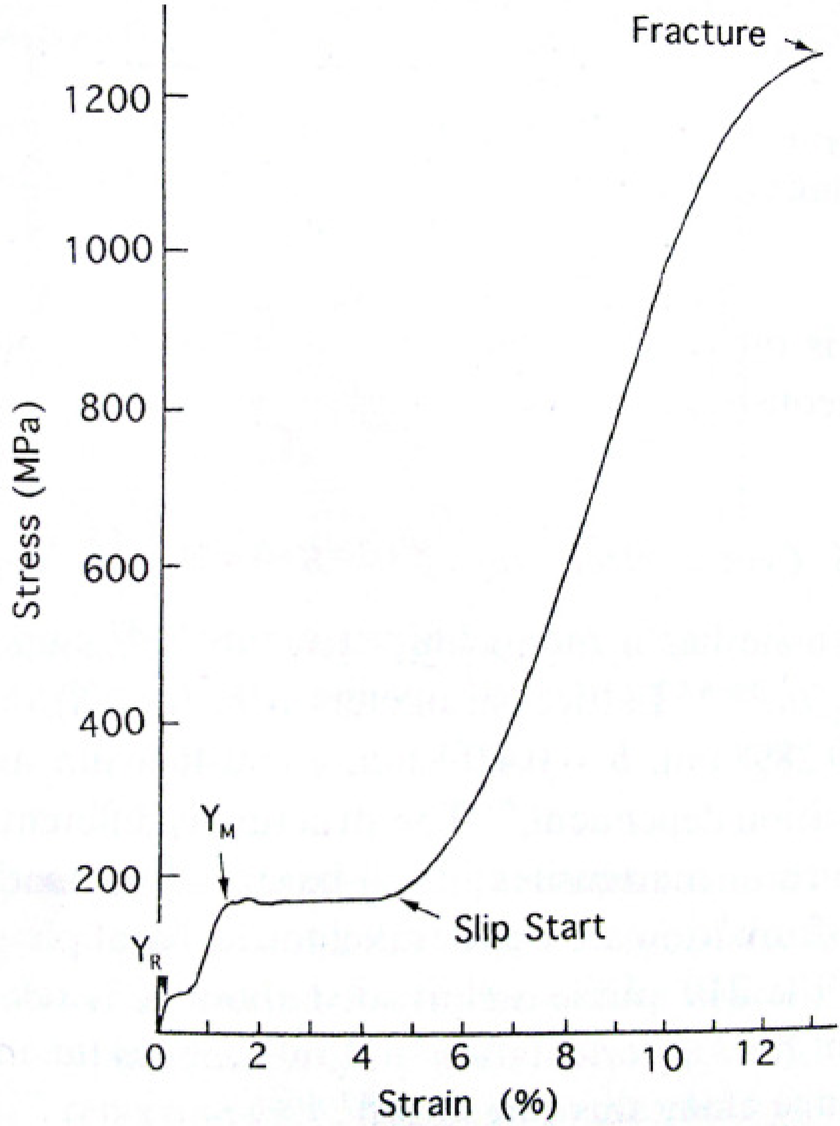

Figure 2.1 – Stress-strain curve of NiTi wire (Otsuka and Wayman, 1998)

There is a first yielding at Y_R. It is the starting point of deformation regarding to the transformation of R phase variants. A second yielding is at Y_M. It is the starting point of martensitic transformation due to stress induction from R phase. This transformation gives approximately 5% of elongation. After martensitic transformation, slipping begins. Stress increases rapidly. Fracture is observed at about 15% elongation. (Otsuka and Wayman, 1998)

2.3.2 Shape Memory Effect

Shape memory effect is an important property of shape memory alloy such as NiTi. Shape memory alloys contain two phases, austenite and martensite phases. Shape memory effect is initiated by the forward and inverse thermoelastic martensitic transformation between these two phases. Shape memory effect is based on the diffusion-less transformation between the martensite which has a lower temperature, and the austenite which has a relatively higher temperature. (Asua et al., 2010). Figure 2.2 shows the graph of strain against temperature of the phase transformations of NiTi caused by thermal and mechanical stimulus. Martensitic transformation is reversible. Upon heating from low temperature, NiTi is in martensite phase. Martensitic transformation starts at M_s and commence above A_s. The process will be completed when the temperature is higher than A_f. When cooling starts and the temperature reaches below M_s from higher temperature, the austenite phase will transform back to martensite. The transformation will finished when the temperature reaches M_f.

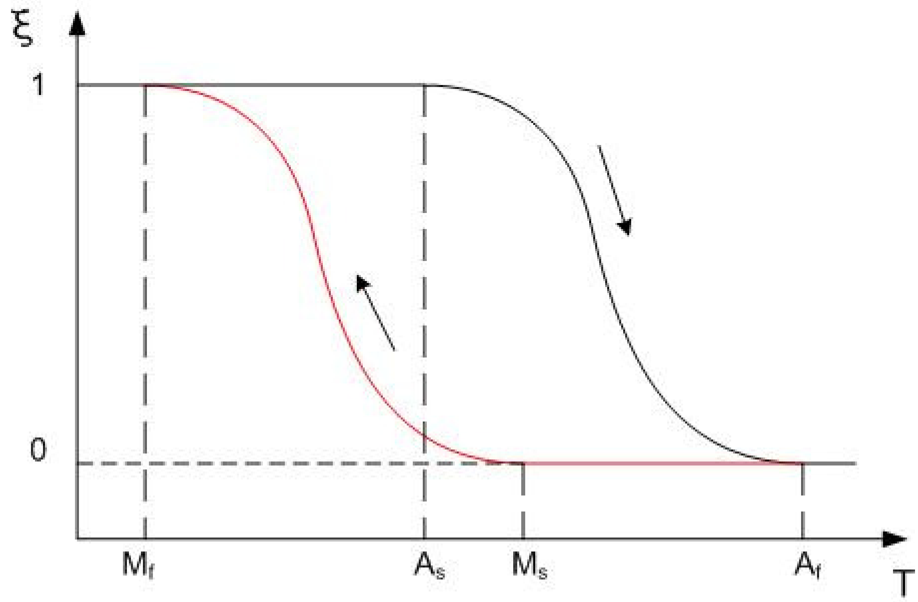

Figure 2.2 – Graph of strain against temperature of the phase transformations of NiTi (Ryhänen, 1999)

ξ(T) represents the martensite fraction. As claimed by Otsuka and Wayman (1998), there may be a shift of characteristic transformation temperatures after repeated use of shape memory effect. This phenomenon is called functional fatigue. It is highly related to the change of microstructure and functional properties of NiTi. Transition from martensite to austenite phase is dependent on temperature and stress. Some of the mechanical energy is lost during the transition process. Hysteresis is therefore raised.

During transformation from higher temperature to lower temperature phase, the transformation stresses caused the microstructure of shape memory alloys by twinning instead of slipping (Asua et al., 2010). Figure 2.3 illustrates the scheme of phase transformation of shape memory alloys by thermal and mechanical stimulus.

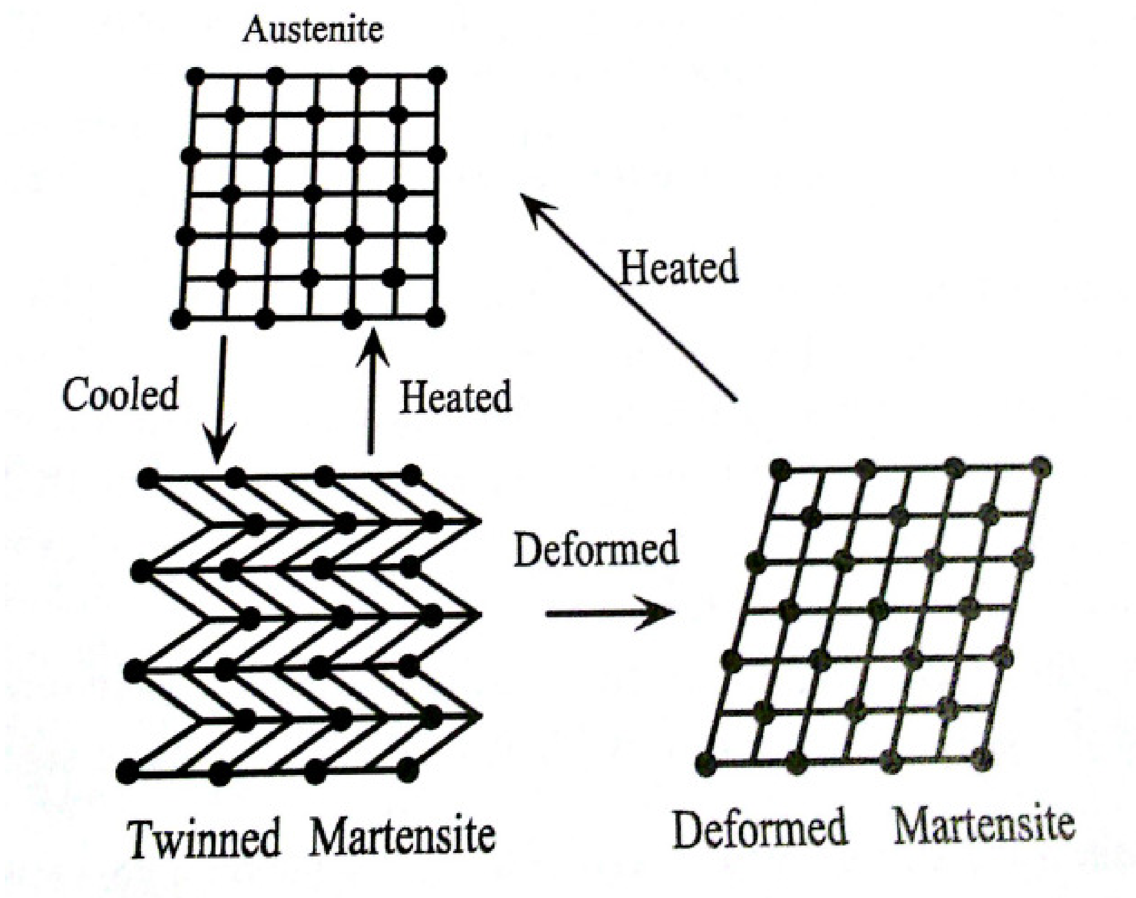

Figure 2.3 – Scheme of phase transformation driven by thermal and mechanical stimulus (Asua et al, 2010)

When a material deforms by twinning, there will be some regions in the crystal that the unique axis of the crystal points in a specific direction. These regions are called variants. (Asua et al, 2010). The unique axis is rotated by an angle related to the difference in length between the longer and shorter axes in the crystal within the nearby variants. Slipping instead, is presented in other general alloys. The dislocation will move to the edge of the crystal. Therefore, general alloys deform inelastically which causes permanent deformation.

2.3.3 Pseudoelastcity or Superelasticity

Phase transformation between the austenite and martensite if the crystal will lead to an elastic response to applied stress. This process is reversible and is called pseudoelasticity. Some other researchers also called it superelasticity. This phenomenon is demonstrated in Figure 2.4.

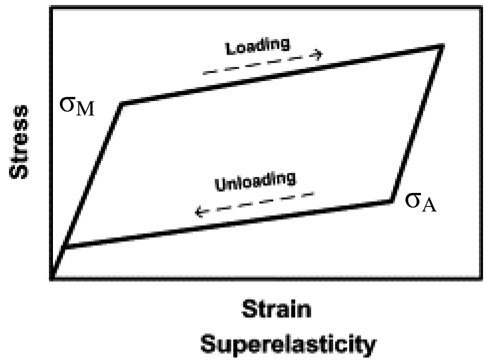

Figure 2.4 – Superelasticity of shape memory alloys (Huang, 2002)

When the applied stress is less than σ_M, stess-strain relationship is nearly linear. When the applied stress is larger than σ_M, martensitic transformation will occur. There will be phase transformation from martensite to austenite. When unloading and the applied stress become less than σ_A, there will be a reverse transformation and the material returns to its original shape. (Huang, 2002)

2.3.4 All-round Shape Memory

Some specially treated NiTi alloys could have a specific behavior called all-round shape memory. Some researchers also called it two-way shape memory. Figure 2.5 illustrates the all-round shape memory phenomenon of NiTi alloy.

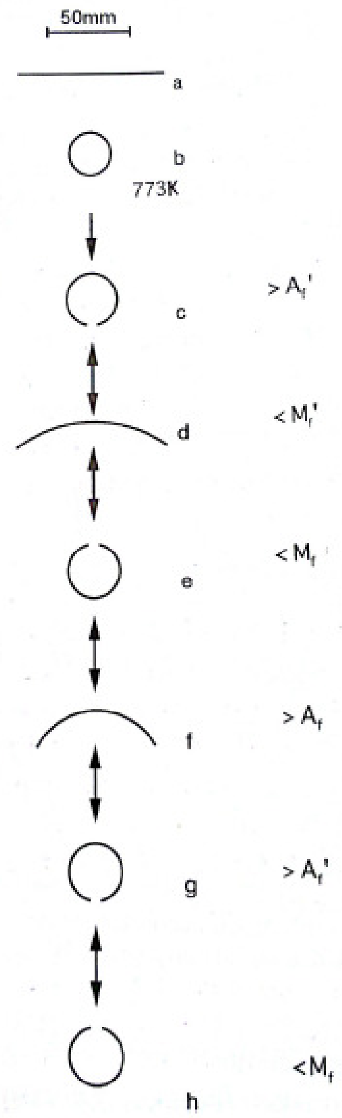

Figure 2.5 – All round shape memory of NiTi alloy (Otsuka and Wayman, 1998)

The all-round shape memory behavior is demonstrated by a thin sheet of NiTi. A sheet of NiTi with 0.3mm thickness was forced into an inner circle of tube with a diameter of 20mm. Its shape became circle. The NiTi was then heat treated at 500°C within the tube. If the applied temperature is higher than the R to B2 phase transformation $A_{f'}$, the sheet could remain the round shape after removal from the tube. After the round shaped sheet was put in air and cooled, its shape changed from (c) to (d). This was related to the B2 to R phase transformation. When the sheet was further cooled, the shape of NiTi would change from (d) to (e), which was rounded upside down. This was due to cooling and the applied temperature was below M_f. This was related to R to B19' phase transformation. The shape transformation between (c) to (e) was reversible. When the NiTi sheet was then heated above A_f, its shape changed as (f) which was similar to that of (d). When further heating and the applied temperature reached $A_{f'}$ again, the shape changed to (g) which was the same as (c). When cooling down to below M_f again, its shape changed to be (h) which is the same as (e).

2.3.5 Applications

NiTi alloys are widely used as prostheses or biomaterials in medicine and dentistry. The main reason for these applications is mainly because of their good biofunctionability and biocompatibility (Miyazaki, 1998). Shape memory alloys have unique properties such as shape memory effect and superelasticity. Moreover, NiTi has good mechanical stability that makes it become one popular biomaterial for clinical application. Titanium and its alloys are widely used for replacement of hard tissue in body, valves of heart, frame of blood vessels and different kinds of medical devices (Liu, 2009). Figure 2.6 shows some common applications of NiTi in medical field.

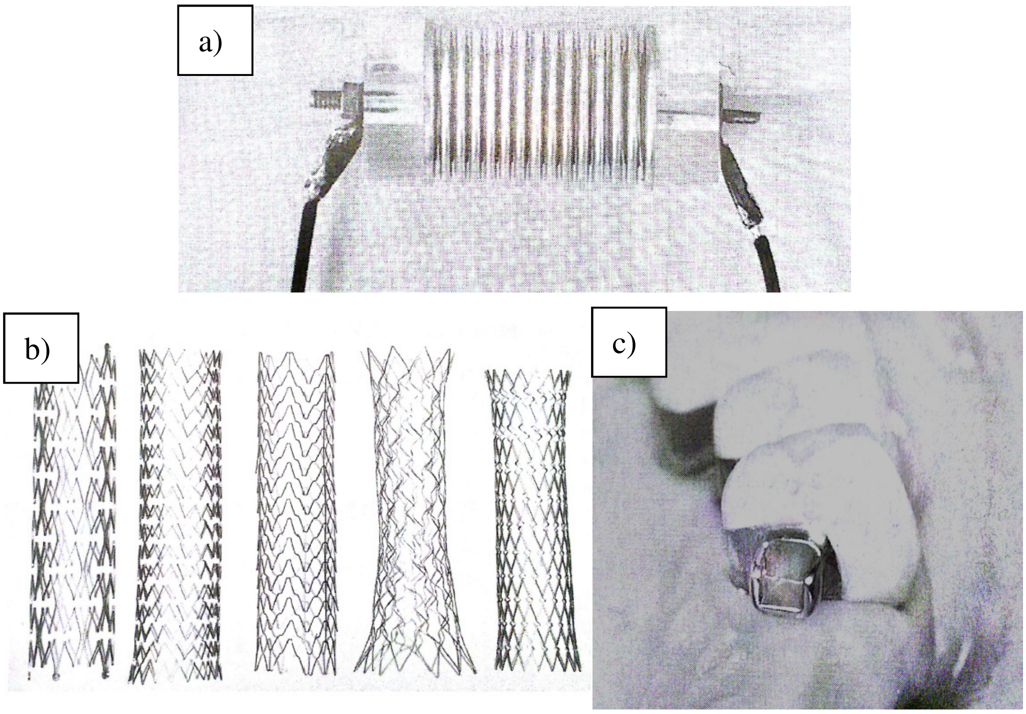

Figure 2.6 – a) Artificial kidney pump (Miyazaki, 1998); b) Blood vessels frames (Yoneyama & Miyazaki, 2009); c) A fixed part for partial denture (Miyazaki, 1998)

2.4 Nitriding of Titanium Alloys

A large number of studies have been conducted into nitriding of titanium alloys. Nitrogen has high solubility in α titanium. Therefore, the strengthen result on titanium alloys is normally significant. Titanium nitride is formed on titanium alloy surface in the form of TiN while at the beneath as Ti_2N with high hardness values (Zhecheva et al., 2005).

2.4.1 Properties of Titanium Nitride

Titanium nitride (TiN) is believed to be an extremely hard ceramic material. It is a common material used as coating on titanium alloys, aluminum alloys and steels in order to improve the surface properties of the substrate. The properties of TiN are described in Table 2.3.

Table 2.3 – Properties of titanium nitride (Pierson, 1996)

Molar mass	61.874 g/mol
Appearance	Golden
Density	5.4 g/cm^3
Melting point	2930℃
Vickers hardness	18 – 21 GPa
Modulus of elasticity	251 GPa
Coefficient of friction	0.65
Crystal structure	Face centered cubic

By surface modification techniques, TiN formed on surface is believed to provide hardening and protective function for the substrate, especially for the protection of sliding or cutting surface. Due to the golden appearance of TiN, it has decorative function as well. TiN is chemically stable in room temperature and has high corrosion resistance. However, it is attacked by hot concentrated acid (Pierson, 1996). Since it is non-toxic in to human body, TiN coating could be applied for medical devices such as artificial implants.

There are four methods for nitriding. They are plasma nitriding, ion beam nitriding, laser gas nitriding and gas nitriding.

2.4.2 Plasma Nitriding

Plasma nitriding is one type of thermo-chemical treatment. Ionized molecules of pure nitrogen are generated by intense electric fields. The ionized molecules of nitrogen forms highly active plasma which is around the target surface. The method supports the formation of specific titanium phase. Moreover, the depth of nitride formed could be controlled and oxidation of titanium could be eliminated (Zhecheva et al., 2005). The processing time for plasma nitriding is ranging from 15 minutes to 32 hours with an operating temperature of 400 - 950℃ depending on the quality and the depth of nitride layer required (Rie & Broszeit, 1995). However, it is believed that plasma nitriding could reduce the fatigue strength of titanium alloys.

2.4.3 Ion Beam Nitriding

In this technique, the target sample is exposed to ion beam of nitrogen and argon. The target surface is bombarded by nitrogen ions and cause desorption and sputtering of impurities. Normally, the working environment of the treatment is ranging from 500 – 900℃ for 30 minutes to 20 hours (Zhecheva et al., 2005). After treatment, nitride layer of 5 – 8 μm with micro-hardness of 800 – 1200 HV could be obtained (Chen & Jaung, 1997).

2.4.4 Gas Nitriding

Ammonia is used as donor for nitrogen in the treatment. A target material is heated and disassociated into hydrogen and nitrogen. Nitrogen diffuses into the target from the surface to the deeper site of the material (Rolinski & Sharp, 2004). It allows nitriding of large batch size. The working temperature is ranging from 650 – 1000 ℃ while the processing time is ranging from 1 – 100 hours (Zhecheva et al., 2005). Nitride layer with a thickness about 2 – 15 μm with micro-hardness from 450 – 1800 HV could be obtained.

2.4.5 Laser Gas Nitriding

Conventional laser gas nitriding use focused laser beam to melt the substrate surface under nitrogen gas environment resulting in the formation of nitride layer on the substrate surface. Nitrogen is supplied in the way through a nozzle into the melt pool. The angle between the nozzle and the substrate surface has to be at least 30° (Zhecheva et al., 2005). Laser gas nitriding is able to form nitride layer toughly on the substrate. This is due to the formation of strong metallic bond between the nitride layer and the substrate. It is believed by many scholars that laser gas nitriding is a fast nitriding process which allows the fabrication of nitride on a specific small area on a substrate (Kannatey-Asibu, 2009). Nitride layer formed on the substrate would generally have the micro-hardness of more than 700 HV depending on the laser parameters (Zhao et al. 2006). The thickness of the nitride layer is 1 – 1.5 μm per scan. Multipass treatment could increase the thickness of nitride layer formed.

2.4.6 Comparison of the Nitriding Methods

A summary included the performance of different nitriding methods is presented in Table 2.4 below. Gas nitriding has the longest processing time while the resulting thickness of nitride layer is not as thick as other methods. Furthermore, the working temperature is relatively higher. This may represent that a higher energy is required for the slow process. Plasma nitriding supports the fabrication of relatively thick layer of nitride. However, the processing time for such thick layer is still very long. In addition, specific high energy ionizing system and vacuum are required for the treatment. Ion beam nitriding has the required equipment similar to that of plasma nitriding, except no specific ionizing system is required. However, the resulting thickness of nitride layer is not as thick as that of plasma nitriding. The thickness of resulting nitride layer for laser gas nitriding is not as thick as other methods. However, the processing time is extremely fast since scanning of laser is a well-known fast process. A fast processing time also enable formation of fine-grained structure which would bring a higher strength and better fatigue resistance (Kannatey-Asibu, 2009). Nevertheless, the process is normally not limit in specific temperature controlled working chamber. Laser gas nitriding enable the treatment of desirable area instead of the whole material.

Table 2.4 – Summary of different nitriding methods

	Plasma nitriding	**Ion beam nitriding**	**Gas nitriding**	**Laser gas nitriding**
Processing time	15 min - 32 hr	30 min – 20 hr	1 – 100 hr	Area dependent 1 – 30 mm/s for each track
Thickness of resulting nitride layer	50μm for 32 hrs process	5 – 8 μm	2 – 15 μm	1 – 1.5 μm per scan
Working temperature	400 – 950 ℃	500 – 900 ℃	650 – 1000 ℃	Room temperature
Hardness of nitride layer	600 – 2000 HV	800 – 1200 HV	450 – 1800 HV	>700 HV
Equipment required	Temperature control system High energy ionizing system Gas supply Vacuum chamber	Temperature control system Ionizing system Gas supply Vacuum chamber	Temperature control system Gas supply Chamber	Laser system Gas supply CNC table Chamber

2.5 Laser Gas Nitriding of Titanium Alloys

It is believed that fast processing time, and formation of strong metallurgical bond between titanium substrate and nitride layer are two major advantages of laser gas nitriding. As mentioned in previous chapter, many studies have proven the effectiveness, reliability and possibility of laser gas nitriding, laser gas nitriding is going to be explored instead of other nitriding methods in this research. In the following section, further discussion on principles and major parameters of laser gas nitriding will be done.

2.5.1 Phase Transitions of Titanium Surface during Laser Gas Nitriding

Formation of nitride on titanium involves several steps. As described by researcher (Zhecheva et al., 2005), the reactions between nitrogen and titanium occur at the edge of the substrate simultaneously. When titanium is located in active nitrogen containing situation under high temperature, there is a nitrogen mass transfer from the surrounding medium to the substrate. After that, nitrogen absorbed diffuses from the surface into the deeper area of substrate. An interstitial solution of nitrogen forms in the hexagonal close packed α phase titanium. The surface layer becomes a diffusion zone named α(N)-Ti. This step of transition continues until the titanium nitrogen matrix could not dissolve any more. If the concentration of nitrogen in the titanium nitrogen matrix becomes higher than the capability of retaining, another reaction occurs and leads to the formation of a new phase named Ti_2N. The structure then becomes a nitrided area containing a compound layer Ti_2N on top and a diffusion zone underneath. When the concentration of nitrogen is then higher than the capacity in Ti_2N, there is a transformation of Ti_2N to TiN afterward. To conclude, the phase transitions of titanium surface during laser gas nitriding could be described as below.

$$\alpha\text{-Ti} > \alpha(N)\text{-Ti} > Ti_2N > TiN$$

In order to explain these phase transitions, other research has proposed a diagram to clearly show the growth of surface nitride layer of titanium by laser gas nitriding. The diagram is presented as Figure 2.7.

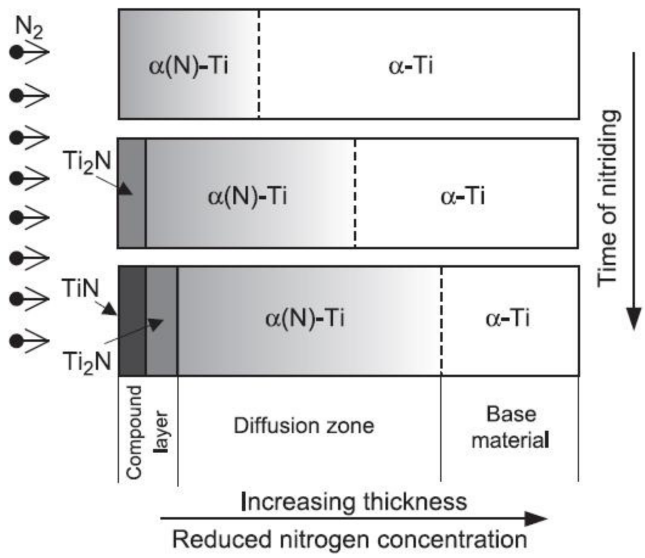

Figure 2.7 – Growth of surface nitride layer during nitriding of titanium (Malinov et al., 2003)

The model could describe mechanism of nitriding of pure titanium appropriately. But this model may not be proper when applying for the nitriding mechanism of titanium alloy. The main reason is the presence of other alloying materials in titanium alloys. There may also be reaction of nitrogen with other alloying material instead of only titanium. However, the presence of other alloying material may not affect the phase transition mechanism very much. This is because the composition of alloying material is not high. Titanium – nitrogen phase diagram could provide useful information about the temperature change and percentage composition during transition. It is presented as Figure 2.8

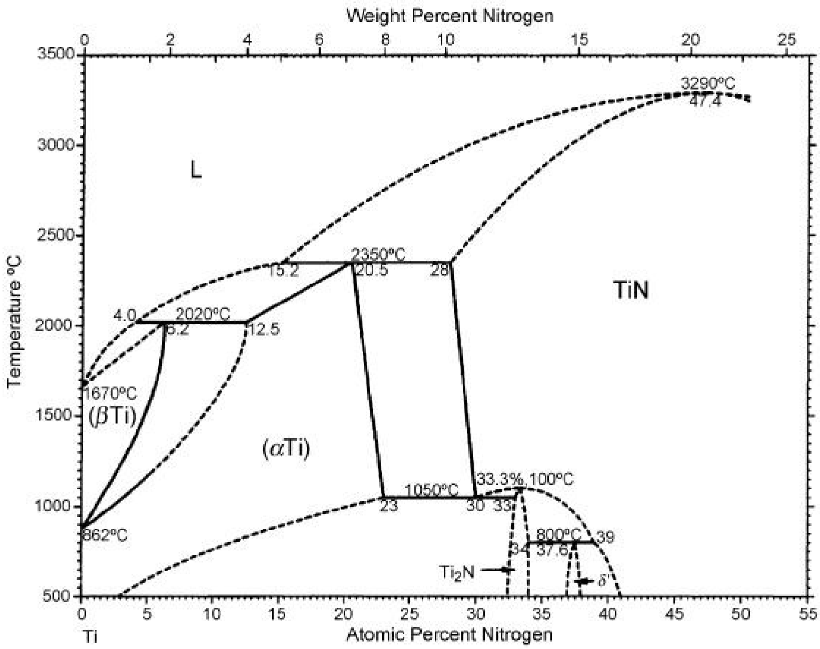

Figure 2.8 – Ti-N phase diagram (Malinov et al., 2003)

2.5.2 Laser Gas Nitriding with Fibre Laser

Fibre laser is recently widely used for material processing. This is mainly because of its advantages. It provides a relatively smaller spot size and higher power intensity than other conventional Nd:YAG and CO_2 laser systems. This allows fibre laser to give a faster energy delivery rate than those Nd:YAG and CO_2 laser systems. Previous research showed that fibre laser could facilitate material processing in a shorter interaction interval (Miyamoto, 2005). Fibre laser could also maintain a high up-time and yield under during production. The reason for this is due to the use of diode instead of flash-lamp as the pumping source for fibre laser. The use of diode could also reduce maintenance of flash-lamp. In addition, mirror alignment which is necessary for other conventional laser could be eliminated.

The advantages of fibre laser include:

- Higher optical quality

  The fibre has waveguiding properties that could help to eliminate thermal distortion of optical path. A high quality optical beam could therefore be produced.

- Better light transmission

  The flexible fiber allows easier delivery of light in a movable focusing element. This is important for laser material processing such as laser surface patterning.

- Smaller size of laser system

  The laser system is much smaller for fibre laser than other conventional laser systems such as Nd:YAG and CO_2 laser. This is because fibre could be bent and stored in a relatively compact area.

- Higher reliability

  Fibre laser systems normally have high vibrational stability and lifetime. This is because a maintenance-free turnkey operation system is used for fibre laser.

2.5.3 Parameters in Laser Gas Nitriding

The nitriding result of laser gas nitriding could be affected by the variation of several parameters include output power of laser, scanning speed, beam diameter, reflectivity of substrate, flow rate of nitrogen, and concentration of nitrogen.

<u>Output power of laser</u>

During nitriding process, laser provides energy for the reaction between nitrogen and titanium for the formation of titanium nitride. Increase laser output could increase the concentration of titanium nitride as well as hardness of nitride layer (Yu et al., 2009).

Scanning speed

Scanning speed of laser on the substrate could be referred to the interaction time between laser beam and the substrate. Higher scanning speed will reduce the interaction time, vice versa. Interaction time is inversely correlated to the depth of diffusion of nitrogen. Previous research has shown the relationship between interaction time, hardness and thickness of nitride layer (Abboud et al., 2008). Reduction of scanning speed led to a slightly increase of hardness of nitride layer. The thickness of nitride layer also increased. Higher scanning speed could eliminate formation of crack and pore. However, too high scanning speed might result in insufficient hardening of surface layer. Figure 2.9 shows the micro-hardness and depth below surface of scanning speed ranging from 0.5 – 5 m/min.

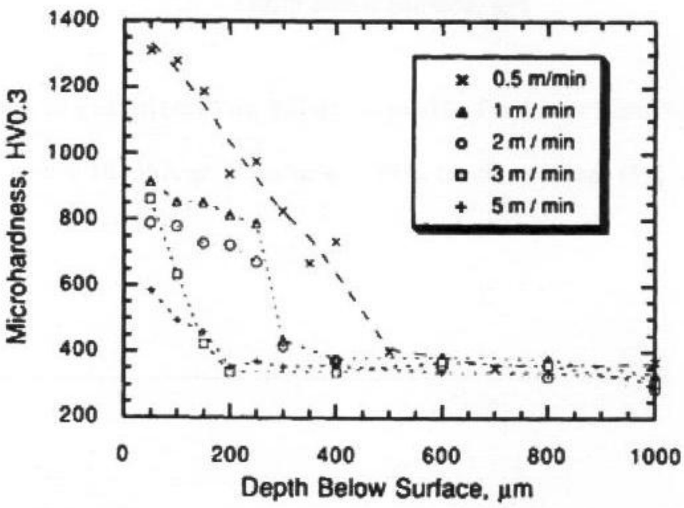

Figure 2.9 - Effect of scanning speed of laser to the micro-hardness and depth of nitride layer on titanium alloy

<u>Beam diameter</u>

Beam diameter is controlled by focal distance of laser to the substrate. A sharp beam spot on the substrate means the energy of laser is concentrated. The beam diameter is small for a concentrated laser beam. When the beam is concentrated, the power acts on the substrate will be higher. Figure 2.10 presents the relationship of laser beam and substrate.

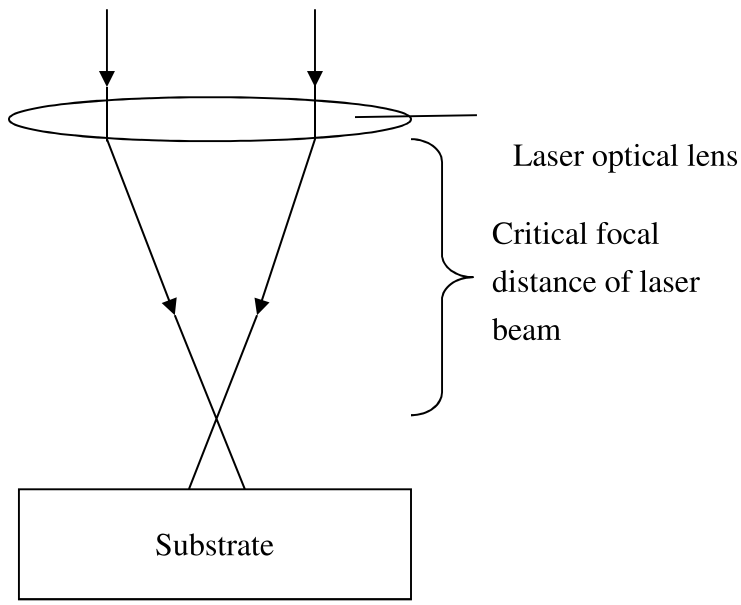

Figure 2.10 – Relationship between beam diameter and focal distance on substrate

Before determining the corresponding focal length for experiment, it is necessary to measure the critical focal length of the laser machine first. As mentioned before, the action of beam on a substrate is most powerful at the critical focal distance. The resulting burn mark on substrate will be larger and darker. To determine the critical focal length, laser spots with gradual change of focal distance are required to create burn marks on a substrate. After that, the burn marks have to be observed under microscope. The few burn marks which are larger and darker in color could be extracted. Fine tune of the focal distance is then required. Finally the focal length of laser machine could be determined. Figure 2.11 shows the burn marks created by laser for determining the focal length. The upper set of spots was for rough estimation while the lower set of spots was for fine tune estimation. It is clearly shown that by changing the focal distance, the burn marks have gradual change of diameter and darkness.

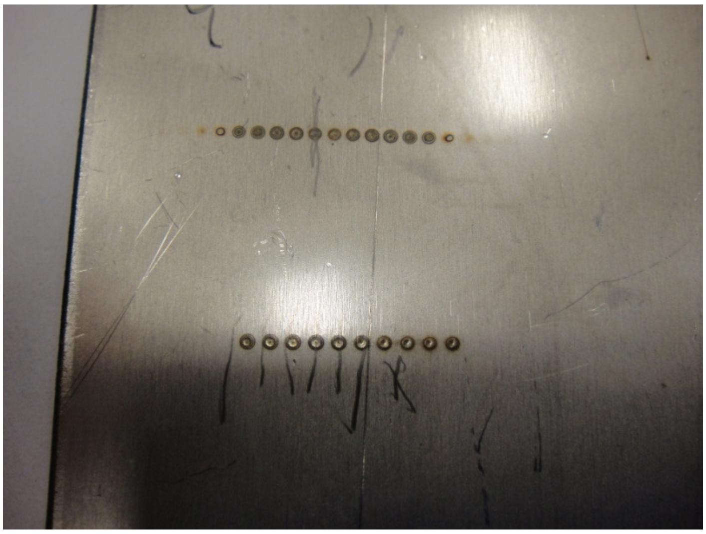

Figure 2.11 - Burn marks for estimating focal length of laser machine

Reflectivity of substrate

Reflectivity of substrate affects the absorption of laser power on the substrate. A proportion of energy is reflected from the substrate surface after a laser beam arrives. Some researchers believe surfaces are less reflective when the roughness is high (Man et al., 2011). It is claimed that laser beam arriving at a rough surface may under two or more reflections, resulting in the increase absorption of laser energy.

Flow rate of nitrogen

The micro-hardness profile change from surface to inner site of substrate under different nitrogen flow rate is presented in Figure 2.12. Flow rate of nitrogen gas mainly affects hardness of nitride layer. Micro-hardness of nitride layer of 1000 L/hr was the lowest at surface. This showed that low nitrogen flow rate might decrease the dissolution of nitrogen as well as the subsequent concentration of titanium nitride dendrites in molten pool on surface, resulting in reduction of hardness (Abboud et al., 2008). However, sharp increase of nitrogen flow rate did not lead to significantly increase of micro-hardness of nitride layer. It indicated that increase in nitrogen flow rate might be related to hardness of nitride layer, but the relationship is not strong.

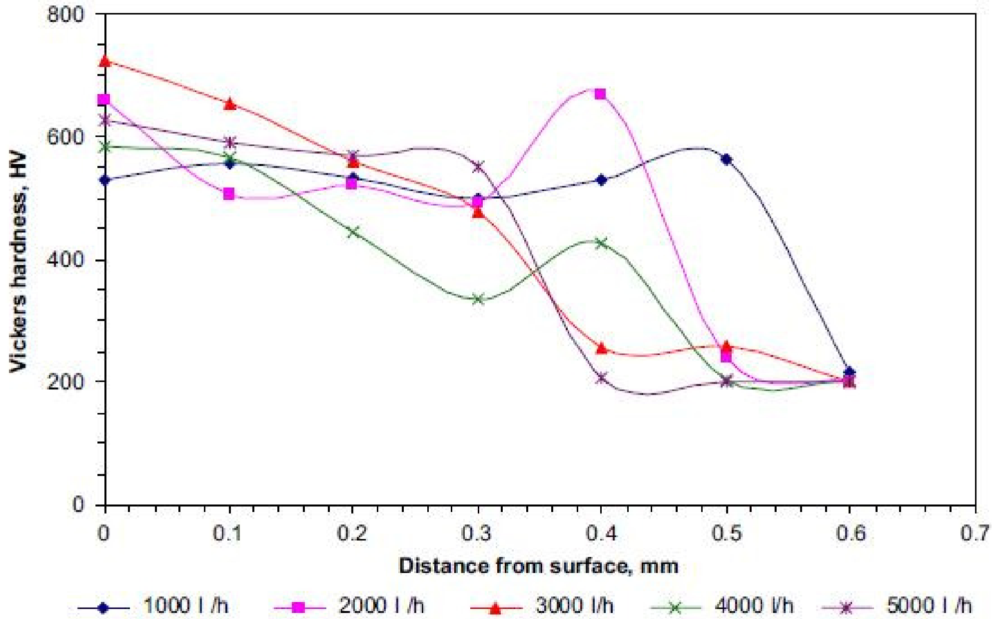

Figure 2.12 - Micro-hardness of TiN in different depth of substrate for various nitrogen flow rate (Abboud et al., 2008)

Concentration of nitrogen gas

A study has shown that nitride layer grows deeper when nitrogen concentration in gas is higher. In addition, the surface color became more golden in color when nitrogen concentration increased. This is due to the increase in nitrogen mixture amount (Abboud et al., 2008). Figure 2.13 indicates that pure nitrogen gas for nitriding could result in high micro-hardness on the surface. This is because high nitrogen concentration could increase dissolution of nitrogen. Titanium nitride dendrites concentration in the molten pool is increase as the same time. Therefore, hardness is increased.

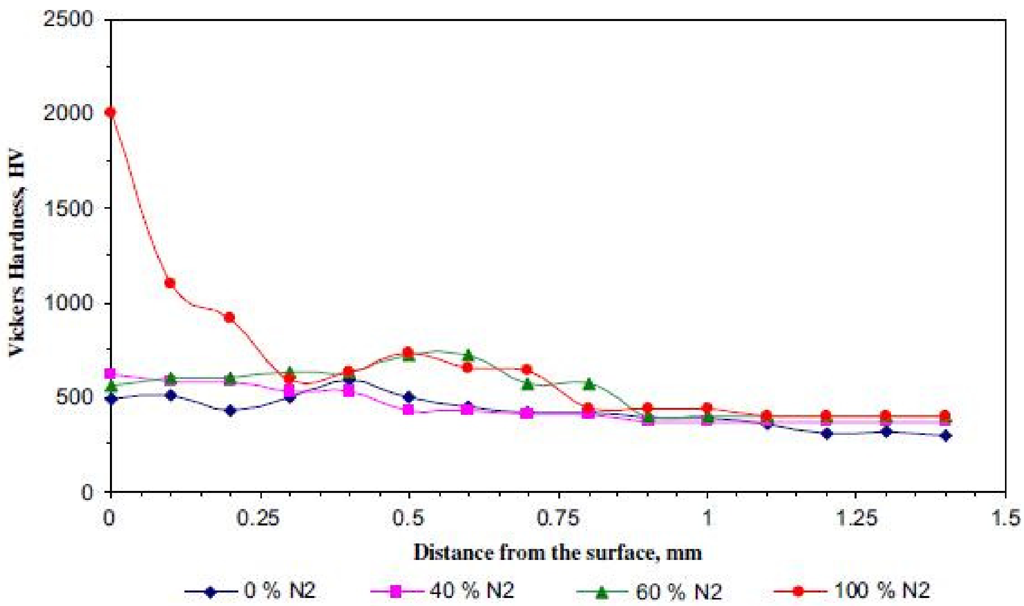

Figure 2.13 - Micro-hardness of TiN in different depth of substrate for various nitrogen concentration (Abboud et al., 2008)

2.5.4 Laser Gas Nitriding on NiTi

As mentioned in the previous chapter, NiTi as a biomaterial and smart material has been widely used for making medical devices. However, one major concern for the application of NiTi would be its high atomic percentage of nickel. Corrosion or wearing during application may bring deleterious effects to body (Cui, Man, and Yang 2003). Studies illustrated that surface layer of TiN produced by laser gas nitriding could successfully prevent the leakage of Ni. Cui et al. (2003) have shown that after laser gas nitriding of the full surface of NiTi substrate using Nd-YAG laser using appropriate parameters could result in the formation of a crack-free thin TiN layer. In addition, there was no nickel signal being detected on the sample surface after treatment, indicating that laser nitriding could reduce the Ni concentration on sample surface. The study also proved that there is a good bonding between TiN surface layer and the laser melted layer of NiTi. Dendrites were observed growing from the surface into the melted inner layer of the NiTi substrate.

In another research project studying laser surface hardening of stainless steel, network pattern of laser tracks were scanned on the material surface. The strength of stainless steel was improved. Therefore, it is believed that such scanning method could also be applied to NiTi for improving its strength. This research project will study the effect to NiTi after applying such network pattern using laser gas nitriding. Laser gas nitriding will alter the surface composition and microstructure so that the properties of material may also change. The influence on the bulk properties may be large when the cross section thickness of the treated sample is thin. Change of microstructure and composition of thin NiTi may affect its shape memory properties. Man et al. (2006) has studied the effects of the presence of nitride layer on NiTi fabricated by laser gas nitriding upon the phase transformation temperature of the alloy. 3-mm thick NiTi plates were used for study. With a set of parameter (500W, 2mm diameter defocused spot size, 150mm focal length Zinc Selenide focusing lens, 99.9% nitrogen flowing at 50L/min, scanning speed 5mm/s), a layer of TiN with 2μm thickness could be fabricated on NiTi. DSC analysis results illustrated that laser gas nitriding of NiTi does not affect the transformation temperatures, so do the shape memory property significantly. Therefore, it could be concluded that laser gas nitriding would not alter the phase transformation characteristics of treated NiTi. (Man and Zhao 2006).

As discussed in many studies, it is believed that the wear resistance of NiTi could be further improved if hard particles were embedded on the alloy. This is because the hard phase particles could withstand the external load. Therefore, it is common to fabricate such nitride on titanium alloy in order to protect the inner material from being worn away during application. Besides investigation of the phase transition characteristics of NiTi after laser gas nitriding, Zhao at el. (2006) has study the wear properties of laser gas nitride NiTi surface. By applying a set of parameters (500W, 2mm spot size and 5mm/s scanning speed), the surface hardness of laser treated NiTi sample could reach 750HV. The result of wearing test showed that the laser nitride coating have better wear resistant capability at room temperature when compared with raw NiTi. By measuring the mass loss, it is found that the weight for raw NiTi is much higher than that of the treated samples. Zhao (2006) believes that the high hardness of TiN/NiTi and stainless steel interface maintain low friction coefficients and wear rates. Therefore, he concludes that the wear resistance increases with TiN amount in the TiN/NiTi composite.

Zhang et al. (2005) also studied the wear behavior of laser gas nitrided NiTi. The parameters for laser gas nitriding were different from that of Zhao (2005). The parameters used in the study were 900W, 25mm/s scanning speed, 1.5mm spot size and 20L/min nitrogen flow instead. A nitride layer with thickness of 1μm to 2μm could be formed on NiTi. In addition, instead of using block-on-wheel wear testing method (Zhao et al. 2006), ball-on-plate wear testing method was used (Zhang et al. 2005). Diamond ball was loaded on the laser treated NiTi surface for 3.5N and turning speed 200 r/min for 15s. Both studies demonstrated that the wear morphology occurred on the laser treated NiTi is mainly adhesive while that for raw NiTi would be adhesive and abrasive together during wear test. Both studies have proved that the surface nitride layer on NiTi could enhance its wear resistance.

Researchers are also interested in the effect of nitride layer on the corrosion properties of NiTi. Nd-YAG laser could be applied to fabricate a compact laser modified gradient layer reinforced with fine TiN particles on NiTi. The corrosion potential and breakdown potential increased with decreasing corrosion current compared with the raw NiTi (Zhang et al., 2011).

Previous studies have demonstrated that laser gas nitriding could be applied for successfully fabricating TiN on NiTi and improving the wear and corrosion properties of the alloy. However, all of them were using Nd-YAG laser for laser process. There is almost no research studying laser gas nitriding using other laser system. In addition, most of the research doing laser gas nitriding on the whole surface of the specimen. The scanning time may be long when the scanning speed is only 5mm/s with at least 50% overlapping of laser tracks.

2.6 Design of Experiments and Taguchi Approach

In 1920, Sir R.A. Fisher developed a statistical technique called Design of experiments (DOE). He developed DOE in order to investigate the way to grow the best crop with various related factors such as level of sunshine, amount of water supply and the use of different fertilizers. He listed out all the possible combination of factors that were supposed to be related to crop growing and created a matrix. He developed schemes to conduct a fraction of the total possibilities. Therefore, all involved factors could be evenly present. As academic knowledge grew, DOE did not only apply in agriculture but also in engineering field. (Roy, 2001)

A Japanese scientist, Dr. Genechi Taguchi was professional in improving the quality of manufacturing. He spent his life on researching and developing a comprehensive quality improvement methodology concerning DOE. The method he devised is called Taguchi method. This method becomes a practical strategy in quality engineering. Taguchi method was developed based on DOE.

There are five phases in applying Taguchi method. They are planning, designing, conducing, analyzing and confirming as illustrated in Figure 2.14.

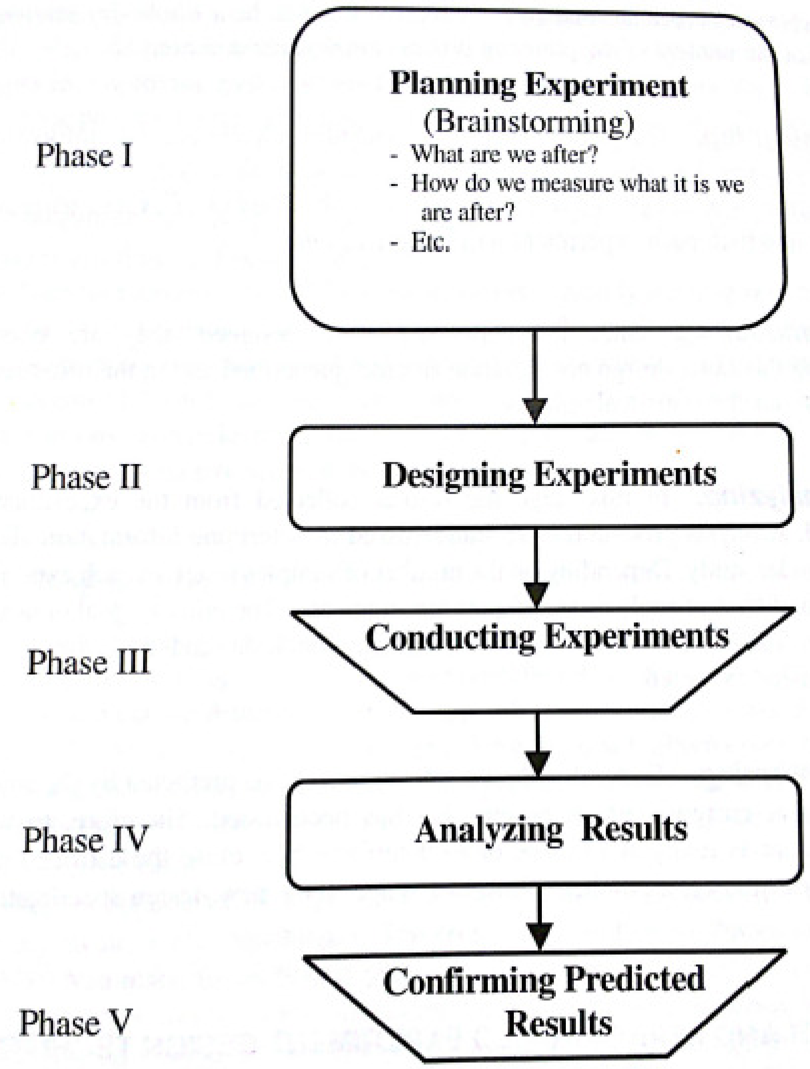

Figure 2.14 – Phases of Taguchi method (Roy, 2001)

According to Roy (2001), planning is like a brainstorming process that all decisions about the project that may affect the results are considered. Then in the designing phase, an experiment could be based on the conclusion from planning phase. This involves to identification of factors and levels in the experiment. In conducting phase, trial experiment will be conducted based on the designed experiment. Different analysis techniques are used in analyzing phase. The main function of this phase is to get the information about the design condition and estimate the expected improvement. Finally in the confirmation phase, the optimum design condition estimated by the analysis will be tested in order to prove whether the estimated improvement could really be achieved.

2.6.1 Signal-to-noise Ratio

In order to evaluate comparison, quality characteristic is required for better measurement of results. Evaluation is a process to measure the performance of results from the analysis according to the objectives. Quality characteristic no matter representing the results bus also give the sense of desirability of the results (Roy, 2001). The quality characteristic could be presented as signal-to-noise ratio, S/N ratio. The three most commonly used S/N ratio are Larger-is-better, Smaller-is-better and Nominal-is-best (Hicks, 1999).

Small-is-better:

$$S/N_{SB} = -10\log_{10}\left[\frac{\sum_{i=1}^{n} Y_i^2}{n}\right] \tag{2.1}$$

Nominal-is-best:

$$S/N_{NB} = -10\log_{10}[S^2] \tag{2.2}$$

Larger-the-better:

$$S/N_{LB} = -10\log_{10}\left[\frac{1}{n}\sum_{i=1}^{n}\left(\frac{1}{Y_i^2}\right)\right] \tag{2.3}$$

$n \geq 2$: the number of observations in a sample of size n

S^2 : variance of the sample

Signal-to-noise ratio is often used for Taguchi analysis. According to Hicks (1999), this is because the treatment combination with the largest true average signal-to-noise ratio could give the least variation in the response variable.

2.6.2 Orthogonal Arrays

Orthogonal arrays are a set of tables of numbers. Each of the number could be used to construct the experiments for a number of experimental situations (Hicks, 1999). Dr. Taguchi conducted research to develop a special set of orthogonal arrays for designing experiments. This special set of orthogonal arrays could standardize the fractional factorial designs.

Orthogonal arrays have their notation L with a subscript or dash. L is come from Latin square while the subscript refers to the number of rows in the table. Number of rows in the table also indicates the number of combinations whom the experimental design contains. Orthogonal arrays sometimes contain numerical notations. It indicates the number of factor involved as well as the full factorial combinations.

2.6.3 Analysis of Mean (ANOM)

Analysis of mean (ANOM) is conducted for determine the best level of each factor that could bring to the most desired result. It involves the process of comparing the mean signal-to-noise ratios obtained from various levels of factor and the interaction. The difference between mean signal-to-noise ratio at the levels could be seen as the effect of each factor or interaction (Chan & Man, 2011).

2.6.4 Analysis of Variance (ANOVA)

Analysis of variance (ANOVA) is one effective statistical method for interpreting the experimental data. Moreover, ANOVA is essential for making decisions by looking at the result from Taguchi method since this method is very objective (Ross, 1996). ANOVA could provide three types of important information:

i) The factors which make a difference

ii) The relative importance of factors involved

iii) The direction for levels of the involved factors that lead to further improvement

Many researchers believe ANOVA is important for judging the statistical significance of factors and interactions. The principle of ANOVA is to break the total variance into individual components. ANOVA involves the following components. They are degree of freedom (DOF), sums of squares (S), mean of squares (V), F-ratio (F), pure sum of squares (S') and percent influence (P). (Taguchi, 1993)

Chapter 3 Experimental Details

Laser gas nitriding was performed on nickel titanium alloy. Different properties were investigated and compared between the treated and untreated samples. This project includes five sets of experiments. They are a) laser gas nitriding on NiTi with different parameter sets for Taguchi analysis; b) tensile test to investigate the effect of laser gas nitriding surface treatment on the tensile stiffness of NiTi; c) wear resistance test to study the effect of surface laser nitride layer to the wear behavior of NiTi; d) corrosion resistance test to investigate the effect of surface nitride layer on the corrosion behavior in sodium chloride solution; e) surface hardness of TiN.

3.1 Taguchi Analysis for Laser Gas Nitriding

As there were numerous factors that could affect the result of laser gas nitriding, design of experiment was employed. Taguchi method, a modified type of design of experiment was conducted in this project. As discussed in Chapter 2, Taguchi method uses orthogonal arrays, which distribute the variables in a balanced manner, to reduce the number of experiments required (Roy, 2001). This experiment is conducted to analyze the effect of different levels of parameters concerning laser gas nitriding to the surface hardness of samples after laser treatment. It is believed that a higher surface hardness would bring to the result of a better wear resistance. Therefore, Taguchi analysis was performed to investigate an optimum parameter set of laser gas nitriding which could give the result of highest surface hardness on NiTi.

3.1.1 Material Preparation

Material used in this study was commercial Ti-55.91 wt. % Ni plate in the form of 200mm × 150mm × 2mm. It was cut into pieces of 20mm × 15mm × 2mm. The surface was polished by SiC paper gradually until 2400 grits. All specimens were degreased with alcohol for 5 minutes, rinsed by distilled water and air dried in room temperature.

3.1.2 Preliminary Study of Surface Hardness of Laser Treated Samples

Before conducting Taguchi experiment, a set of samples was treated by laser gas nitriding in order to briefly understand the effect of different parameters on the surface hardness of NiTi. The results from this preliminary study were important for examine whether the fibre laser was suitable for laser gas nitriding as well as providing consistent results for further analysis in the project. This preliminary study was necessary to gather potential levels that are used in the Taguchi experiment. The reason is that in order to obtain the optimum parameter set from Taguchi experiment, the potential range of different factors should be identified. The focal point for this preliminary study is the output power and the scanning speed of laser, while the potential ranges for other parameters include nitrogen flow rate were referenced from literature. The setting in the preliminary study is presented in Table 3.1.

Table 3.1 – Experimental setting in preliminary study

Output power (W)	**Scanning speed (mm/min)**	**Beam diameter (mm)**	**Nitrogen flow rate (L/min)**
60 - 90	300 - 900	0.4	20

The surface hardness was measured by Vickers hardness test through Mitutoyo Hardness Testing Machine Microwizard. Hardness is a measurement of the resistance of solid material to permanent shape change after a force is applied. There are various types of hardness measurement methods such as scratch hardness, indentation hardness and rebound hardness. Indentation test was employed in this project. This type of hardness measurement examines the resistance of a material to material deformation caused by a constant compression load from a sharp object. The indentation left on the sample surface was measured. It was marked by a specifically dimensioned and loaded indenter. A pyramidal shape indenter of 136° angle was pressed by 200g force into the surface of the samples. The holding time was set to be 8 seconds.

Two diagonals of the indentation were measured and the average was used to compute the hardness (HV) based on the following equation:

$$\mathrm{HV} = \frac{2000P\sin(\alpha/2)}{d^2} = \frac{1854.4P}{d^2} \qquad (3.1)$$

d: length of diagonals in μm

α: face angle (136° for Vickers hardness in this project)

P: load applied on the material in gf

The schematic of the specially designed indenter and appearance of indentation is demonstrated in Figure 3.1.

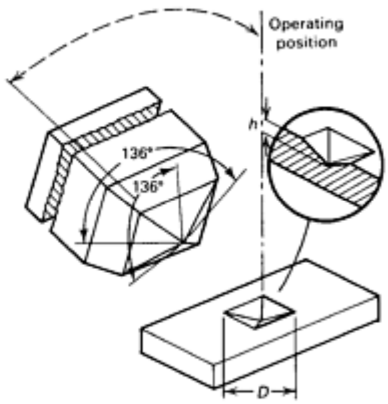

Figure 3.1 – Schematic of the indenter and indentation (Frohlich et al., 1977)

3.1.3 Orthogonal Array of Taguchi Experiment Selection

The potential ranges for parameters concerning laser gas nitriding were identified. The results were applied for the Taguchi experiment. An L-27 orthogonal array was employed. As discussed in Chapter 2, orthogonal array of Taguchi method could minimize the number of trial experiments at the same time investigate the major effects of factors and interactions. It could also be useful to conclude the performance of the factors to the experimental results with scientific data such as the statistical level of confidence.

The three levels in Taguchi analysis were presented as 1, 2, 3. For selection of orthogonal array for analysis, calculation of degree of freedom (DOF) is necessary. It is an important step to compare the DOF of the orthogonal array with the DOF of all factors and interactions involved in the experiment (Chan & Man, 2011). The DOF of orthogonal array is required to be equal to or greater than that of the total DOF of factors and interactions. The four factors involved in this Taguchi analysis were as A, B, C, D as short term. Therefore, their relevant interactions were as AXB, AXC, AXD, BXC, BXD, CXD.

$$\text{DOF of 4 factors} = 4 \times (3 - 1) = 8$$

$$\text{DOF of 6 interactions} = 6 \times (3 - 1) \times (3 - 1) = 24$$

$$\text{Total DOF} = 24 + 8 = 32$$

The total DOF is 32 and it is larger than the total DOF of L-27 orthogonal array. Chan and Man (2011) suggested that it is possible to share two-factor interactions in three columns in the L-27 orthogonal array. After such modification, the total DOF is reduced to 26 and is suitable to be analyzed in an L-27 orthogonal array.

It was also possible to analyze four factors with three levels condition in L-16 orthogonal array. However, L-27 orthogonal array was used instead of L-16. This is because an L-27 orthogonal array in this case could help to analyze the interaction between factors at the same time with the analysis of optimum parameter set. The results could give an even better understanding about the relationship between the factors. Table 3.2 showed the factor setting for L-27 orthogonal array.

Table 3.2 – L-27 (3^{13}) array

Column													
	A	**B**	**C**	**D**	**AXD**	**AXD** **BXC**	**BXD**	**CXD**	**BXC**	**BXD** **AXC**	**AXC**	**CXD** **AXB**	**AXB**
Trial	1	2	3	4	5	6	7	8	9	10	11	12	13
1	1	1	1	1	1	1	1	1	1	1	1	1	1
2	1	1	1	1	2	2	2	2	2	2	2	2	2
3	1	1	1	1	3	3	3	3	3	3	3	3	3
4	1	2	2	2	1	1	1	2	2	2	3	3	3
5	1	2	2	2	2	2	2	3	3	3	1	1	1
6	1	2	2	2	3	3	3	1	1	1	2	2	2
7	1	3	3	3	1	1	1	3	3	3	2	2	2
8	1	3	3	3	2	2	2	1	1	1	3	3	3
9	1	3	3	3	3	3	3	2	2	2	1	1	1
10	2	1	2	3	1	2	3	1	2	3	1	2	3
11	2	1	2	3	2	3	1	2	3	1	2	3	1
12	2	1	2	3	3	1	2	3	1	2	3	1	2
13	2	2	3	1	1	2	3	2	3	1	3	1	2
14	2	2	3	1	2	3	1	3	1	2	1	2	3
15	2	2	3	1	3	1	2	1	2	3	2	3	1
16	2	3	1	2	1	2	3	3	1	2	2	3	1
17	2	3	1	2	2	3	1	1	2	3	3	1	2
18	2	3	1	2	3	1	2	2	3	1	1	2	3
19	3	1	3	2	1	3	2	1	3	2	1	3	2
20	3	1	3	2	2	1	3	2	1	3	2	1	3
21	3	1	3	2	3	2	1	3	2	1	3	2	1
22	3	2	1	3	1	3	2	2	1	3	3	2	1
23	3	2	1	3	2	1	3	3	2	1	1	3	2
24	3	2	1	3	3	2	1	1	3	2	2	1	3
25	3	3	2	1	1	3	2	3	2	1	2	1	3
26	3	3	2	1	2	1	3	1	3	2	3	2	1
27	3	3	2	1	3	2	1	2	1	3	1	3	2

3.1.4 Factors and Levels Identification

As discussed in Chapter 2, there were four major factors that affect the result of laser gas nitriding. The four factors are listed as follow:

i) Output power

ii) Scanning speed

iii) Beam diameter

iv) Nitrogen flow rate

Each factor had three levels. By referencing from other research (Chan & Man, 2011), L-27 Taguchi experiment is efficient and suitable for the analysis of four factors with three levels setup. Larger orthogonal array such as L-54 orthogonal array may not be suitable for this analysis. This is because there would be no confusion between on factor and two-factor interactions when the design of resolution is too high. In addition, large orthogonal array would increase the difficulty for no matter the experiment logistic but also the further analysis of Taguchi experiment. The factor levels of the L-27 Taguchi experiments are presented in Table 3.3.

Table 3.3 – Factor levels of L-27 Taguchi experiment

Material	**Shape memory NiTi of 2mm in thickness**		
Factor	1	2	3
A. Output power	70W	80W	90W
B. Scanning speed	300mm/min	600mm/min	900mm/min
C. Beam diameter	0.4mm	0.5mm	0.6mm
D. Nitrogen flow rate	10L/min	15L/min	20L/min

For L-27 factorial design, 108 trial experiments are required to be conducted. When Taguchi method is applied, there are only totally 27 trial experiments that are required for analysis. The experiment time could be greatly reduced. In addition, Taguchi method could help to randomize all the levels of factor to have equal chance of being affected by the noise factors. Because of these two reasons, Taguchi method was applied in this project.

3.1.5 Signal-to-noise Ratio Consideration

As discussed in Chapter 2, there were three signal-to-noise ratio formula which are commonly used. In this project, larger-the-better signal to noise ratio was applied in order to maximize surface hardness after laser gas nitriding. The formulae for larger-the-better signal to noise ratio is as below:

$$S/N_{LB} = -10\log_{10}\left[\frac{1}{n}\sum_{i=1}^{n}\left(\frac{1}{Y_i^2}\right)\right] \qquad (3.2)$$

S/N_{LB} : Signal-to-noise ratio

Y_i^2 : Mean of responses

n: Number of replications

3.1.6 ANOM and ANOVA Analysis

Analysis of mean (ANOM) and analysis of variance (ANOVA) were employed in this project. ANOM was conducted for examine the best level in each factor that would bring to the most desirable result. It is also possible for ANOM to rank the importance of each factor. In this project, L-27 orthogonal array was applied for analysis. Each three-level factor would give a result in three averages of signal-to-noise ratio. They are m_1, m_2 and m_3. The best level would be the factor at the level with highest mean signal-to-noise ratio. During ANOVA analysis, the total variance of signal-to-noise ratio was separated into values in terms of contribution. The variance would therefore associate with a factor or an interaction. This variance was then being compared with the mean variance from estimated error. The factor or interaction was said to be significant when the associated variance was larger than the estimated error. The quantities which are important for ANOVA analysis could be computed by using the following equations:

DOF = (number of factors / interactions) x (number of levels – 1)

$$\mathrm{S} = \sum(y_i - \bar{y})^2 \tag{3.3}$$

$$\mathrm{V} = \frac{S}{DOF} \tag{3.4}$$

$$\mathrm{F} = \frac{V}{V_{error}} \tag{3.5}$$

$$\mathrm{S}' = \mathrm{S} - (DOF)(V) \tag{3.6}$$

$$\mathrm{P} = \frac{S\prime}{S_{total}} \tag{3.7}$$

DOF: degree of freedom

S: sums of squares

V: variance

F: F-ratio

S’: pure sum of squares

P: percent influence

Pooling is common practice in ANOVA analysis. It is important for revising and re-estimating the ANOVA results (Roy, 2001). A factor or an interaction was pooled when it fails the test of significance.

3.2 Laser Gas Nitriding

After Taguchi analysis, the optimum parameter for laser gas nitriding in order to obtain the highest surface hardness could be obtained. This set of optimum parameters would be used through the experiment.

The laser system used in this project was 100W continuous wave fibre laser (SP-100C-0013) with output wave length of 1091nm. The system includes a laser head, power electronics modules, computer control and cooling system. The laser beam is transmitted by doped fibre. The laser head consisted of a BK-7 re-collimating lens. A red spot from a He-Ne laser was used to indicate the location of the laser beam on the specimen. Scanning movement of specimens was controlled by a 3 axis CNC table. A computer control system was connected to control the movement of the table. Figure 3.2 presents the method of beam spreading of the fibre laser used in this project.

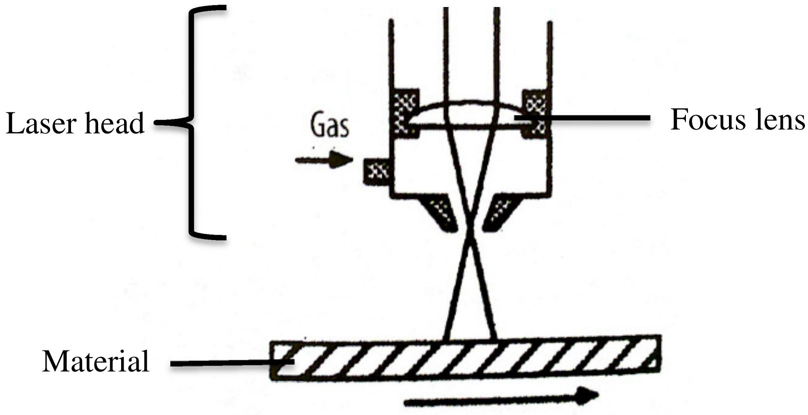

Figure 3.2 – Schematic diagram of focusing lens of fibre laser

Laser emission was first transmitted by the optic fibre and then focus by the focus lens. In some cases, there is another protective lens located under the focus lens to further protect the focus lens from reflection of laser emission on the sample surface. It is possible that laser emission could be reflected from the sample surface and damages the focus lens. The protective lens is coated with specially designed material. This material works like a photo filter to prevent light from entering back to the laser head. The protective lens allows single direction pathway of laser emission. During laser surface processing, smoke consists of small particles of the treating material may be generated due to high energy absorbed. These small particles may diffuse in the atmosphere and enter the laser head. Some of the particles may adhere to the lens of laser. This kind of adhesive material may lead to serious damage to the laser lens. If there are adhesive materials on the lens, they absorb much energy form laser emission during operation. Absorbed energy could be converted as heat energy which may burn up the coating on the lens as well as the lens itself. Damage lens could not allow laser emission to pass out successfully during operation. Figure 3.3 shows the photo of a damaged protective laser lens. It is clearly shown that there is a serious broken point at the center of the lens. This damage may be caused by the adhesive materials on the lens.

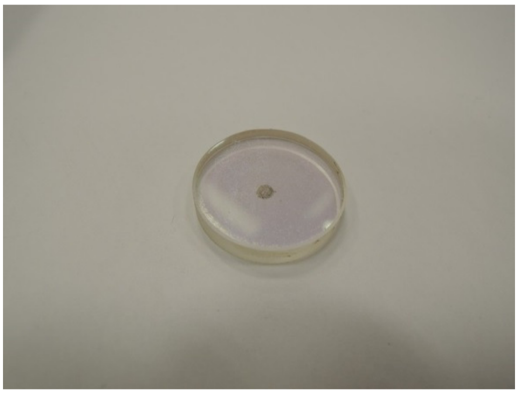

Figure 3.3 – Broken protective laser lens

In order to prevent small particles from entering the laser head, gas is blown as in Figure 3.2 to create a gas flow down to the treating material surface. This could help to reduce the change of small particles from entering the laser head.

For laser gas nitriding, nitrogen gas is one major component for the process. Figure 3.4 illustrated the operation set up for laser gas nitriding in this project.

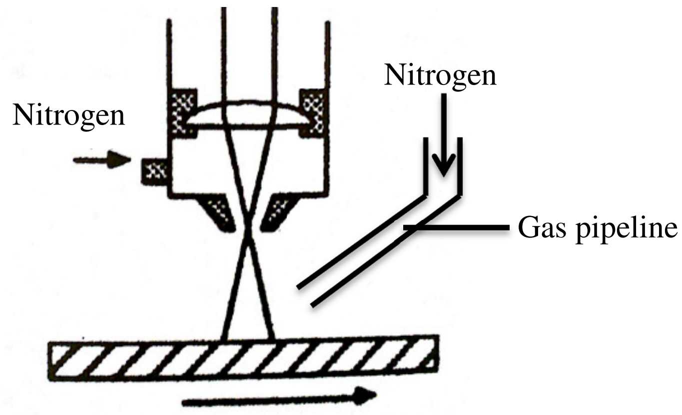

Figure 3.4 – Schematic diagram for set up of laser gas nitriding

Nitrogen gas was pumped into the laser head and a gas pipeline. The gas pipeline could deliver nitrogen gas to the site of laser gas nitriding on the sample. This could improve the efficiency of laser gas nitriding. Sufficient amount of nitrogen gas could be supplied for laser gas nitriding. In addition, nitrogen blowing could help to reduce the amount of oxygen surrounding the nitriding site during the process. A special designed nozzle was located at the end of the gas pipeline near the nitriding site. The nozzle could help to covert the blowing mode of the ejected nitrogen gas on the sample surface in order to obtain a better result of laser gas nitriding. The nitrogen gas blew the small particles vaporized form the material and prevented oxidation during laser gas nitriding. The whole set up was surrounded by a plastic box so that nitrogen gas could be trapped in the box for a longer period of time for laser gas nitriding. One important criterion for successful laser gas nitriding is the sufficient surrounding of nitrogen gas at the site of laser gas nitriding. If there is not sufficient nitrogen gas at the site, laser gas nitriding could not perform well. Instead of TiN, oxides will form on material surface during laser processing.

The movement of samples was controlled by CNC table. The minimum movement of the CNC table could reach 0.0001 mm. Therefore, adjustment of the focal length between the laser head and the sample could be done precisely. This is important for the adjustment of beam diameter for laser gas nitriding.

Cooling system is necessary for a laser processing operation system. High energy generated from laser system could result in rapid temperature increasing during laser gas nitriding process. If there is overheat of laser system, the feedback safety control within the laser system would start automatically. This safety control will lock the laser system to prevent further laser emission. Laser gas nitriding could be directly affected if the laser emission is suddenly locked during processing. Therefore, the cooling system held an important role during laser gas nitriding. The experimental apparatus involved for laser gas nitriding are presented in Figure 3.5i to 3.5iv.

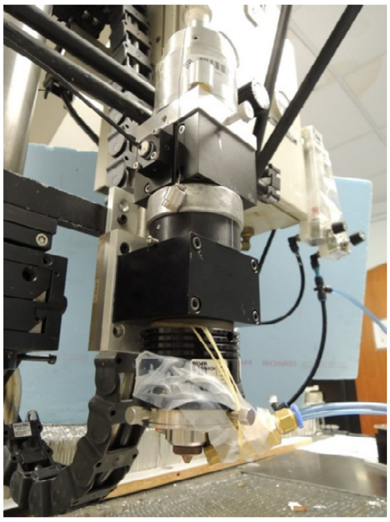

Figure 3.5i – Laser head with gas pipeline attached

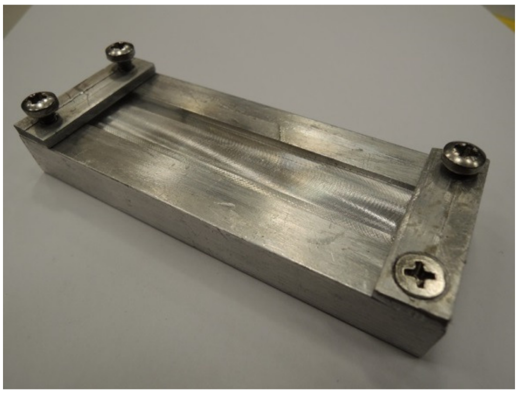

Figure 3.5ii – Specially designed clamp

Figure 3.5iii – CNC table control system

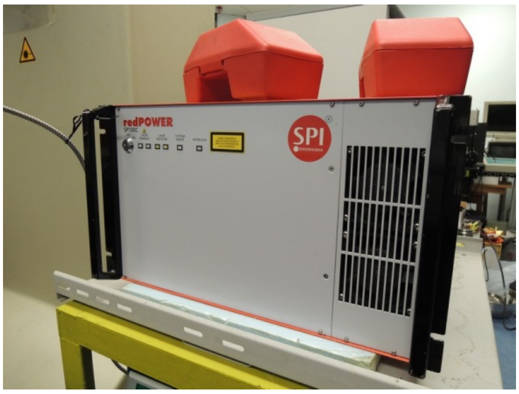

Figure 3.5iv – Fibre laser system

3.3 Tensile Test

3.3.1 Preparation of I Shaped Beams

Tensile test was conducted to investigate the effects of laser gas nitriding on the tensile stiffness of NiTi. I shaped beams of NiTi were prepared by wire cutting. The dimension of I shaped beams were also referred to ASTM E8 standard. The dimensions of I shaped beams is illustrated in Figure 3.6.

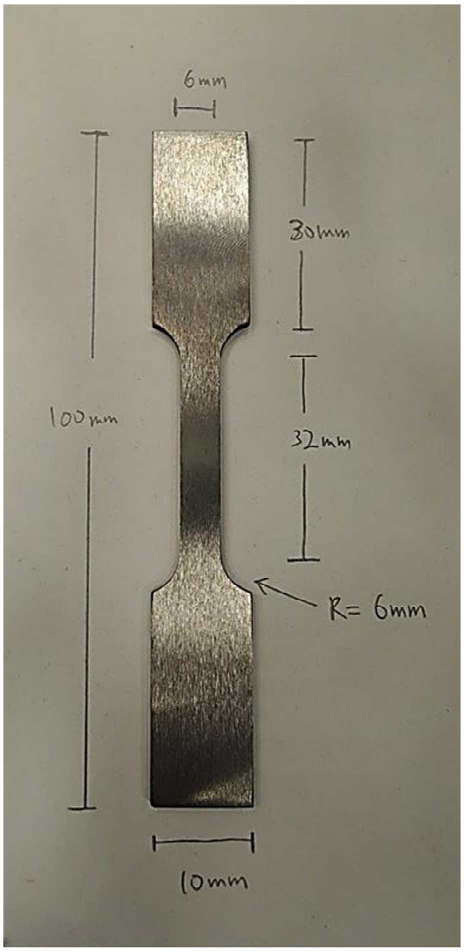

Figure 3.6 – Dimensions of I shaped beams

After wire cutting, the I shaped beams were polished by SiC paper gradually until 2400 grits. All the beams were cleaned by detergent. After that they were degreased with alcohol for 5 minutes under ultrasonic, rinsed by distilled water and air dried in room temperature.

3.3.2 Laser Gas Nitriding with Varying Percentage Coverage of TiN on NiTi

Laser gas nitriding was conducted on the I shaped beams. The parameters for laser gas nitriding were according to the optimum parameter set computed from L-27 Taguchi analysis. The aim for this test is to investigate how the percentage coverage of TiN on sample surface would affect the tensile stiffness of NiTi. Laser gas nitriding was conducted on I shaped beams to fabricate various percentage coverage of TiN on NiTi surface within the gage region. Table 3.4 presents the coverage of TiN on I shaped beams. Figure 3.7 illustrated the morphologies of the laser treated I shaped beams.

Table 3.4 – Percentage coverage of TiN on I shaped beams

Sample	**A0 (untreated NiTi)**	**A1**	**A2**	**A3**
Percentage coverage of TiN	0%	20%	40%	60%

Figure 3.7 – Morphologies of laser treated I shaped beams

(90W, 300mm/min, 0.4mm, 20L/min)

In a preliminary study of tensile test, longitudinal and transverse laser nitrided tracks were fabricated on I shaped beams. However, it was found that some of the samples had the broken site exactly on the transverse track of the transverse track on the sample as presented in Figure 3.8. ‘A’ represents one longitudinal laser track while ‘B’ represents the transverse laser track. ‘C’ shows the broken site of the sample. This phenomenon may show that the transverse tracks could create cracks on the samples. In addition, they me lead to fatigue during tensile test. The fatigue may influence the result of tensile test as well as the accuracy of measuring the tensile stiffess of samples. Therefore, only longitudinal tracks were fabricated on the I shaped beams.

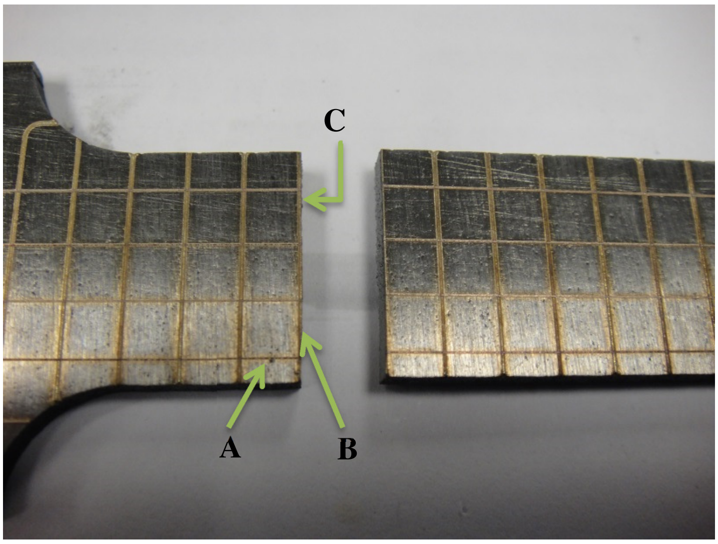

Figure 3.8i – Broken site at transverse track on sample

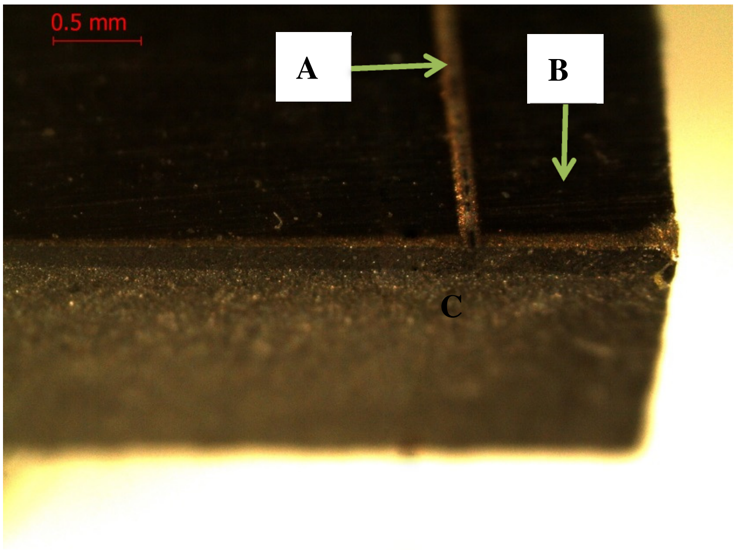

Figure 3.8ii – Broken site at tranverse track with higher magnification

In order to balance the force acted on the sample during tensile test, laser gas nitriding was conducted on both sides of I shaped beams. The percentage coverage of laser nitrided region was the same on both sides. However, laser gas nitriding on such thin material may cause deformation of sample pieces. Deformation was due to heating during nitriding. Therefore, a specially designed clamp was applied to fix the I shaped beam during nitriding. The clamp was also important to prevent the I shaped beam from moving during laser gas nitriding. If the sample moves during treatment, laser tracks with unexpected pattern would form as shown in Figure 3.9.

Figure 3.9 – Unexpected pattern formed when no clamp was used

3.3.3 Tensile Test of I shaped beams

Static tensile tests were conducted using Material Test System (MTS 810) at room temperature. They were at low-strain rates with a cross-head displacement velocity of 0.15 mm/min. Three replicate samples were used for each parameter of sample.

3.4 Corrosion Behavior Analysis

Due to the unique shape memory, super-elasticity, high resistance to fatigue, NiTi alloys become one important material in engineering, especially for medical application (Duerig et al., 1999). NiTi has good corrosion resistance, mainly due to the presence of a thin passive film which consists of titanium oxide. However, previous report showed that breakdown of the passive film may occur and recovering process is relative slow (Rondelli, 1996).

Many researchers have also proved that surface nitriding of titanium alloys could improve their corrosion resistance effectively (Gorji & Sanjabi, 2012; Man et al., 2003). One important advantage of laser gas nitriding is that a metallurgical bond between nitride and NiTi substrate could be created. Many studies have reported the corrosion behavior of nitride layer on NiTi substrate (Starosvetsky & Gotman, 2001; Kumar & Kaur, 2009).

This part of analysis investigates the feasibility of applying laser gas nitriding technique to improve the corrosion resistance of NiTi in simulated body fluid. A continuous wave fibre laser was used to perform laser gas nitriding process under a pure nitrogen environment on the substrate of commercial NiTi plates. A reinforcement network grid of titanium nitride (TiN) tracks with various densities produced by laser gas nitriding will be fabricated on the alloy surface. The TiN network grid is metallurgically integrated into the TiN alloy matrix at the surface. It is postulated that by varying the TiN grid density the corrosion resistance could be improved to the level similar to the material with the whole surface treated by laser gas nitriding. Compared with laser gas nitriding of whole surface of material, it is believed that surface grid reinforced MMC would have lower production cost and processing time. Corrosion behavior of NiTi and the treated samples was investigated by electrochemical polarization conducted in 0.9% (by weight) sodium chloride solution.

3.4.1 Sample Preparation

NiTi plates with dimensions of 10mm X 10mm X 2mm were prepared by wire cutting machine. The plates were then treated by laser gas nitriding with the optimum parameter set obtained from Taguchi analysis. Different percentage coverage of TiN was fabricated on the plates according to Table 3.5. The morphologies of samples are shown in Figure 3.10.

Table 3.5 – Percentage coverage of TiN on each sample

Sample	H0 (untreated sample)	H1	H2	H3	H4
Percentage coverage of TiN	0%	27.5%	47.5%	76.3%	100%

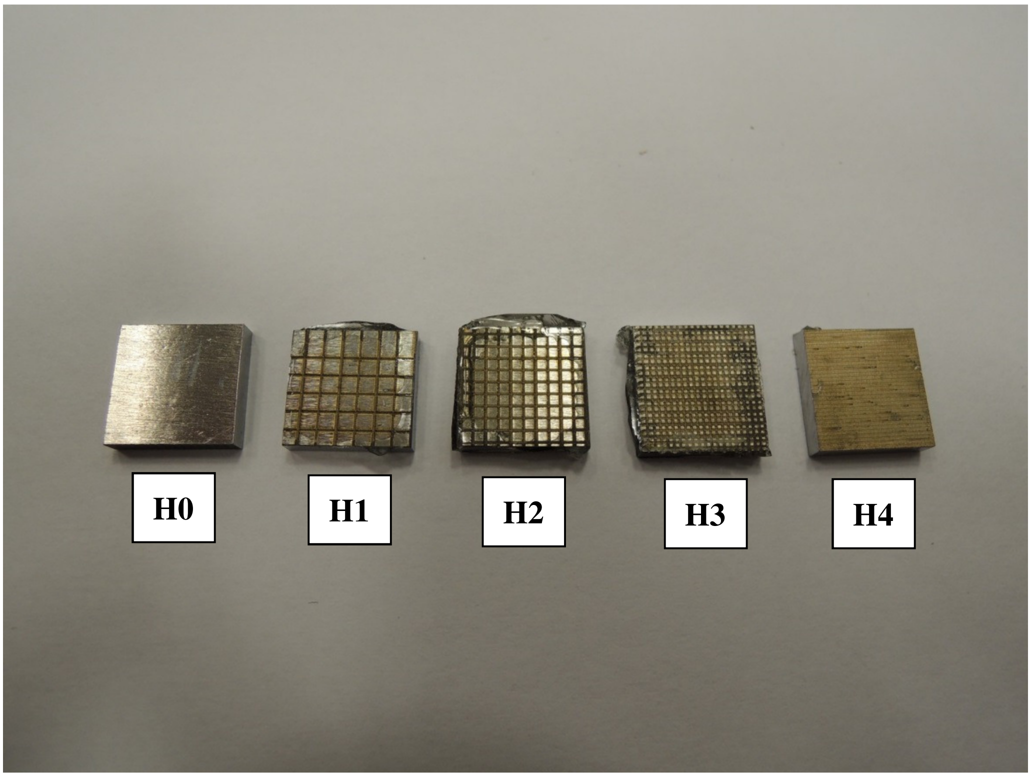

Figure 3.10 – Samples prepared for potentiodynamic polarization measurement

(90W, 300mm/min, 0.4mm, 20L/min)

The samples were slightly ground by SiC papers to guarantee consistent surface roughness. All the samples were ultrasonically cleaned by alcohol for 5 minutes. They were then rinsed by distilled water and dried thoroughly by cool blowing before measurement.

3.4.2 Potentiodynamic Polarization

The corrosion resistant properties were evaluated by potentiodynamic polarization measurements (EG & G Princeton Applied Research, model 273A) with a standard three electrode system in 0.9% (by weight) NaCl solution under a temperature of 37°C ± 1°C. Samples for corrosion study were mounted in epoxy and exposed a surface area of 1cm^2. Graphite rods were used as counter electrodes. The reference electrode was SCE. All samples were immersed in the electrolyte for 1 hour before starting the measurement in order to achieve equilibrium in the solution at open-circuit potential. The scanning rate was 2mV/s. By TAFEL lines extrapolation method, corrosion current density could be computed by the software of potentiostat. Figure 3.11 shows the schematic diagram of a glass cell used for polarization measurement in the study. It is conformed to ASTM Standard G5-94.

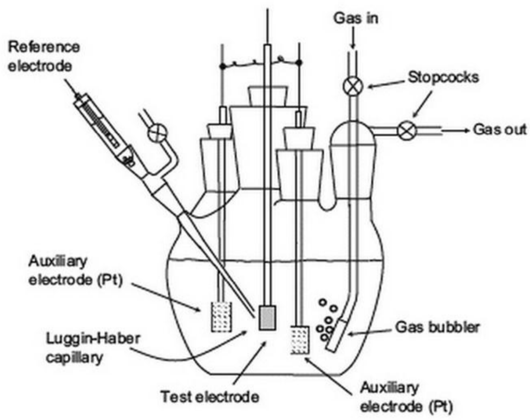

Figure 3.11 – Schematic diagram of a standard three electrode system (Mccafferty, 2010)

3.4.3 Electrochemical Impedance Spectroscopy Measurement

Electrochemical impedance spectroscopy (EIS) measurement was employed to study the change in passive film during immersion in 0.9%w.t. sodium chloride solution. The whole setup for EIS was maintained in the temperature of 37°C ± 1°C under water bath. The EIS results were illustrated in Bode plots. A fully nitrided sample was tested. EIS measurement was conducted with a frequency response detector installed in the potentiostat (EG & G Princeton Applied Research, model 273A). A sine wave with amplitude of 10mV was applied during the experiment and the impedance spectra at one hour with immersion in 0.9% w.t. sodium chloride solution at 37°C ± 1°C were obtained in the frequency ranging from 100 kHz to 1 mHz.

3.5 Analysis Concerning Surface Hardness to Parameters of Laser Gas Nitriding

An analysis was conducted to relate the influence of different parameter of laser gas nitriding to the resulting surface hardness. Laser gas nitriding was conducted according to the parameter setting listed in Table 3.6. Laser tracks were fabricated on each sample by 50% overlapping in order to create a larger area of TiN for investigation.

Table 3.6 – Parameter sets for analyzing their influence to surface hardness

Sample	Output power	Scanning speed	Beam diameter	Nitrogen flow rate
L0	N/A	N/A	N/A	N/A
L1	90W	300mm/min	0.4mm	20L/min
L2	90W	600mm/min	0.4mm	20L/min
L3	90W	900mm/min	0.4mm	20L/min
L4	90W	300mm/min	0.5mm	20L/min
L5	90W	300mm/min	0.6mm	20L/min
L6	70W	300mm/min	0.4mm	20L/min
L7	80W	300mm/min	0.4mm	20L/min

The resulting surface hardness of sample after laser gas nitriding using the parameters listed in Table 3.6 would be measured by Vickers hardness test. The surface hardness would be then related to the laser parameter of samples. Surface hardness was conducted by using Vickers hardness test using Mitutoyo Hardness Testing Machine

Microwizard. A loading force of 200g was applied with loading time of 8 seconds.

X-ray diffraction (XRD) would be used for examining the content of laser tracks. In addition, the peak intensity obtained from XRD spectrum is believed to be able to evaluate the relative amount of material in the track. X-ray diffraction was conducted by using Rigaku SmartLab at 45kV and 200mA at a rate of 1°/min. The scanning start angle and end angle was 30° and 100° respectively.

3.6 Wear Resistance Analysis

The wear resistance of samples after laser gas nitriding with network reinforcement of TiN was investigated by using linearly reciprocating ball-on-slab sliding wear test. The results of wear resistance of the laser treated samples were then being compared with the untreated sample.

The samples were prepared by laser gas nitriding by using the optimum set of parameter obtained in Taguchi analysis (Table 3.7). NiTi plate with thickness of 6mm was wire cut into samples with dimension of 15mm X 20mm. Laser tracks were fabricated on the NiTi substrate forming longitudinal and transverse pattern. TiN network was formed. The width of the laser track was 0.24mm. The percentage coverage of TiN on samples was described in Table 3.8.

Table 3.7 – Laser parameters of samples for wear test

Parameter for laser gas nitriding	**Output power**	**Scanning speed**	**Beam diameter**	**Nitrogen flow rate**
	90W	300mm/min	0.4mm	20L/min

Table 3.8 – Percentage coverage of TiN of samples for wear test

Sample	W0 (untreated sample)	W1	W2	W3	W4 (fully scanned)
Percentage coverage of TiN	0%	27.5%	47.5%	76.3%	100%
Size of TiN grid (mm^2)	N/A	5.0176	1.5376	0.5476	N/A
Size of untreated groove within the grid (mm^2)	N/A	3.0976	0.5776	0.0676	N/A

The apparatus used for measurement of wear resistance in this experiment would be Phoenix Tribology TE99 Universe Wear Machine as shown in Figure 3.12. The test was designed and conformed to ASTM-G133 standard.

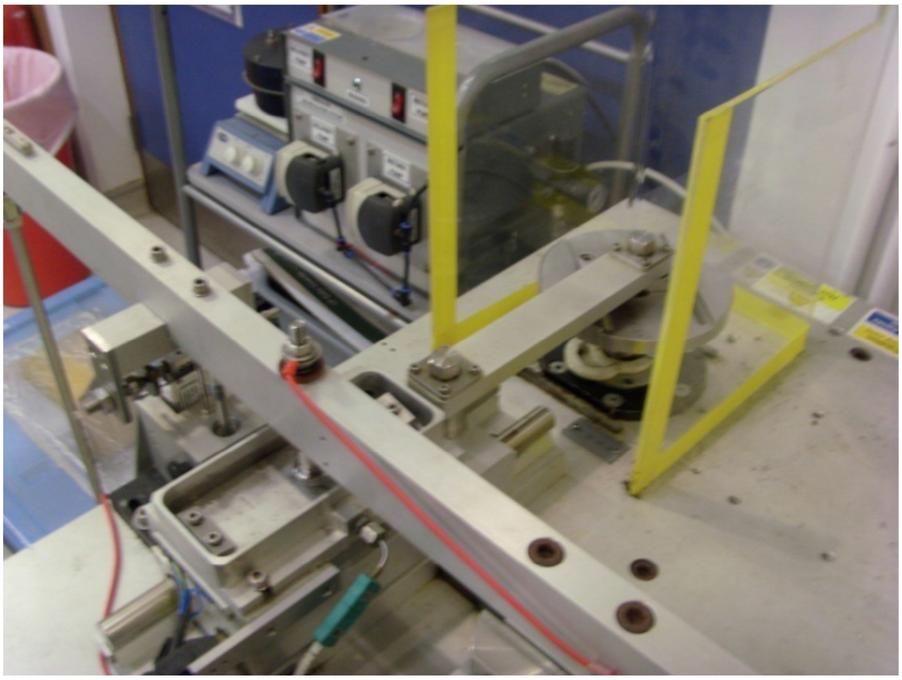

Figure 3.12 – Apparatus applied for wear resistance measurement

By a linear and reciprocating ball-on-flat plan geometry, the ball-on-slab test could be able to determine the sliding wear of samples. The direction of the motion between the surfaces involved in the experiment reverses in a periodic pattern. A ball used for measurement moved back and forth within a straight line. The major quantities of this experiment were the wear volumes of the countered ball and the flat sample surface. The frequency was set to be 1Hz while the testing time was 600s. Stroke length was 10mm. A load of 0.5kg was applied. A stainless steel ball with diameter of 6.33 mm was used during the test. Figure 3.13 illustrates the mechanism of ball-on-slab test in this experiment.

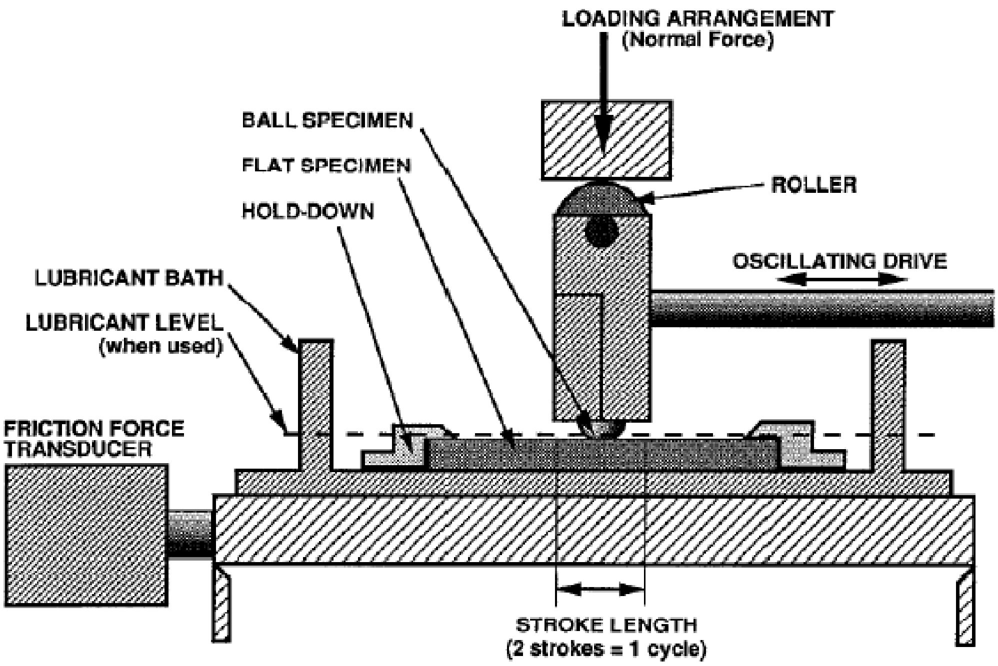

Figure 3.13 – Schematic diagram of ball-on-slab wear resistance measurement apparatus

The stroke length was long enough to cover several laser tracks on the sample surface as well as the untreated grooves. In addition, the testing site was chosen so that the ball could contact both the laser tracks and the untreated grooves alternatively during the wearing movement. Therefore, the result of the wear test could be representable. Average volume loss of sample surface was measured as indicator for wear resistance. Measurement with equally spacing along the wearing track on the sample surface was measured. According to standard, if the volume loss due to wearing of three initial profiles had 25% or lower difference between each other, those profiles were accepted for taking average. When it was larger than 25%, six cross sectional profiles would be measured for evaluating the average volume loss.

The surface profile of sample was measured by Taylor-Hobson Form Talysurf Series 2 in this experiment. A sharp tip was installed in this apparatus. During measurement, the sharp tip moved across the wearing track. The upward and downward movement of tip was detected and recorded by a sensor. Such movement could be then transferred to be the cross sectional profile of wearing track. Figure 3.14i and ii shows the apparatus and the tip used for measurement respectively.

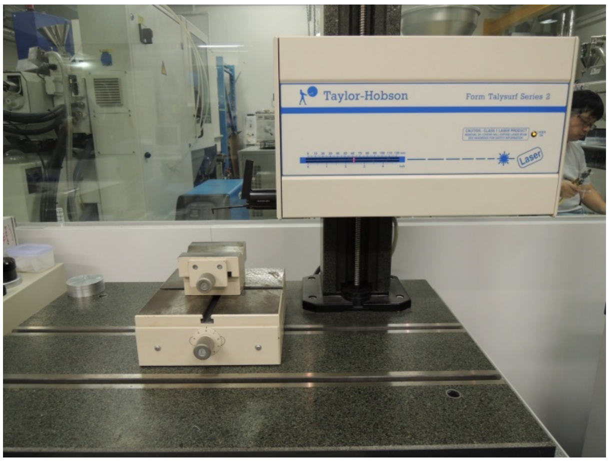

Figure 3.14i –Taylor-Hobson Form Talysurf Series 2

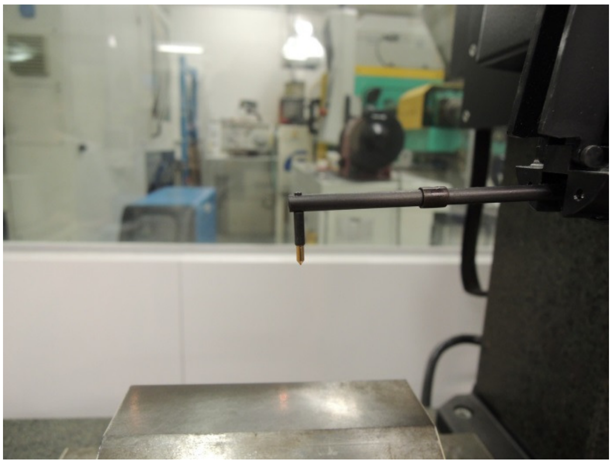

Figure 3.14ii – Tip for measurement

3.7 Nano-indentation Hardness Analysis

Nano-indentation hardness analysis was conducted using diamond Berkovich indenter. The analysis is suitable to determine the mechanical properties of thin film. This is because the indentation depth for nano-indentation test is much smaller than that in conventional indentation hardness test, and so substrate effect can be significantly reduced.

Hardness H_N and reduced Young's modulus E_r were determined from load-displacement curves from the nano-indentation hardness analysis. The loading segment to peak load and the unloading segment is each 17 s. The holding segment at peak load is 3 s.

Chapter 4 Results and Discussions

4.1 Characterization of the TiN Layer Formed

Laser gas nitriding was conducted by 100W continuous wave fibre laser (SP-100C-0013) with output wave length of 1091nm. X-ray diffraction analysis was conducted to examine the presence of TiN layer on the laser treated samples. This measurement is important to prove the successful fabrication of TiN layer on NiTi substrate by using the current methodology.

Two samples were prepared for the analysis. The first sample was an untreated sample, which means that no laser processing was conducted on that sample. The other sample was treated by laser using output power of 90 W, scanning speed of 300 mm/min, nitrogen flow rate of 20 L/min and beam diameter of 0.4 mm. All the samples were cleaned thoroughly by alcohol ultrasonically for 10 minutes for degreasing before the test. For convenience, laser tracks were fabricated on the whole sample with 50% overlapping for easier investigation. Figure 4.1 shows the morphology of both samples. For the laser treated sample, a golden hard layer was formed on the sample surface. Laser treatment only affected the surface of bulk NiTi plate.

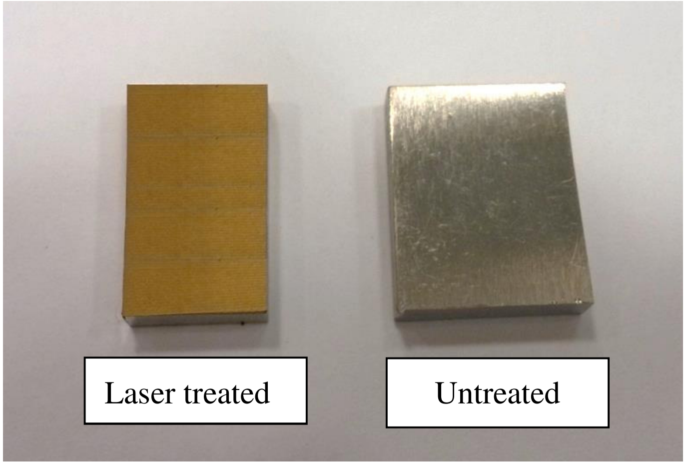

Figure 4.1 – Samples for XRD analysis

(left: 90W, 300mm/min, 0.4mm, 20L/min; right: untreated NiTi)

Both samples were under X-ray diffraction analysis and their spectrums are illustrated in Figure 4.2. The X-ray diffraction scanning was set to fit this analysis. Only the surface layer of the sample would be scanned. Therefore, the result for the analysis would only focus on the surface layer of the sample.

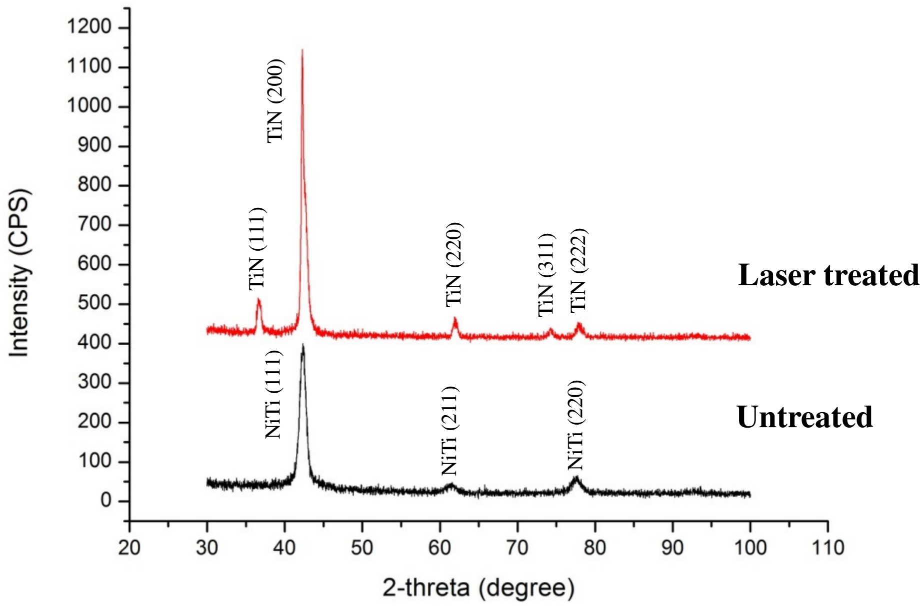

Figure 4.2 – XRD spectrum for the surface layer of samples

As observed, the XRD spectrums for laser treated and untreated samples are different from each other. This illustrates that the surface layers of the samples are composed of different materials. Peaks pertaining to TiN can be identified on the treated sample. While for the untreated sample, only peaks of austenitic NiTi can be identified. Together with the golden appearance of the laser treated sample as compared with the silvery appearance of untreated NiTi, the XRD patterns indicate that the treated sample consists a layer of TiN on the sample surface, while there is no TiN on the untreated sample.

The cross-sectional morphology of the TiN layer was by the SEM image in Figure 4.3.

A continuous thin surface layer of TiN was formed on the surface of the sample with thickness between 10 µm and 20 µm. A discrete dendritic phase could also be observed below the sample surface in the melted zone of laser nitriding. The dendritic structures become smaller gradually from the sample surface towards to the interior.

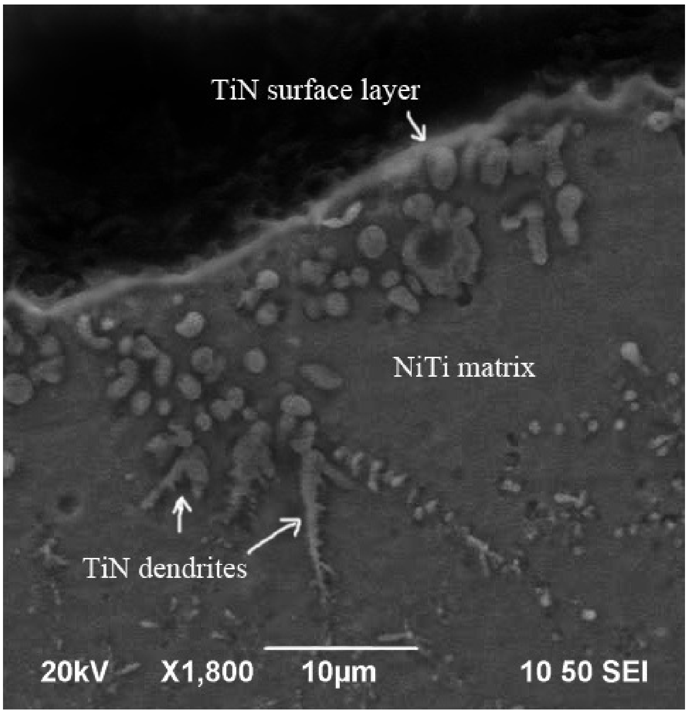

Figure 4.3 – Microstructure of the cross-section of laser gas nitrided NiTi sample (90W, 300mm/min, 0.4mm, 20L/min)

Figure 4.4 shows the dendritic phase with a larger magnification. EDX analysis was conducted in order to identify of the dendritic phase. The site of testing was on the dendritic structure. EDX results, which presents in Figure 4.5, show that the testing area contains elements included titanium, nickel and nitrogen and the dendritic phase is believed to be TiN, while Ni could be coming from NiTi, which was also probed by

EDX.

During laser gas nitriding, Ti from the alloy was consumed for formation of TiN in a nitrogen atmosphere. Such TiN appears as a continuous layer on the surface due to the richness of nitrogen there, and also as dendrites below the surface layer. Ni may be vaporized during laser treatment. This is due to the lower melting point (1453°C) of Ni than Ti (1720°C) (Man and Zhao 2006). Condensed Ni may then combine with Ti which remained in the melt pool to form NiTi again. In agreement with previous research and the result of EDX mapping shown in Figure 4.6, it is possible to retain NiTi phase in the laser gas nitrided layer.

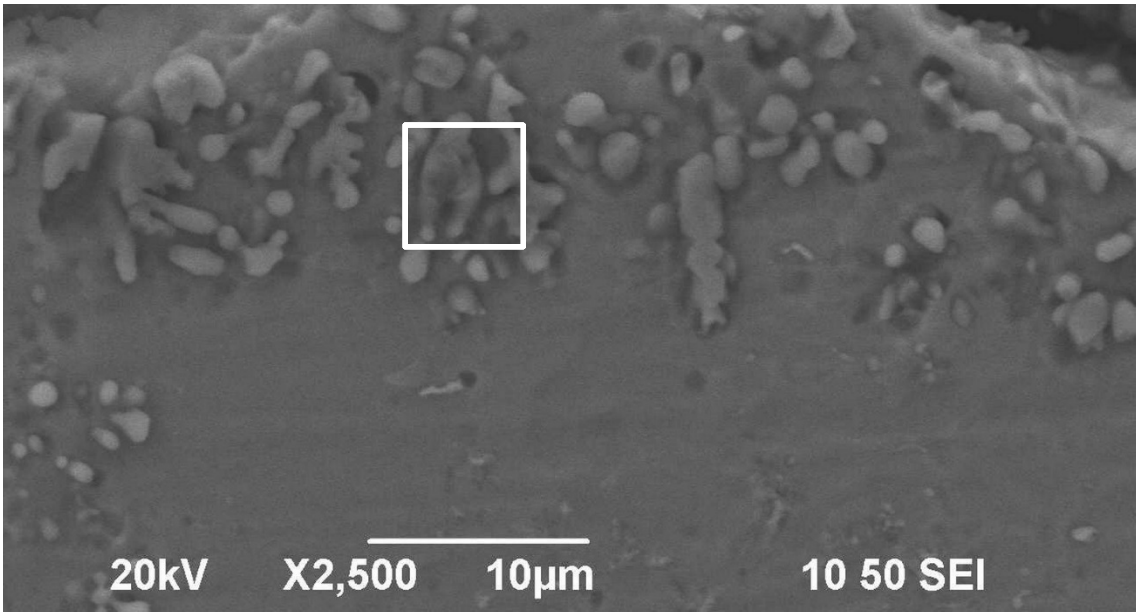

Figure 4.4 – Site of EDX analysis for the dendritic structure (marked in square)
(90W, 300mm/min, 0.4mm, 20L/min)

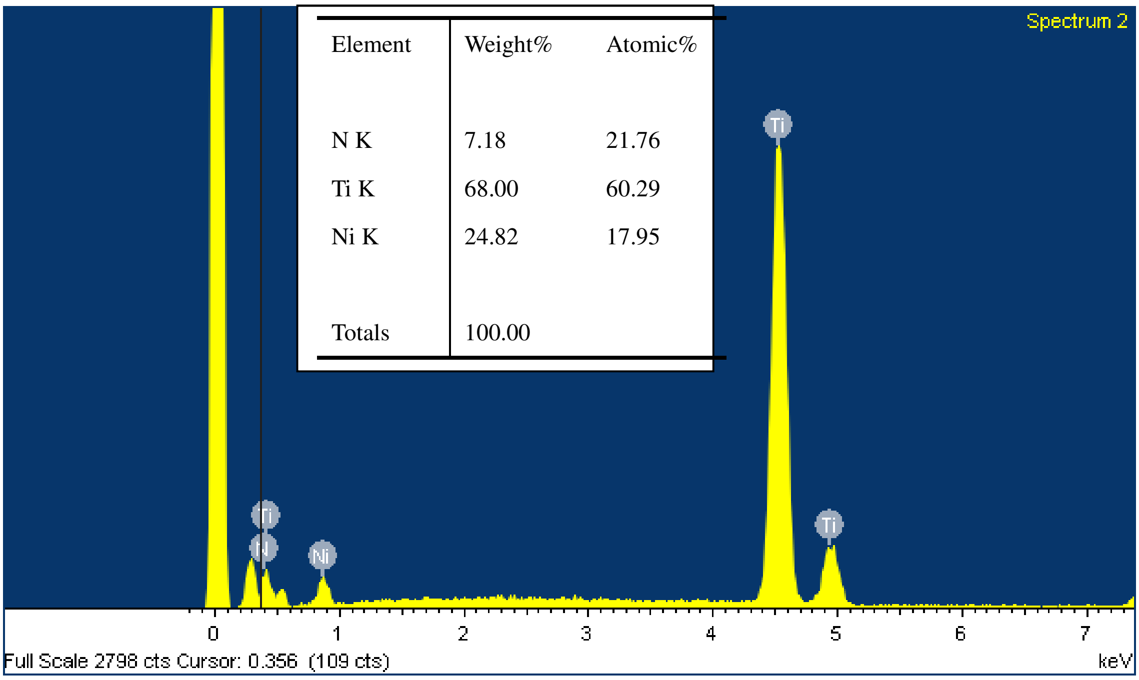

Element	Weight%	Atomic%
N K	7.18	21.76
Ti K	68.00	60.29
Ni K	24.82	17.95
Totals	100.00	

Figure 4.5 – Testing results of EDX analysis for the dendritic structure

EDX mapping was also conducted to further investigate the components on the sample. Spots were marked on the site when the relevant element was present as presented in Figure 4.6a to 4.6d. The more the spots, the higher the concentration for that particular element presence.

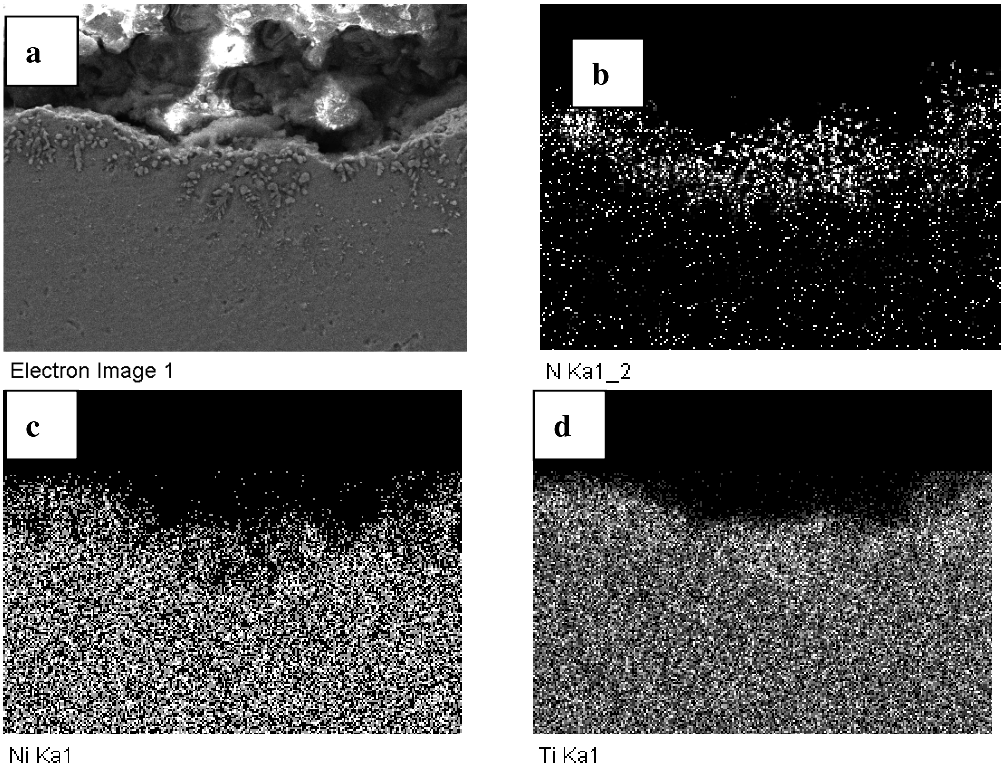

Figure 4.6 – EDX mapping a) SEM image; b) Nitrogen; c) Nickel; d) Titanium

(90W, 300mm/min, 0.4mm, 20L/min)

The whole sample contains much titanium and nickel. As shown in 4.6b, nitrogen is present mainly on the outermost top layer of the sample. When looking down towards the inner site, the nitrogen content becomes lower. It is believed that laser gas nitriding could fabricate TiN on NiTi sample surface. The presence of nitrogen at the inner site of the sample could be related to the formation of solid solution after laser treatment. The formation of TiN on the sample surface reduces the nickel content on the outermost site as illustrated in 4.6c. Therefore, the surface layer of sample may contain mainly TiN.

4.2 Preliminary Study

The XRD and EDX results illustrated that TiN could be fabricated on NiTi by laser gas nitriding using fibre laser. A preliminary study concerning the change of output power and scanning speed to the resulting surface hardness was conducted. The other parameters include beam diameter and nitrogen flow rate were kept constant through the study. The parameters setting and the resulting surface hardness were recorded in Table 4.1. The results were converted into graphical format for easier analysis and are shown in Figure 4.7.

Table 4.1 – Change of output power and scanning speed to the resulting surface hardness after laser gas nitriding

Track	Output power (W)	Scanning speed (mm/min)	Average hardness (HV)
Plain	N/A	N/A	320.70
A	60	1200	371.06
B		900	478.32
C		600	538.65
D	70	1200	429.03
E		900	450.33
F		600	527.00
G	80	1200	434.77
H		900	479.85
I		600	556.57
J	90	1200	508.90
K		900	568.08
L		600	663.80

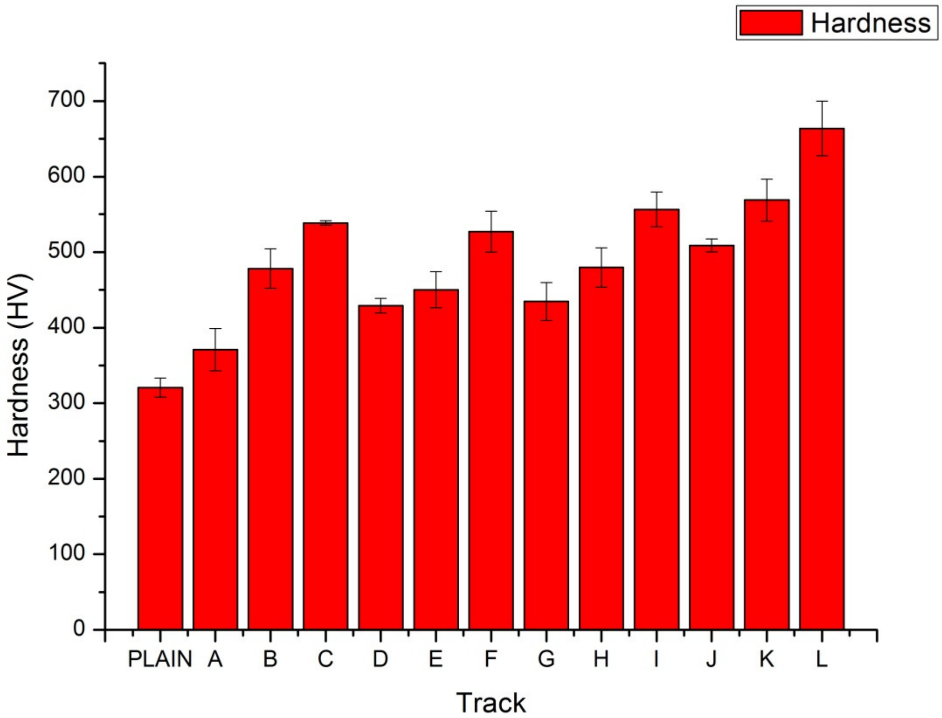

Figure 4.7 – Resulting hardness of various laser tracks

In the experiment, the beam diameter and nitrogen flow rate were kept constant. It is found that when output power increase, surface hardness increase. The surface hardness increases from about 371HV at 60W to 508HV at 90W when Track A and Track J are compared. There is more than 30% increase of surface hardness due to the increase of output power. When the scanning speed was at 900mm/min, there is no significant increase of surface hardness. This may conclude that increase of laser output power could increase the surface hardness. However, the influence of power may not be significant within the range of 60W to 90W.

Surface hardness also increases with the reduction of scanning speed. For example when Track G to I are investigated, the surface hardness increase gradually from 434HV to 556HV. The improvement of hardness is significant. This phenomenon could also been observed in other pairs of results. Scanning speed could be identified as an important factor that could greatly affect the surface hardness of NiTi. All the laser treated samples give a higher surface hardness than the sample without treatment. This may show that laser gas nitriding could help for improvement surface hardness of NiTi.

By looking at the preliminary results, it is found that the increase of output power could lead to the increase of surface hardness. When three levels for this factor were required to be selected, output power of 70W to 90W was selected for L-27 Taguchi analysis. No further increase of output power would be selected since this range has reached the maximum output power of the fibre laser used in this project. By investigating effect of varying scanning speed to the surface hardness, it is found that increase of scanning speed could bring to significant improvement of surface hardness on NiTi. Therefore, three levels with lower scanning speed were chosen for L-27 Taguchi analysis. Laser gas nitriding was carried for scanning speed lower than 300mm/min. It was expected that the surface hardness could be even higher. However, particles may evaporate and attach on the laser lens during laser operation. These particles will absorb large amount of laser energy and cause overheat of the lens. When scanning speed was lower than 300mm/min, the whole scanning process would be longer. Thus, there will be higher chance for damaging the lens due to overheating. Under this consideration, scanning speed lower than 300mm/min would not be used. Scanning speed ranging from 300mm/min to 900mm/min was selected for L-27 Taguchi analysis.

4.3 Taguchi Analysis

4.3.1 Signal-to-noise Ratio

A set of trial experiments for Taguchi analysis had been conducted. Laser gas nitriding was conducted on NiTi plates. The surface hardness after laser treatment of each sample was collected and then converted to larger-the-better signal-to-noise ratio in order to minimizing the variability of response. Table 4.2 summarizes the result of the trial experiments for Taguchi analysis. The morphology of each sample is shown in Figure 4.8 (i) to (xxvii).

Figure 4.8 showed the cross sectional morphologies of laser tracks after laser gas nitriding with varying laser parameters. Nitride layer is formed on the surface. The treated area shows different microstructure compared with the untreated area. Small grains form at the fusion zone. The grain size increases toward to the boundary of the heat affect zone. The heat affected area increases with the increase of laser output power. Vickers microhardness test was conducted on each sample. The mean surface hardness is 537 HV. Compared with the hardness of NiTi, which is about 330 HV, there is improvement of surface hardness after laser gas nitriding.

Table 4.2 – Surface hardness and the corresponding S/N ratio of L-27 Taguchi experiment

Trial	A (W)	B (mm/min)	C (mm)	D (L/min)	Surface hardness (HV)	S/N ratio (Larger-The-Better)
1	70	300	0.4	10	740.60	57.39
2	70	300	0.5	20	597.20	55.52
3	70	300	0.6	15	576.00	55.21
4	70	600	0.4	20	572.30	55.15
5	70	600	0.5	15	517.10	54.27
6	70	600	0.6	10	362.10	51.18
7	70	900	0.4	15	525.70	54.41
8	70	900	0.5	10	530.30	54.49
9	70	900	0.6	20	419.00	52.44
10	80	300	0.4	20	656.40	56.34
11	80	300	0.5	15	585.90	55.36
12	80	300	0.6	10	511.40	54.18
13	80	600	0.4	15	559.10	54.95
14	80	600	0.5	10	502.30	54.02
15	80	600	0.6	20	521.00	54.34
16	80	900	0.4	10	543.05	54.70
17	80	900	0.5	20	527.58	54.45
18	80	900	0.6	15	342.40	50.69
19	90	300	0.4	15	488.37	53.78
20	90	300	0.5	10	514.04	54.22
21	90	300	0.6	20	634.16	56.04
22	90	600	0.4	10	565.70	55.05
23	90	600	0.5	20	545.68	54.74
24	90	600	0.6	15	532.06	54.52
25	90	900	0.4	20	635.04	56.06
26	90	900	0.5	15	514.10	54.22
27	90	900	0.6	10	511.83	54.18

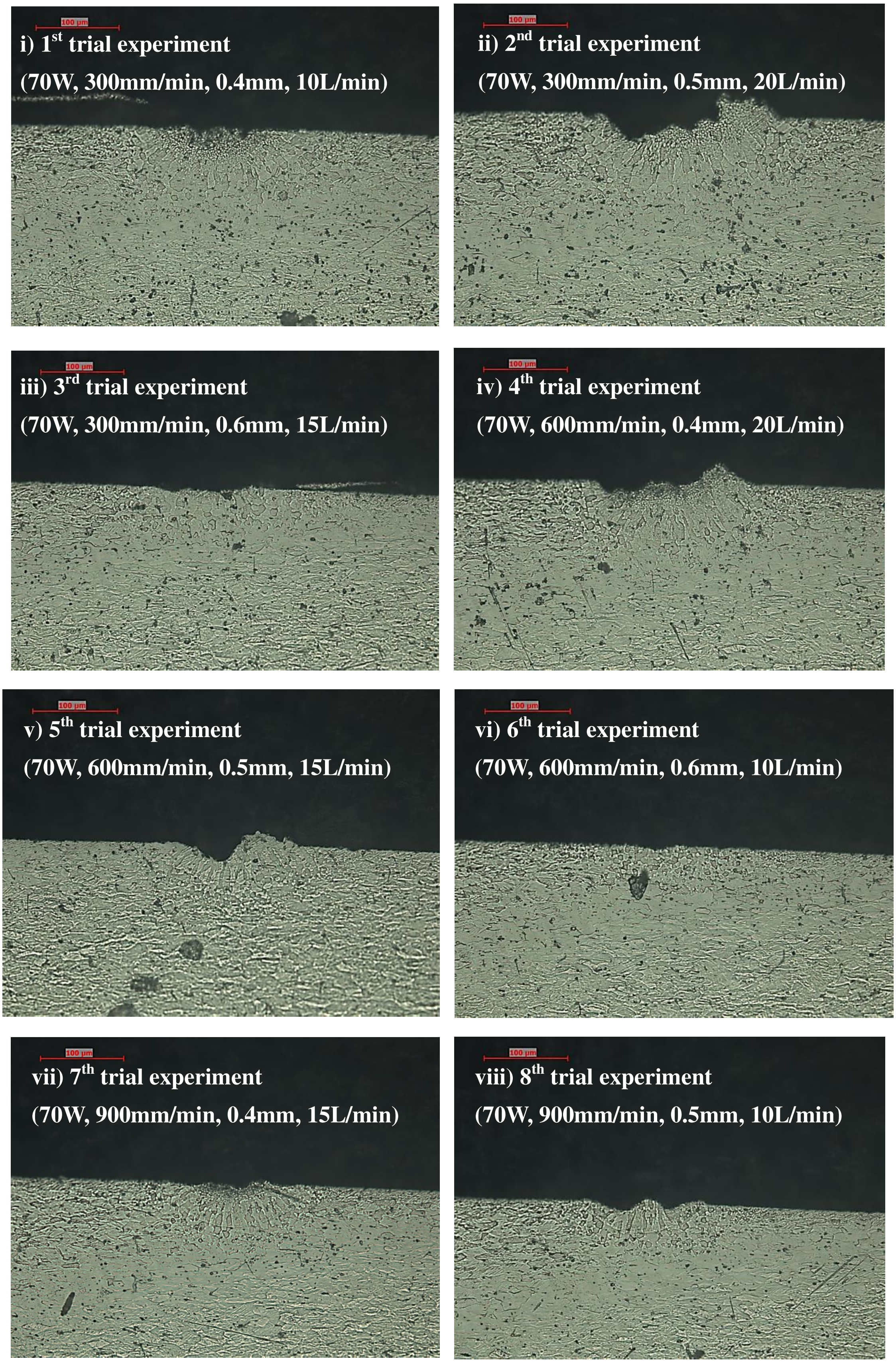
i) 1st trial experiment
(70W, 300mm/min, 0.4mm, 10L/min)
ii) 2nd trial experiment
(70W, 300mm/min, 0.5mm, 20L/min)
iii) 3rd trial experiment
(70W, 300mm/min, 0.6mm, 15L/min)
iv) 4th trial experiment
(70W, 600mm/min, 0.4mm, 20L/min)
v) 5th trial experiment
(70W, 600mm/min, 0.5mm, 15L/min)
vi) 6th trial experiment
(70W, 600mm/min, 0.6mm, 10L/min)
vii) 7th trial experiment
(70W, 900mm/min, 0.4mm, 15L/min)
viii) 8th trial experiment
(70W, 900mm/min, 0.5mm, 10L/min)

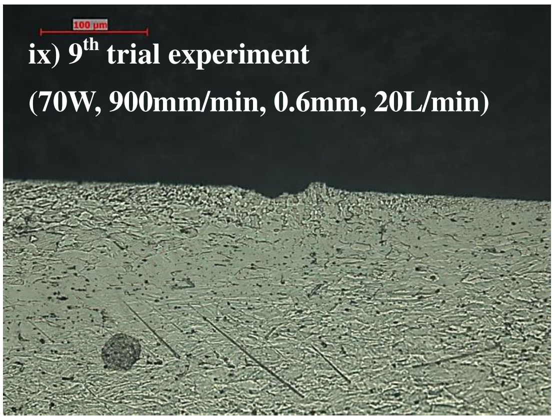
100 µm
ix) 9th trial experiment
(70W, 900mm/min, 0.6mm, 20L/min)

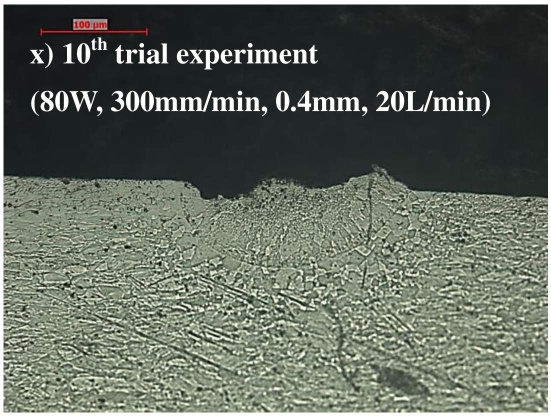
100 µm
x) 10th trial experiment
(80W, 300mm/min, 0.4mm, 20L/min)

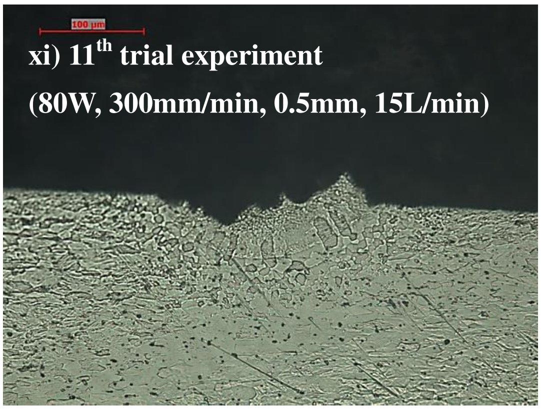
100 µm
xi) 11th trial experiment
(80W, 300mm/min, 0.5mm, 15L/min)


100 µm
xii) 12th trial experiment
(80W, 300mm/min, 0.6mm, 10L/min)

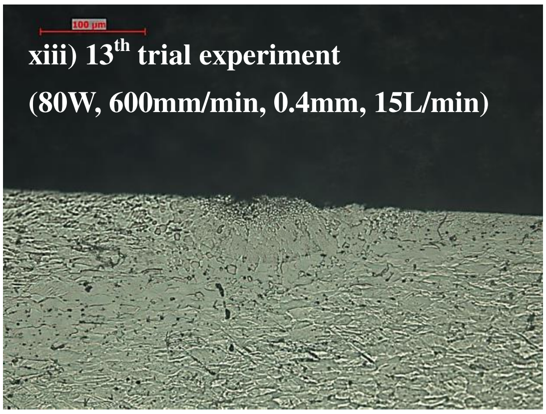
100 µm
xiii) 13th trial experiment
(80W, 600mm/min, 0.4mm, 15L/min)

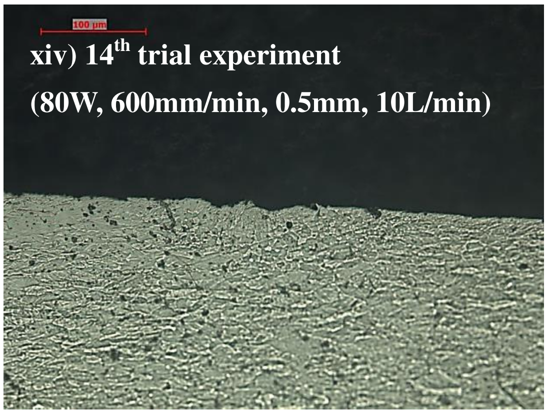
100 µm
xiv) 14th trial experiment
(80W, 600mm/min, 0.5mm, 10L/min)

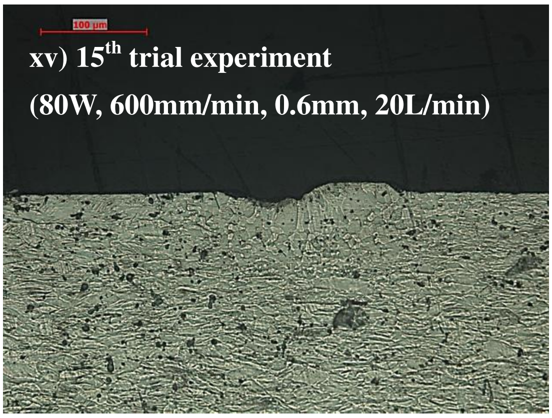
100 µm
xv) 15th trial experiment
(80W, 600mm/min, 0.6mm, 20L/min)

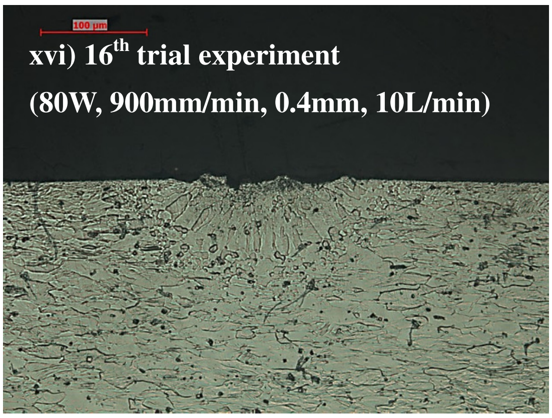
100 µm
xvi) 16th trial experiment
(80W, 900mm/min, 0.4mm, 10L/min)

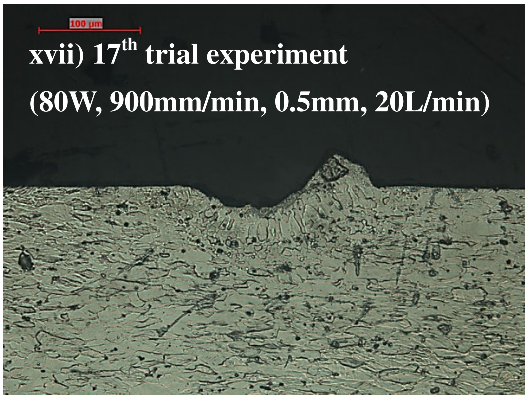
xvii) 17th trial experiment
(80W, 900mm/min, 0.5mm, 20L/min)

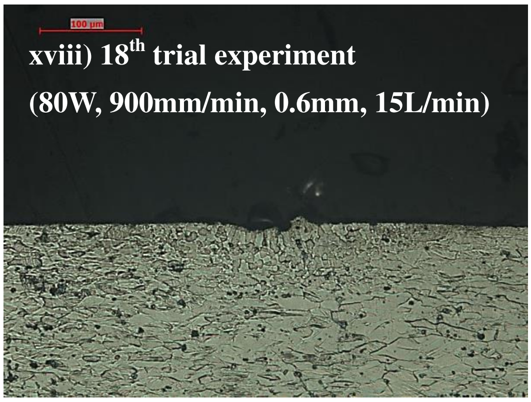
xviii) 18th trial experiment
(80W, 900mm/min, 0.6mm, 15L/min)

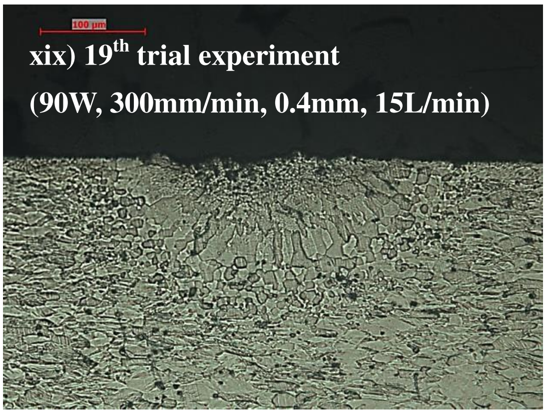
xix) 19th trial experiment
(90W, 300mm/min, 0.4mm, 15L/min)

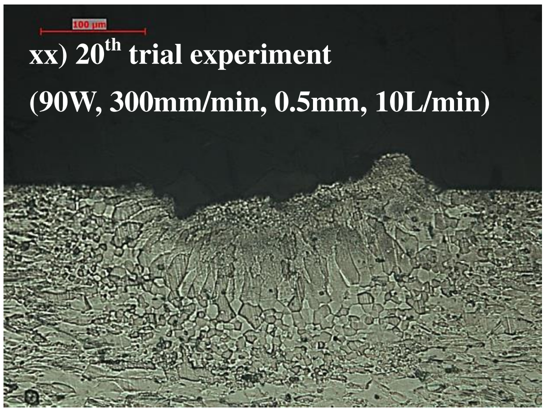
xx) 20th trial experiment
(90W, 300mm/min, 0.5mm, 10L/min)

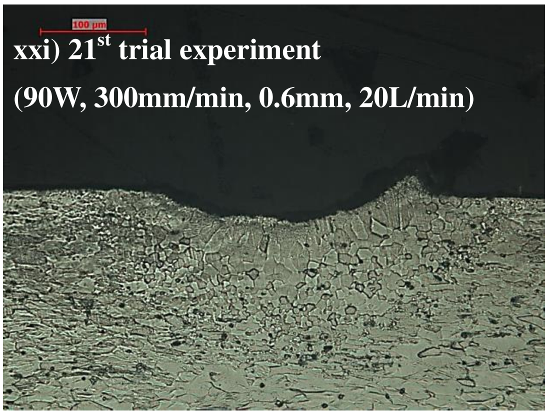
xxi) 21st trial experiment
(90W, 300mm/min, 0.6mm, 20L/min)

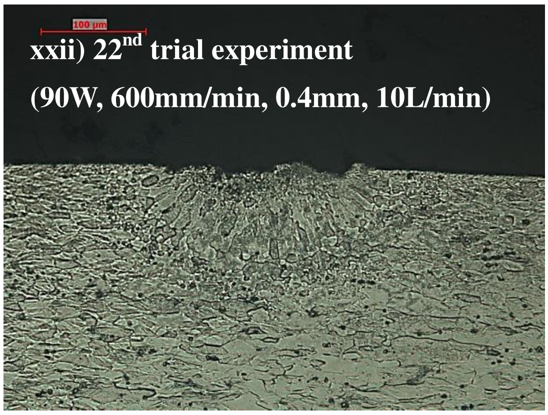
xxii) 22nd trial experiment
(90W, 600mm/min, 0.4mm, 10L/min)

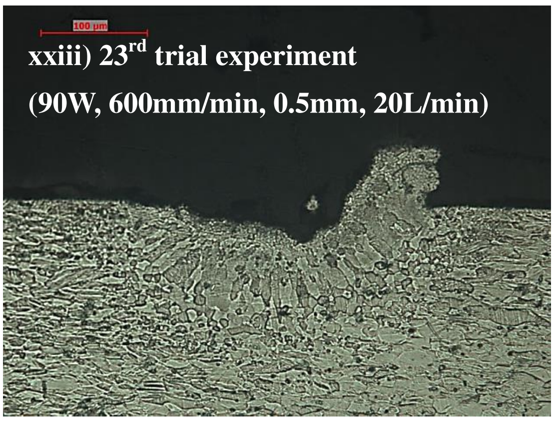
xxiii) 23rd trial experiment
(90W, 600mm/min, 0.5mm, 20L/min)

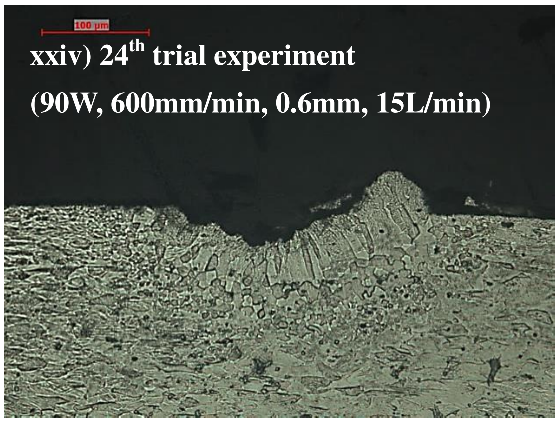
xxiv) 24th trial experiment
(90W, 600mm/min, 0.6mm, 15L/min)

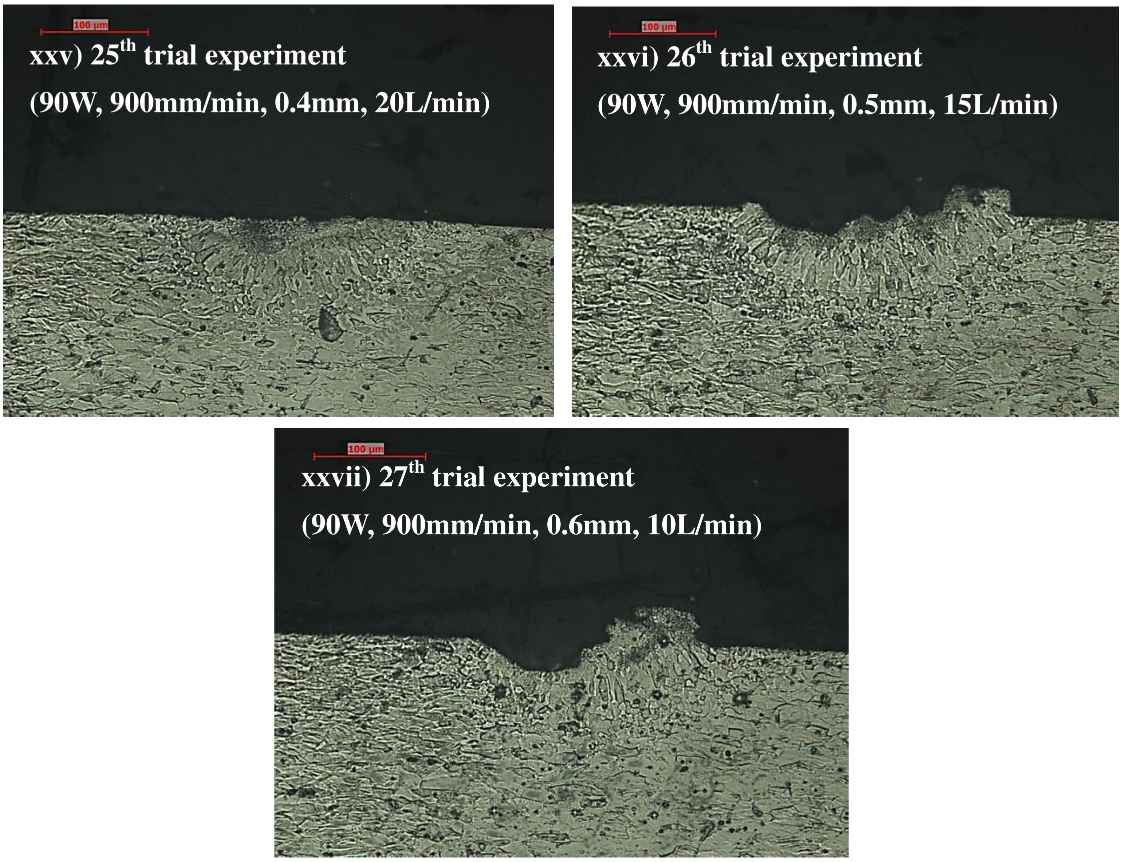

Figure 4.8 – Morphology of laser track under

4.3.2 Analysis of Mean (ANOM)

The mean signal-to-noise ratio of factor A to D and the influence of interaction AXB to CXD for the L-27 Taguchi analysis are computed respectively. It is believed that the factor which has the highest point in the graph is the suggested level for that factor. This is because the measured surface hardness was converted into larger-the-better signal-to-noise ratio. The effect of interactions is investigated by graphical plotting method in ANOM. By observing the graph, if the plotted lines are crossed significant, there is a strong interaction between the factors. Variation of such level combination of that interaction may significantly affect the resulting hardness. The graphical results of ANOM are presented in Figure 4.9.

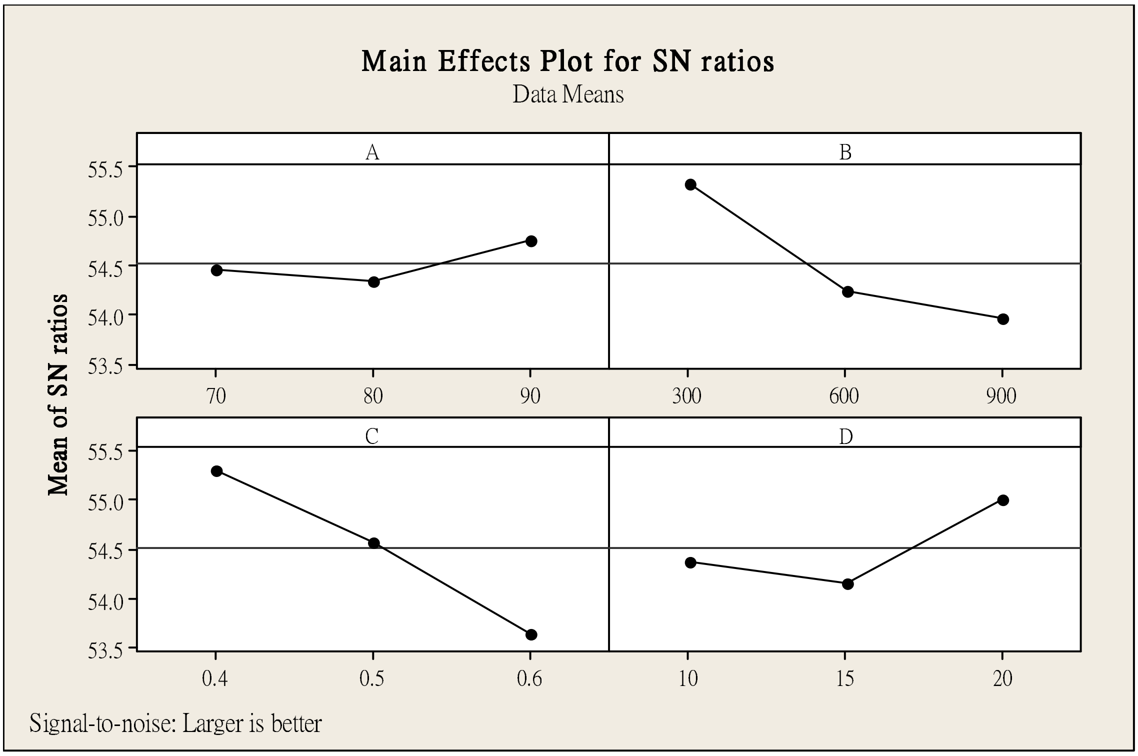

Figure 4.9 – Graphical ANOM results of L-27 Taguchi analysis

According to ANOM analysis, the suggested parameter for each factor is listed in Table 4.3.

Table 4.3 – Optimum parameter for each factor according to ANOM

Factor	**A: Output power**	**B: Scanning speed**	**C: Beam diameter**	**D: Nitrogen flow rate**
Optimum parameter	90W	300mm/min	0.4mm	20L/min

This parameter set could likely produce the desired result. The difference between the three levels of mean of signal-to-noise ratio could briefly show the relevant influence of each factor to the surface hardness of NiTi. As presented in Table 4.4, factor B and C have relatively higher value than other factors. This indicates that factor B and C, scanning speed and beam diameter, give a higher influence to the surface hardness than the output power and nitrogen flow rate.

Table 4.4 – Difference between three levels of mean S/N ratios for the four factors in L-27 Taguchi experiment

Level	A	B	C	D
m_1	54.45	55.34	55.31	54.38
m_2	54.33	54.25	54.59	54.16
m_3	54.76	53.96	53.64	55.01
Delta	0.42	1.38	1.67	0.85

The interaction plots for the factors involved in the L-27 Taguchi analysis are shown in Figure 4.10 (i) to (vi).

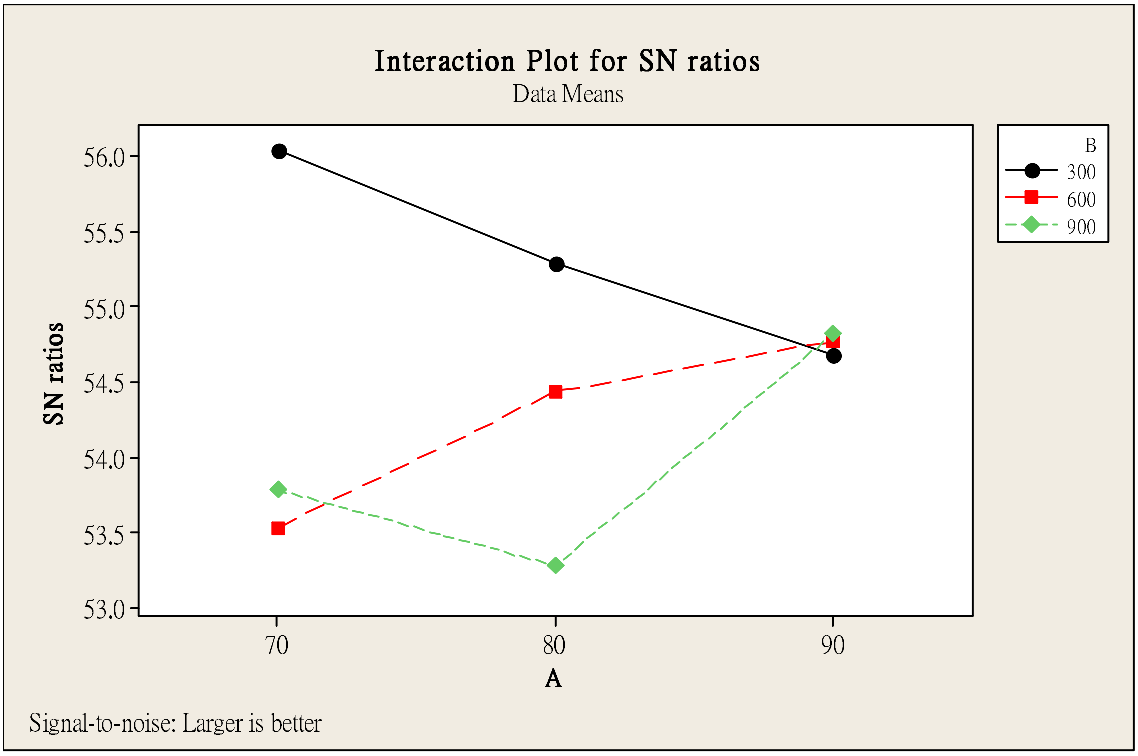

Figure 4.10i – Interaction plot of AXB

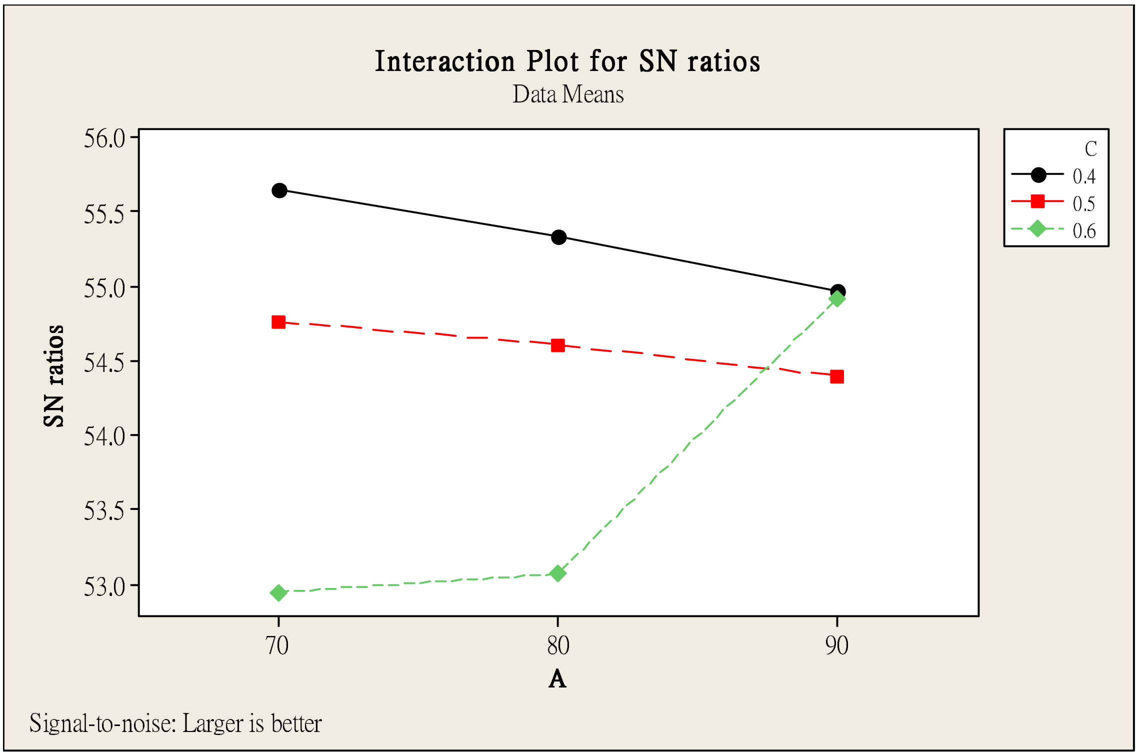

Figure 4.10ii – Interaction plot of AXC

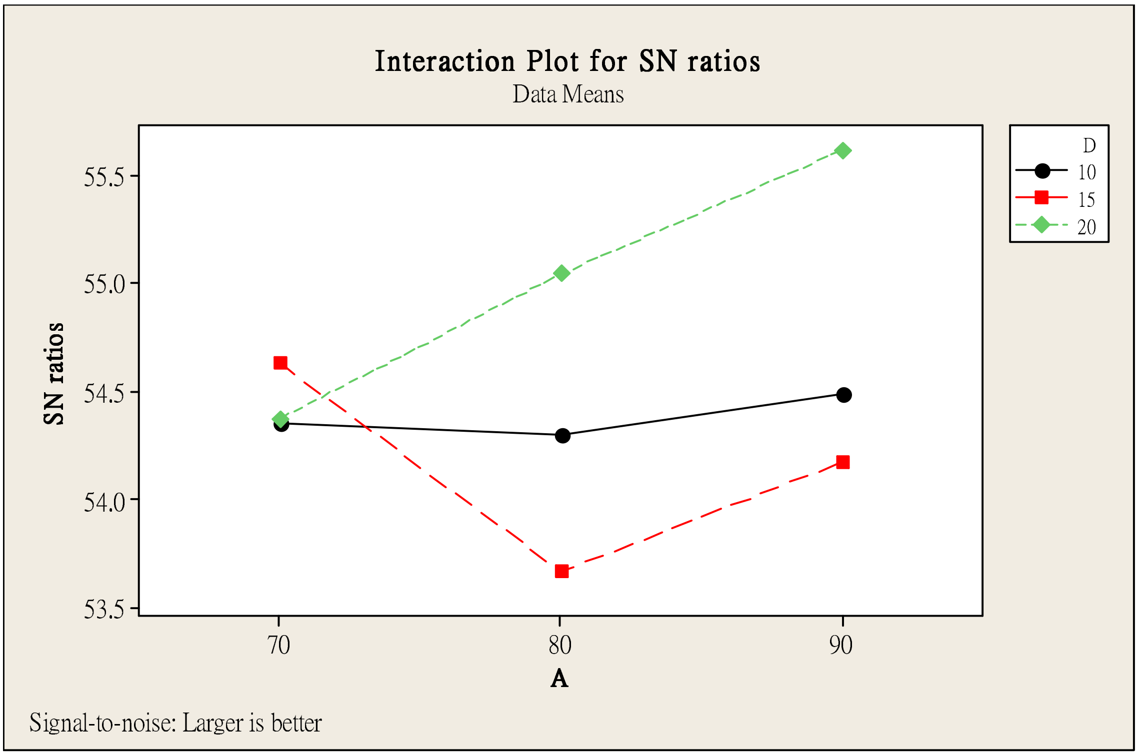

Figure 4.10iii – Interaction plot of AXD

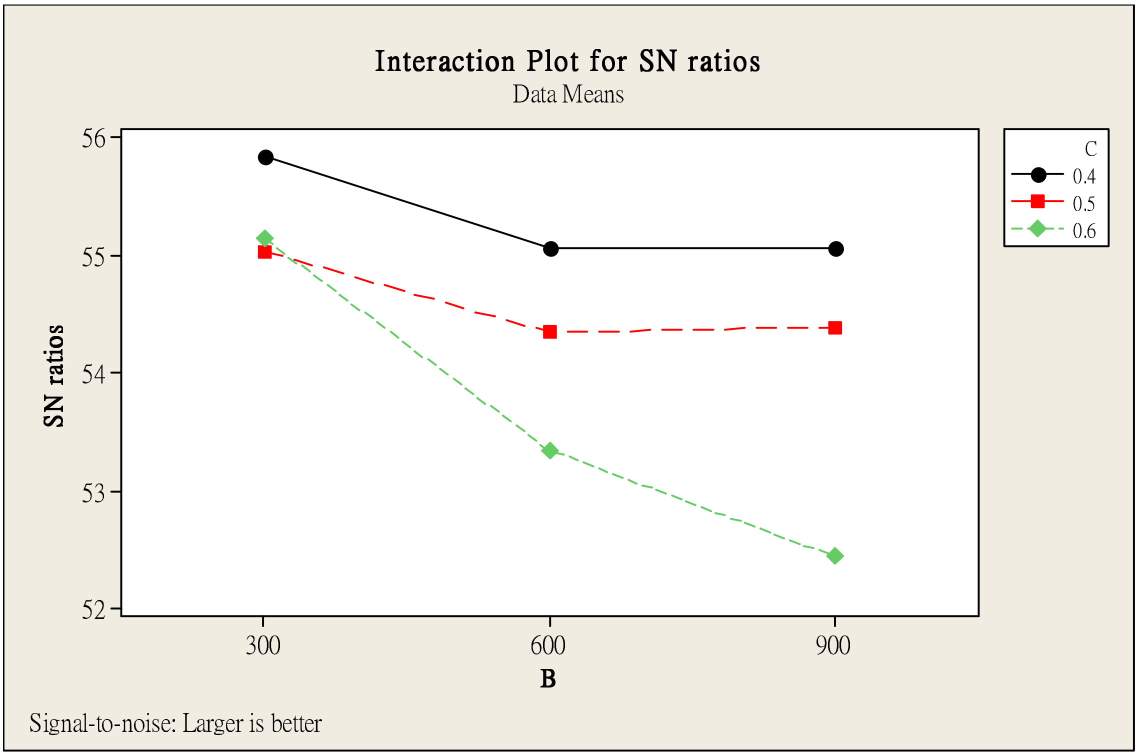

Figure 4.10iv – Interaction plot of BXC

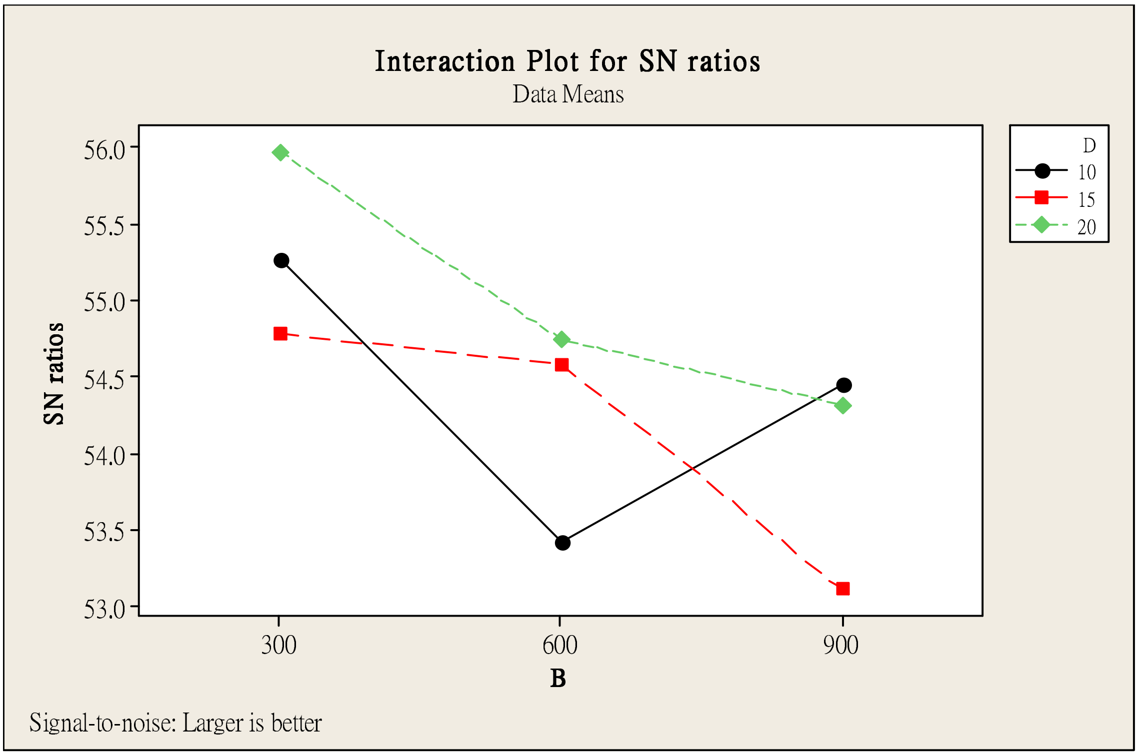

Figure 4.10v – Interaction plot of BXD

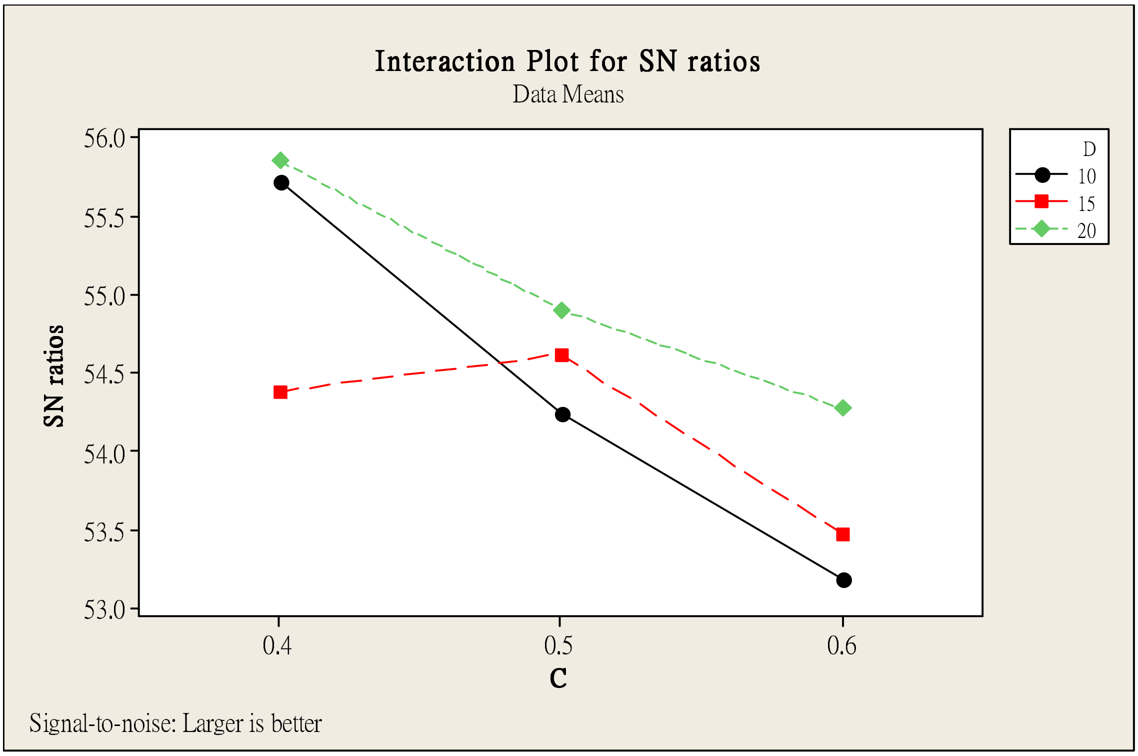

Figure 4.10vi – Interaction plot of CXD

The interaction plots for AXB (interaction between output power and scanning speed) and BXD (interaction between scanning speed and nitrogen flow rate) consist of more intersection points between the three lines. This may indicate that AXB and BXD are more significant interactions. ANOM could be a simple method for briefly study the effect of interactions on the response. However, it is whether difficult to state the importance of factors and interactions in a scientific manner by only examining the graphical plots of ANOM.

4.3.3 Analysis of Variance (ANOVA)

Analysis of Variance (ANOVA) could provide two types of importance value for a more scientific analysis of the factors and interactions to the response. They are F-ratio (F) and percent influence (P). A statement containing the analytical data of the L-27 Taguchi experiment is shown in Table 4.5. The data necessary for further analysis of the degree of influence of factors or interactions to the response is listed in the table. As discussed in Chapter 2, they are degree of freedom (DOF), sums of squares (S), mean of squares (V), F-ratio (F), pure sum of squares (S') and percent influence (P). Factors and interactions which have a lower S value would be pooled so that the statistical power of investigating the relative importance of remaining factors and interactions could be raised.

Table 4.5 – Statement for ANOVA analysis of L-27 Taguchi experiment

Factor / Interaction	**Pool**	**S**	**DOF**	**V**	**F**	**S'**	**P**
A	Y	0.85					
B		9.51	2	4.75	6.67	8.08	15.89%
C		12.66	2	6.33	8.89	11.24	22.09%
D		3.53	2	1.76	2.48	2.10	4.13%
AXB		8.10	4	2.02	2.84	5.25	10.32%
AXC		7.39	4	1.85	2.59	4.54	8.93%
AXD	Y	0.88					
BXC		3.98	4	0.99	1.40	1.13	2.22%
BXD	Y	1.67					
CXD	Y	2.30					
Error estimate		5.70	8	0.71			36.41%
Total		50.86	26				100%

As in the ANOVA study, Factor B and C, scanning speed and beam diameter, have relatively larger influence to the response. They have the percent influence (P) of 15.89% and 22.09% respectively. Factor D, nitrogen flow rate has less influence to the response, while Factor A, output power, has the least influence to the response. This is also agreed with the results in ANOM. According to literature, output power is one major and importance factor that could highly affect the results of laser gas nitriding. However, it is rather less important in this ANOVA analysis. One reason for this phenomenon may be that the range of output power chosen for Taguchi analysis, 70W to 90W, is within the optimum range for maximizing the surface hardness. Therefore, the change of output power within this range may not give significant influence to the surface hardness. Therefore, the sums of squares (V) for output power is relatively small. Factors and interactions were pooled according to their S value. It is better for S_{error} to be lower than 10% of the total S value. After pooling, the S_{error} is 5.7 which is lower than 10% of total S value. The error for percent influence in the L-27 Taguchi experiment is less than 50%, it could be assumed that all important elements have been identified. Hence, pooling in this ANOVA analysis is accepted. The percent influence (P) of AXB is the highest in ANOVA analysis. In addition, the percent influence (P) of Factor B and C, scanning speed and beam diameter is higher than other factors. These results from ANOVA also give good agreement to the ANOM results.

F-test has done to further evaluate the results of ANOVA. F-test is usually applied for comparing statistical models which have been fitted to a set of data. The aim of F-test is to identify the model that fits the population the most when the data were sampled (Lomax, 2007). During F-test, the F-ratio calculated from ANOVA was compared with the tabulated F-ratio with the corresponding DOFs in the form of numerator and denominator. If the F-ratio calculated form ANOVA is higher than that of the corresponding tabulated F-ratio, it may conclude that the relevant factor or interaction is important at a certain confidence level. As shown in Table 4.6, the numerator and denominator are 18 and 8 respectively. The tabulated values for 90%, 95% and 99% confidence level could be referenced form the table of F-test. Their corresponding values are 2.444, 3.184 and 5.437 respectively.

Table 4.6 – DOFs form L-27 Taguchi experiment and the tabulated values

Numerator (m)	Denominator (n)	Tabulated values		
f_b, f_c, f_d, f_{axb}, f_{axc}, f_{bxc}	f_e	90%	95%	99%
18	8	2.444	3.184	5.437

Table 4.7 - Confidence level of factors and interactions after pooling for the L27 experiment

Factor / Interaction	B	C	D	AXB	AXC	BXC
F value	6.67	8,89	2.48	2.84	2.59	1.40
Confidence level	99%	99%	90%	90%	90%	<90%

Factor B and C are statistically important at the confidence level of 99% in the Taguchi analysis. This means that scanning speed and beam diameter are important up to at least 99% confidence level. Nitrogen flow rate is less important when compared with scanning speed and beam diameter. It is important up to at least 90% confidence level. Interaction between power and scanning, and interaction between power and beam diameter have statistically important up to at least 90% confidence level. However, Interaction scanning speed and beam diameter may be considered as a weak interaction since the confidence level is less than 90%.

4.4 Tensile Test of Laser Treated Samples

A tensile test was conducted to investigate the fraction of surface coverage of TiN on the tensile stiffness of sample. Laser gas nitriding was conducted using the optimum parameter set determined in the Taguchi analysis (output power: 90W, scanning speed: 300mm/min, nitrogen flow rate: 20L/min, beam diameter: 0.4mm). Load-elongation curves for the tested sample were plotted after tensile test as shown in Figure 4.11.

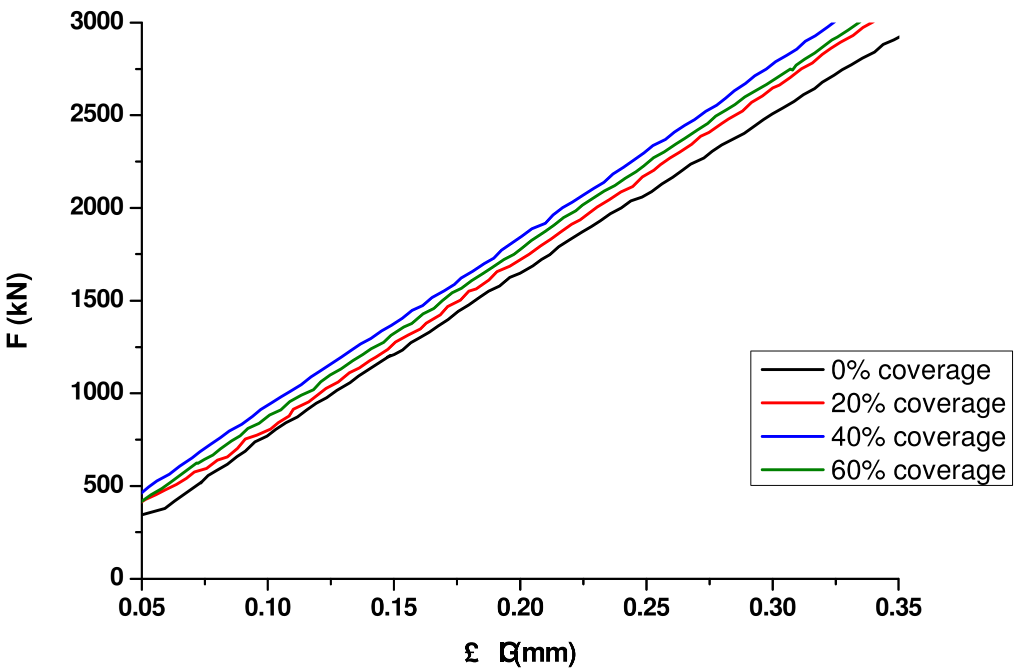

Figure 4.11 – Load-elongation curves for samples

There is an increasing trend of stiffness when the surface coverage of TiN is increased. Untreated NiTi has the lowest stiffness among all the samples. It is believed that the increase of stiffness is closely related to the presence of TiN on sample surface. TiN, being much harder and stiffer than NiTi, may act as reinforcing elements when force is applied on the sample during tensile test. During tensile test, the force applied on sample is shared by the TiN layer. NiTi with surface tracks of TiN may be regarded as a type of surface metal-matrix-composites. Figure 4.12 illustrates the phenomenon of reinforcement, with a reinforcing fibre (here it is a track of TiN) fabricated in a matrix (here it is the NiTi substrate) in a normal state while Figure 3ii shows the matrix under tensile load.

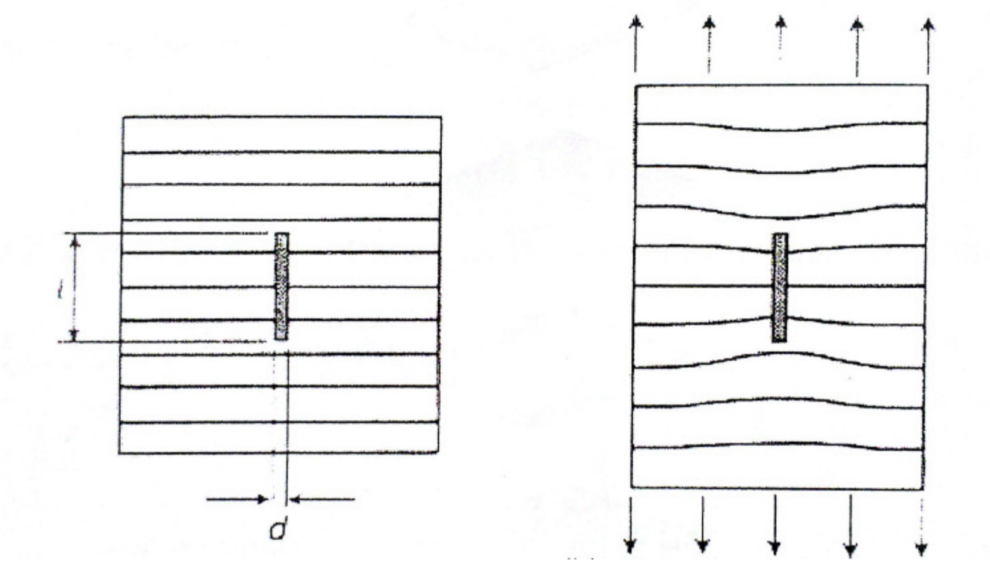

Figure 4.12 – i) Reinforcing fibre in a polymer matrix in normal state; ii) under tensile load

During loading condition as presented in Figure 4.12ii, a fibre which reinforces the matrix deforms less. This reduces the overall elongation of the matrix. The reinforcing fibre provides a restraining effect on the matrix, which depends on the strength of the fibre and the strength of the interfacial bond between the fibre and matrix. Therefore, the increase of the amount of fibre and interface leads to the increase of reinforcement effect to the whole matrix. The idea of strength reinforcement of NiTi by laser gas nitriding is supposed to be similar to this type of fibre reinforcement. The higher percentage coverage of TiN means the higher volume fraction of reinforcements, and the higher the stiffness could be obtained. The reinforcing fibre could increase the stiffness of sample, but the deformability may be reduced.

However, the stiffness of sample does not increase proportionally to the surface coverage of TiN. According to the result, sample A2 (40% TiN surface coverage) has the highest stiffness, which is even higher than that of sample A3 (60% TiN surface coverage). This could be explained as follows. During laser gas nitriding, the NiTi substrate was heated up at the same time. Heating may induce an annealing effect on the substrate. Hence, the stiffness may be reduced. Laser gas nitriding and annealing induce opposing effects on the overall tensile properties of laser-treated NiTi samples at the same time. To demonstrate the annealing effect, the bulk microhardness of NiTi samples with different TiN coverage (that is, samples with different heat input and thus different degrees of annealing) was measured. As shown in Figure 4.13, the microhardness of NiTi substrate decreases with the increase of surface TiN coverage.

This suggests that more heat input results in a higher degree of annealing, leading to lower bulk hardness. Thus laser nitriding induces two opposing effects on the tensile properties of the NiTi samples, namely, strengthening due to the formation of TiN tracks and annealing due to heat input. It is believed that for samples with TiN coverage up to about 40%, the effect of strengthening due to laser gas nitriding dominates. This leads to increase of stiffness with TiN coverage. When the TiN coverage further increases up to about 60%, annealing effect dominates. The microhardness of substrate is reduced accordingly. Hence, the stiffness is reduced.

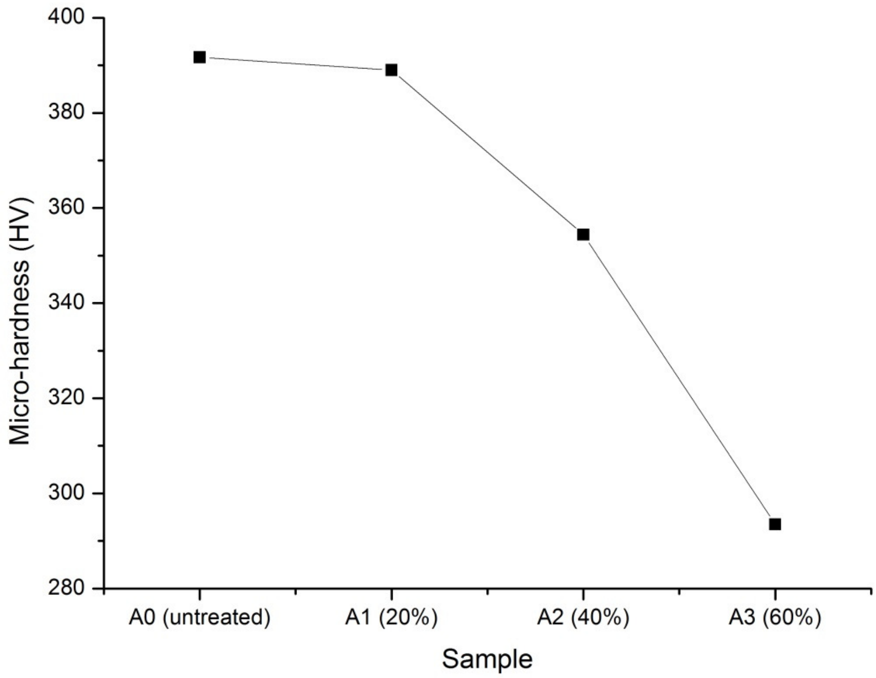

Figure 4.13 – Change of micro-hardness of samples

4.5 Corrosion Behavior Analysis

4.5.1 Potentiodynamic Polarization Measurement

Table 4.8 shows the results of potentiodynamic polarization measurements for laser gas nitriding treated samples with different percentage of TiN coverage. All the samples exhibited passive behavior in the 0.9% (by weight) NaCl solution at 37°C ± 1°C. Samples were prepared by applying output power: 90 W, scanning speed: 300mm/min, nitrogen flow rate: 20 L/min and beam diameter: 0.4 mm. The results show the influence of coverage of TiN on the corrosion behavior of samples.

Table 4.8 – Corrosion behavior of samples

Sample	**H0**	**H1**	**H2**	**H3**	**H4**
Coverage of TiN	0%	27.5%	47.4%	76.3%	100%
E_{corr} **mV** Vs SCE	-324.880	-324.541	-246.613	-222.206	-166.660
i_{corr} **μA/cm²**	3.468	9.420e-1	4.958e-1	3.357e-1	2.139e-1
E_{pit} **mV**	170.9	212.0	235.6	325.5	359.8

It is found that the corrosion behavior of sample H0 (untreated) has the lowest corrosion resistance in sodium chloride solution. It has the lowest (most active) E_{corr} and highest i_{corr} among all the samples. In addition, the E_{pit} value for NiTi is also low, which is only 170.9 mV. From these results, it is believed that NiTi has lower corrosion resistance and easier to initiate pits when compared with other samples in this analysis. There is a gradual increase of E_{corr} and decrease of i_{corr} values for the nitrided samples as the nitride coverage increases. The corrosion resistance to sodium chloride solution becomes stronger when the coverage of TiN increases from 27.5% to 100%. E_{pit} values also give an increasing trend with the increase of percentage coverage of TiN. This experiment shows that surface network reinforcement of TiN fabricated by laser gas nitriding could help to improve the corrosion behavior of NiTi in sodium chloride solution. By comparing sample H0 (untreated) with sample H1 – H4 (laser treated), it could be concluded that laser treated samples could give significant improvement regarding to corrosion. The higher the percentage coverage of TiN network, the better the corrosion performance of material. Such a trend results from the fact that TiN, which is a ceramic, is more inert than bare NiTi, which is metallic. Figure 4.14 shows the polarization curves of the samples. Figure 4.15 to 4.17 further illustrate the results in graphical format.

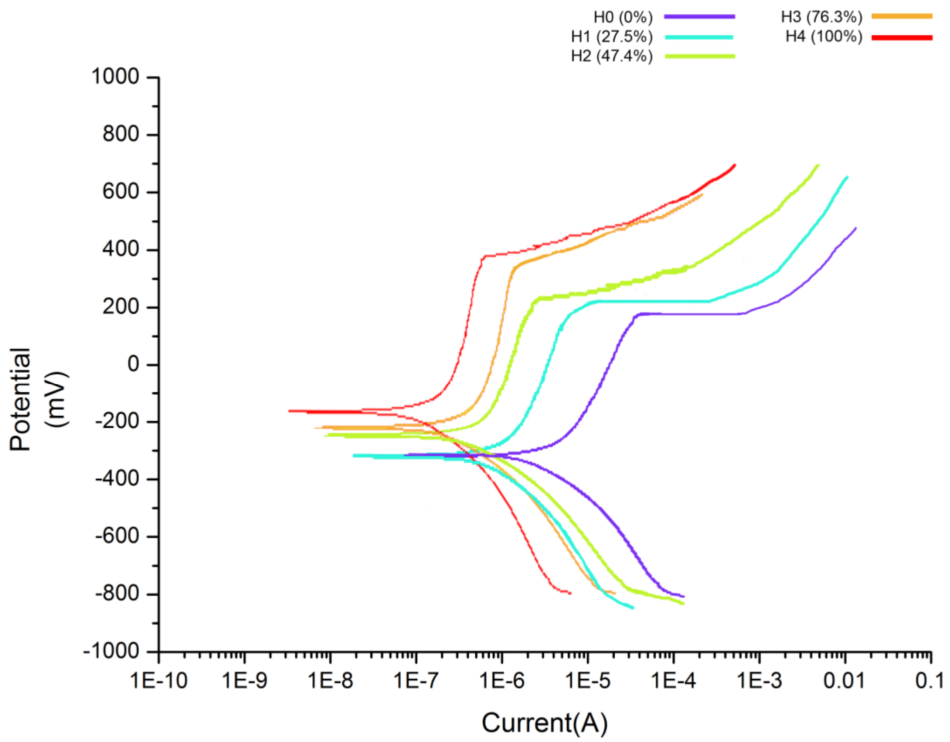

Figure 4.14 – Polarization curves of various samples

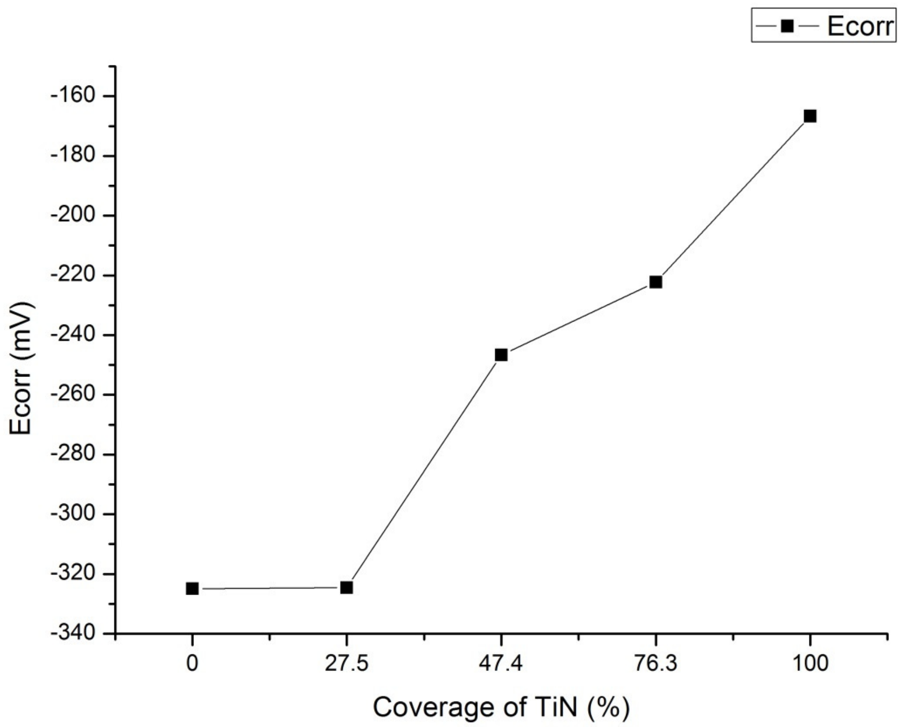

Figure 4.15 – Change of E_{corr} with coverage of TiN

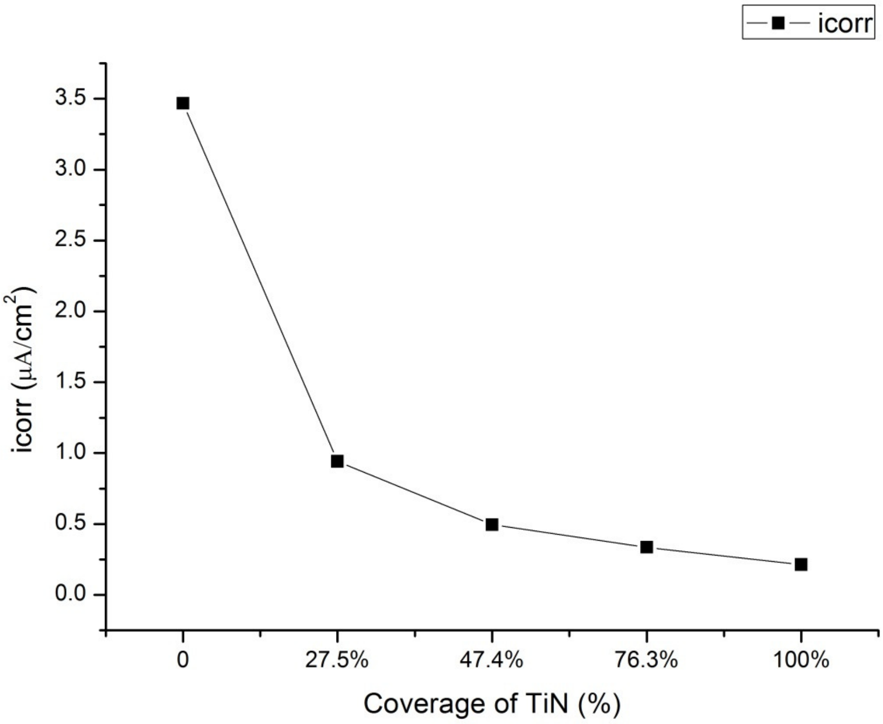

Figure 4.16 – Change of i_{corr} with coverage of TiN

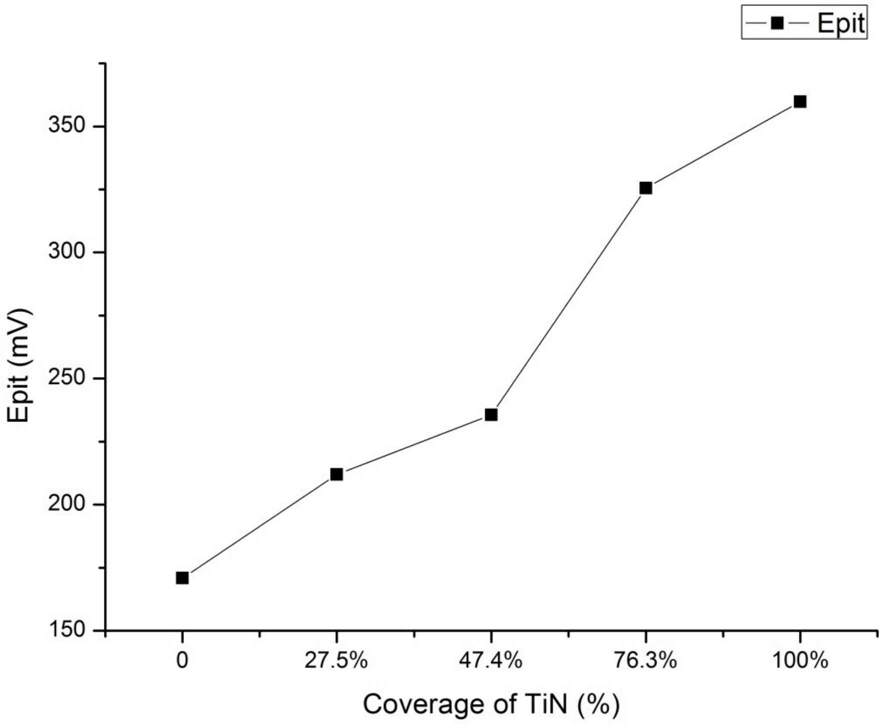

Figure 4.17 – Change of E_{pit} with coverage of TiN

The morphologies of samples after potentiodynamic polarization measurement were shown in Figure 4.18i to 4.18v. As illustrated in the figures, there are more pits on the untreated area than the nitrided area. Some of the pits were formed at the interface between the laser nitrided tracks and the untreated zone. In sample H1 (27.5% coverage), there are still many pits formed on the surface. When there is increase in percentage coverage of TiN, the number of pits formed on the sample gradually decreased. Finally on the fully nitrided sample, there is rarely formation of pits on the surface.

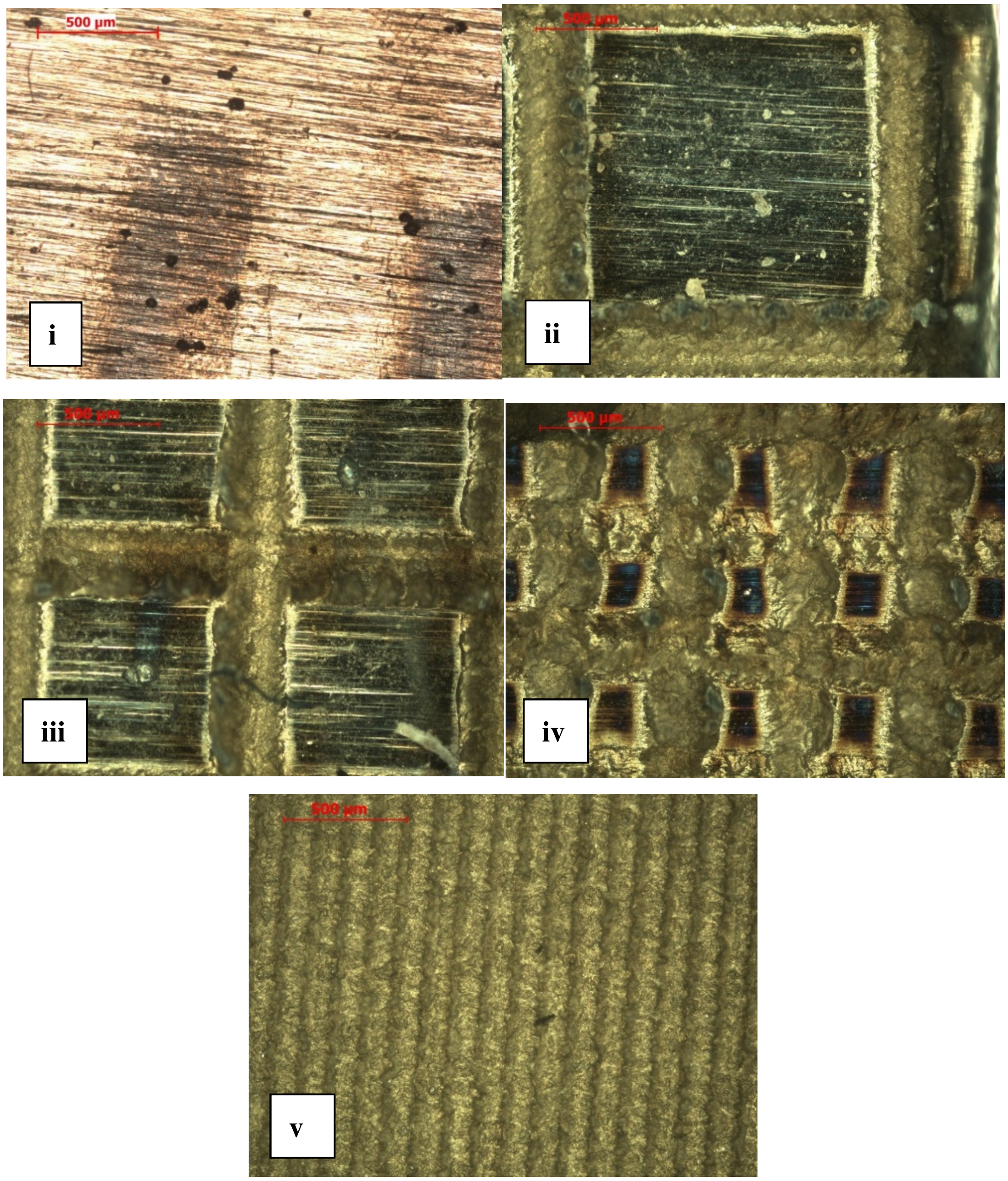

Figure 4.18 – Morphology of sample after corrosion test i) untreated NiTi; ii) 27.5% TiN coverage; iii) 47.4% TiN coverage; iv) 76.3% TiN coverage; v) 100% TiN coverage

(output power: 90W, scanning speed: 300mm/min, nitrogen flow rate: 20L/min and beam diameter: 0.4mm)

4.5.2 Electrochemical Impedance Spectroscopy Measurement

The electrical resistance of fully laser nitrided sample was examined by electrochemical impedance spectroscopy (EIS) using AC voltage. The sample was prepare by applying output power: 90W, scanning speed: 300mm/min, nitrogen flow rate: 20L/min and beam diameter: 0.4mm. The study was conducted by using 0.9% w.t. NaCl solution with temperature of 37°C ± 1°C. The EIS data for the samples were simulated by employing the equivalent electrical circuit, R_s (Q_c (R_{pore} (Q_sR_t))), as shown in Figure 4.19.

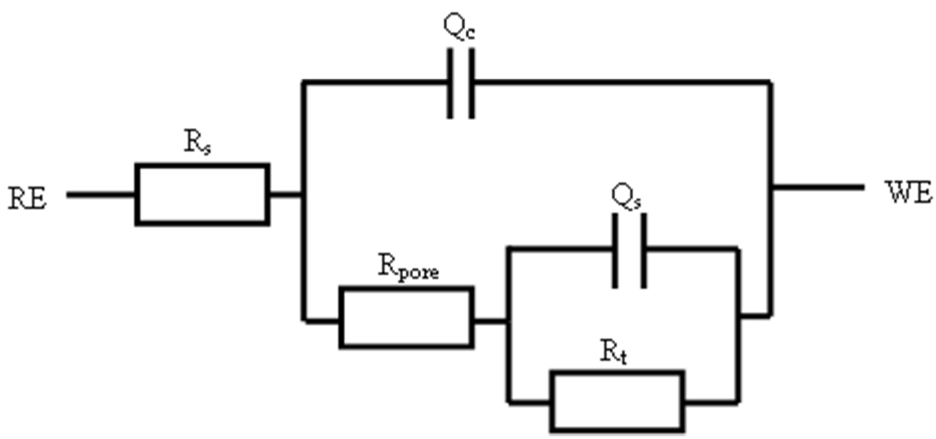

Figure 4.19 – Equivalent circuit for TiN on NiTi substrate

The equivalent circuit contains a solution resistance R_s, a capacitance Q_c and a pore resistance R_{pore}, a capacitance Q_s and a charge transfer resistance R_t for defects in the coatings. Q_c and Q_s are constant-phase elements. From the study, it is found that the simulation data fits well with the experimental data. The chi-squared value between the simulation data and the experimental data is $1.57e^{-3}$ which is very small. This represents that the experimental data fits the proposed circuit model. The experimental data collected for EIS analysis was compared with model R_s (Q_c (R_{pore} (Q_sR_t))) by software (ZSimpWin). Figure 4.20 graphically shows the fitting for the model. It shows that the data of the sample is closed to the model for both Nyquist plot and Bode plot.

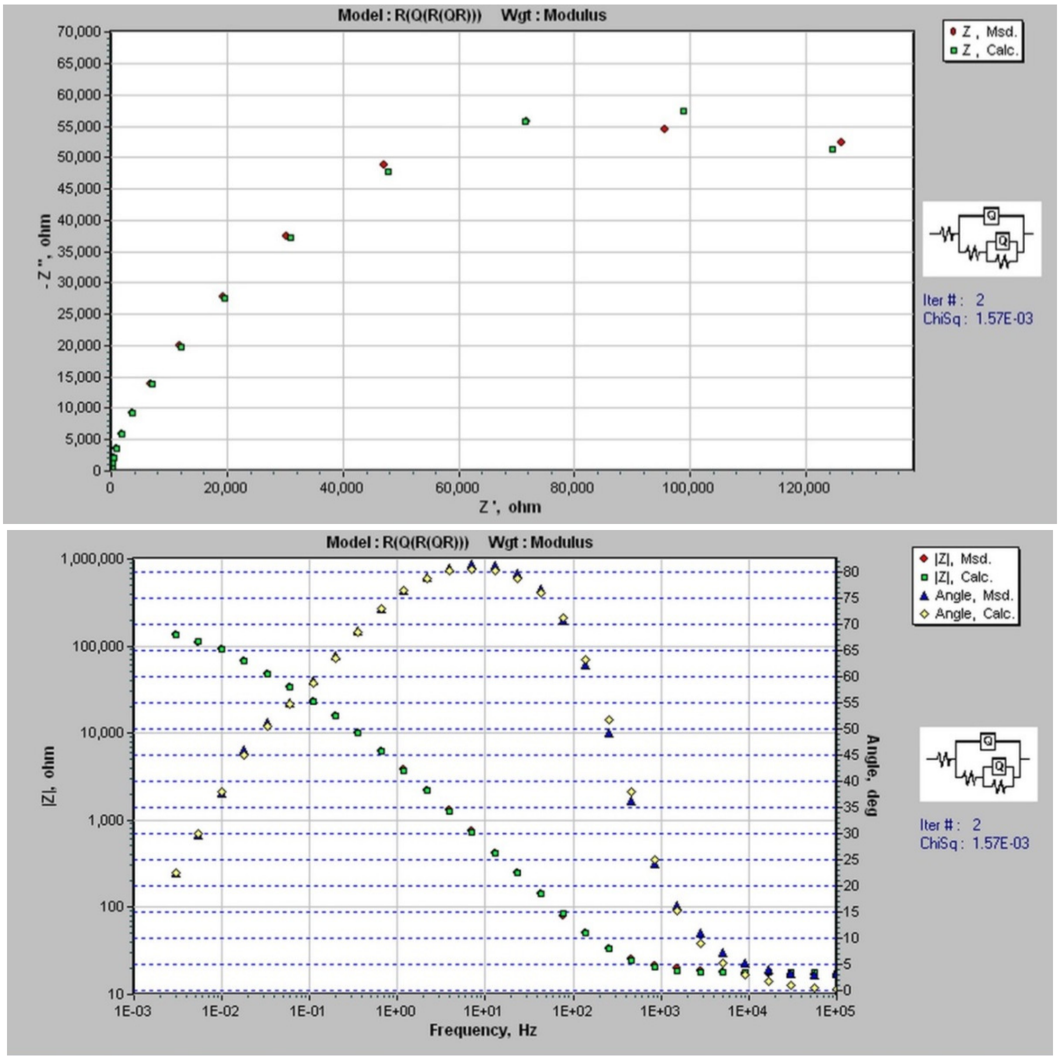

Figure 4.20 – Fitting curve for TiN with the desired model

The presence of a large semi-circle in Nyquist plot represents capacitance impedance. Figure 4.21 represented the Bode plots of the experimental data after immersion in 0.9% w.t. NaCl solution in 37°C ± 1°C after 1 hour. In the medium frequency region, the impedance shows a linear relationship with phase angle near to 80°. This shows a behavior of capacity of the electrolyte and electrode interface. In the high frequency region, the phase angle is near approaching to 0°. This indicates ohmic resistance dominates the impedance.

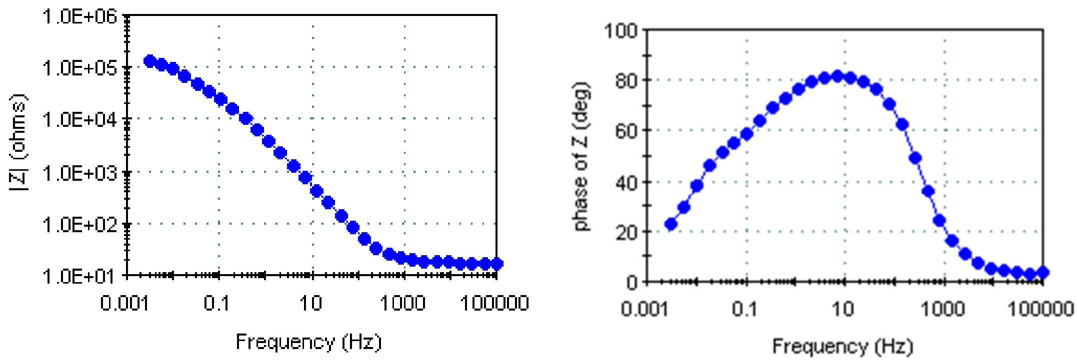

Figure 4.21 – Bode plot of EIS spectra of fully laser treated sample

Table 4.9 – Electrochemical parameters obtained from EIS spectra using the equivalent circuit

Sample	**R_s (Ωcm^2)**	**Q_c (F/cm^2)**	**n**	**R_{pore} (Ωcm^2)**	**Q_s (F/cm^2)**	**n**	**R_t (Ωcm^2)**
Laser nitrided sample	17.68	4.07e-5	0.9255	2.855e4	4.747e-5	0.6829	1.499e5

The high n value of 0.9255 of 1 hour immersion time gave a strong capacitive response between NaCl solution and TiN. In addition, there is no reveal of degradation of the substrate.

As studied by other research, the equivalent circuit of NiTi could be simulated by $R_s(Q_{c1}R_p)$ (Bayat, Sanjabi, & Barber, 2011; Chan, Man, & Yue, 2012). Figure 4.22 illustrates the equivalent circuit of NiTi. R_s represents the resistance of the electrolyte between the working and reference electrode which is NaCl solution. Q_{c1} is a capacitance represented by constant-phase element. R_p is a polarization resistance.

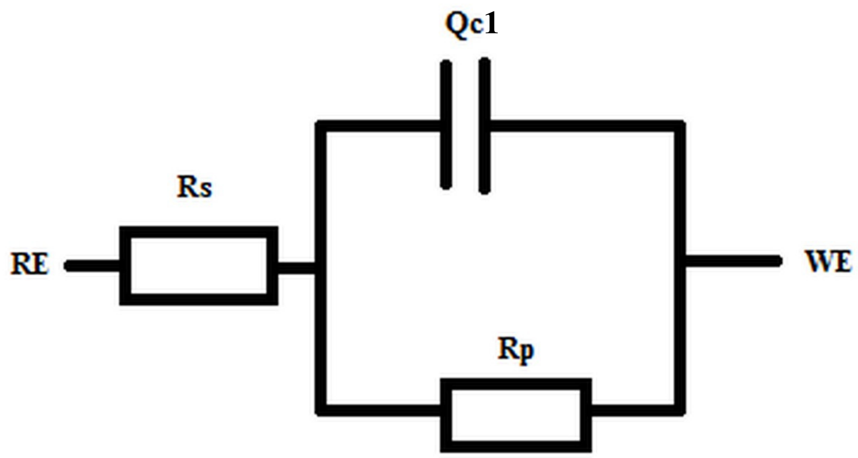

Figure 4.22 – Equivalent circuit model for the corrosion interface of NiTi

The current laser treated sample consists of both TiN coverage and bare NiTi untreated sites. Therefore, the equivalent circuit model for the sample with TiN surface network should combine both equivalent circuit models of bare NiTi and TiN on NiTi substrate. The combined equivalent circuit model is suggested as shown in Figure 4.23. The equivalent circuit for TiN on NiTi substrate may be parallel to that for bare NiTi. The components included in this circuit may be weighted for their area function.

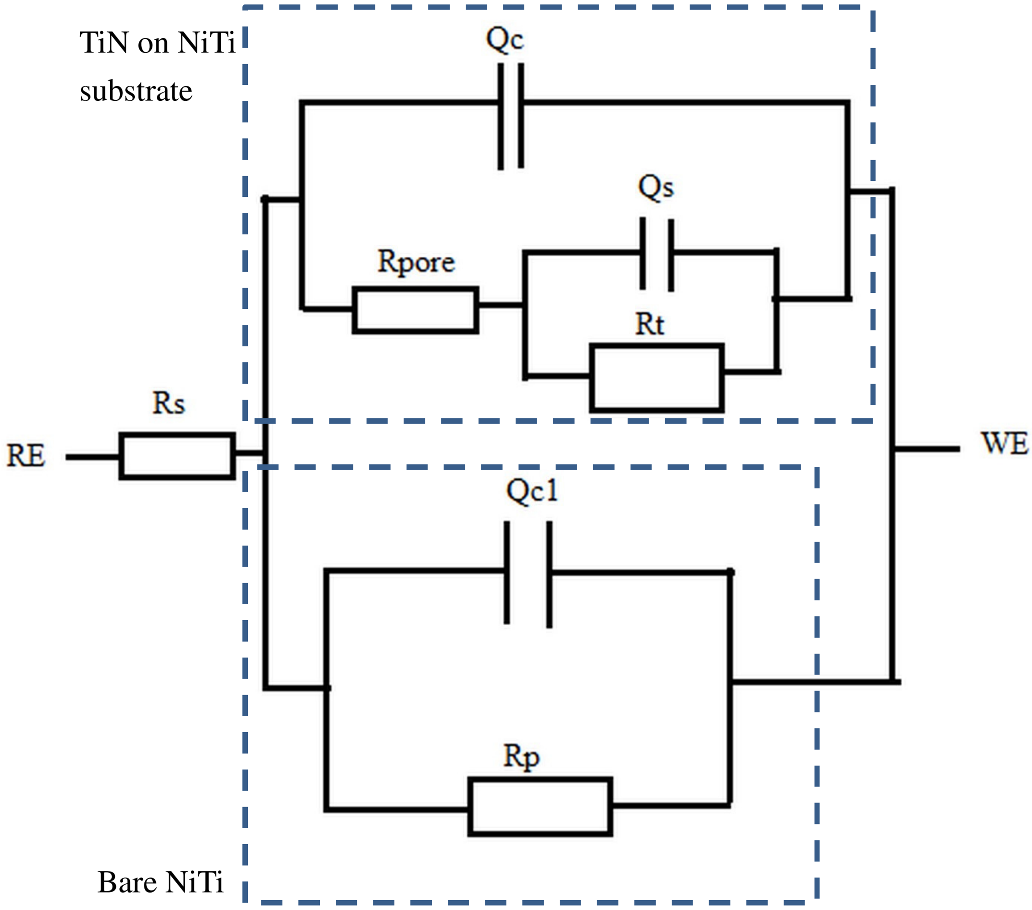

Figure 4.23 – Equivalent circuit model for NiTi with TiN network

4.6 Effect of Varying Laser Parameters to Surface Hardness

Laser gas nitriding was conducted for eight sets of samples with different parameter setting. As discussed by Steen (2003), normally for laser surface treatment, the higher the output power, the smaller the beam diameter. In addition, lower scanning speed could bring to larger hardening effect to a material. Therefore, laser energy density is suggested to relate these three important factors for laser surface treatment. Laser gas nitriding, as one type of laser surface treatment, could therefore use laser energy density for relating those three factors. In this study, output power, scanning speed and beam diameter were converted to laser energy density for further analysis. The resulting hardness for each sample is presented in Table 4.10. Figure 4.24 graphically presents the relationship between laser energy density and surface hardness. The following equation was used for converting the parameters:

$$F = \frac{P}{DV} \tag{4.1}$$

P: Output power

D: Beam diameter

V: Scanning speed

Table 4.10 – Laser energy density of each sample and their hardness

Sample	L0	L1	L2	L3	L4	L5	L6	L7
Laser energy density ($J\ mm^{-2}$)	N/A	2.3873	1.1936	0.7958	1.5279	1.0610	1.8568	2.1221
Hardness (HV)	353.2	739.3	635.3	558.7	697.0	564.6	663.0	673.8

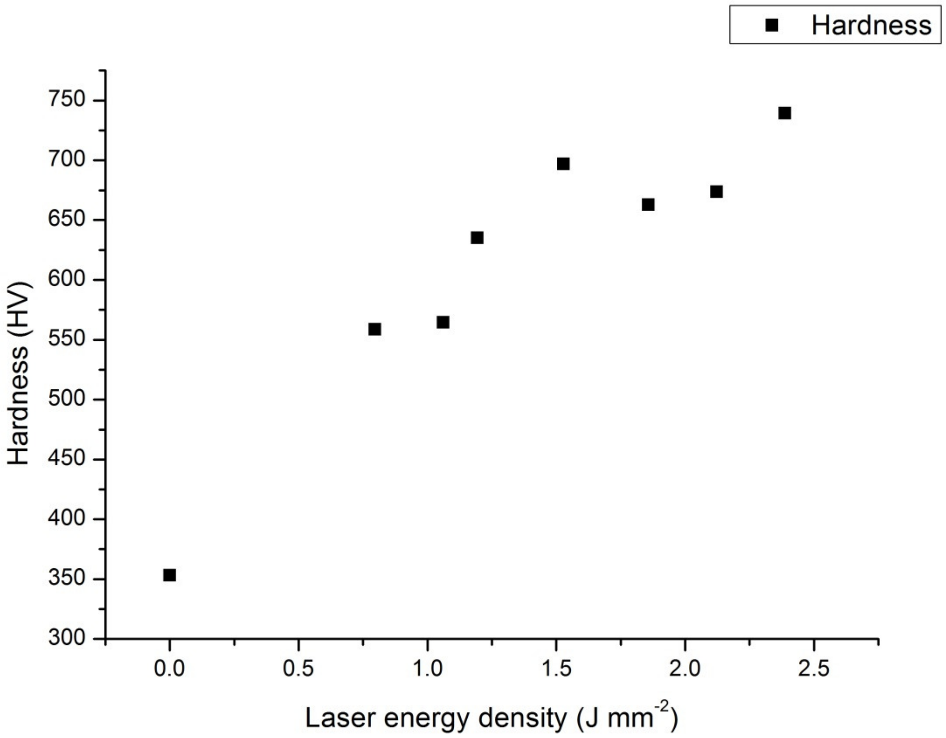

Figure 4.24 – Change of surface hardness to laser energy density

L0 represents the untreated NiTi sample. It has the lowest surface hardness. The surface hardness was highly related to the laser density. From the result, it is found that the higher density, the higher surface hardness of sample. This may be explained by the relative content of TiN formed on sample surface by laser gas nitriding. The XRD results (Figure 4.25) showed the relative amount of TiN in the fabricated TiN tracks.

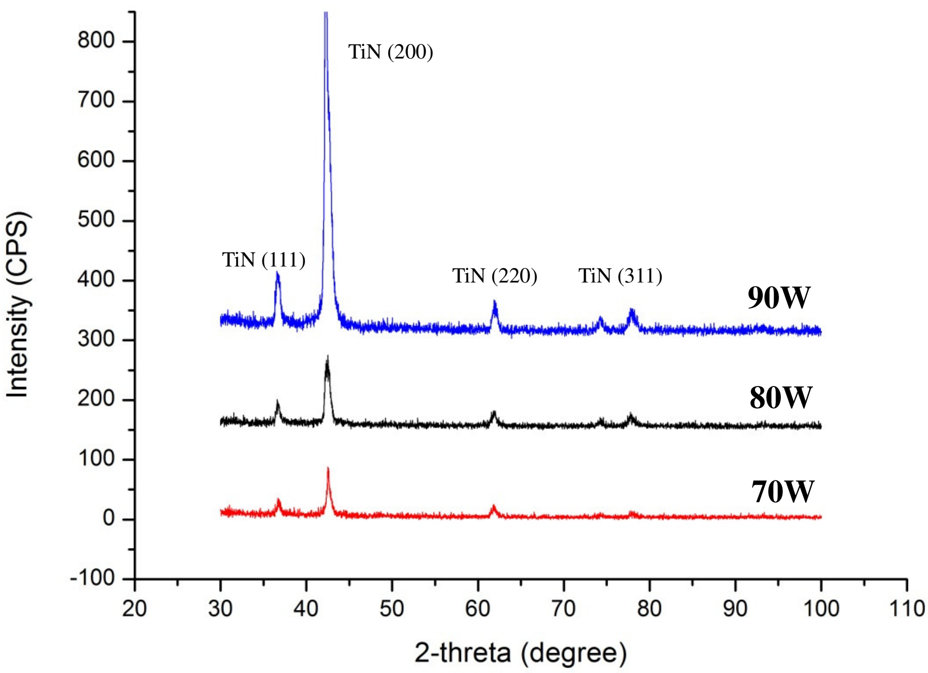

Figure 4.25i – XRD spectrum when changing power

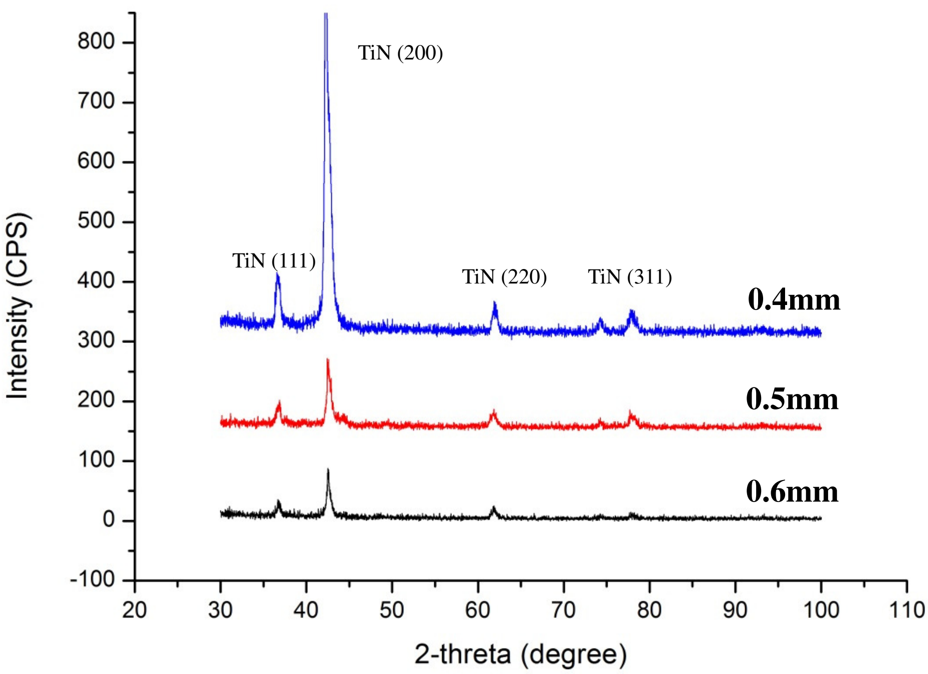

Figure 4.25ii – XRD spectrum when changing beam diameter

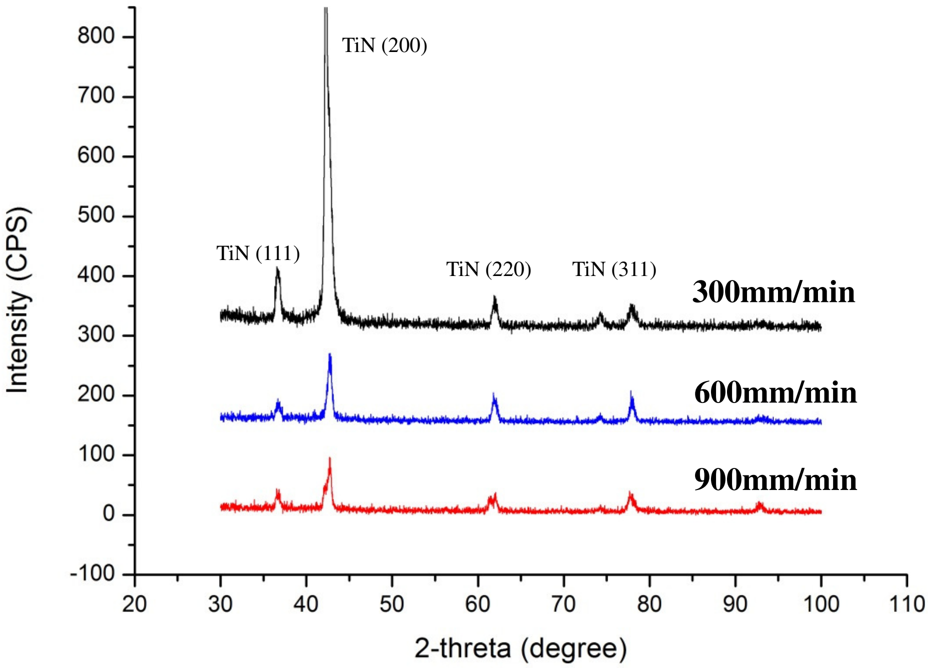

Figure 4.25iii – XRD spectrum when changing scanning speed

As shown in Figure 4.25i, the intensity decrease with the decrease of laser power. As in Figure 4.25ii, larger beam diameter would lead to the lower of the intensity. Also, slower scanning speed lead to the increase of intensity. The result is consistent to the laser density. Therefore, it is believed that a higher laser density could result in a higher content of TiN formed. A higher TiN content could lead to the increase of surface hardness.

4.7 Wear Resistance Analysis

Samples were laser nitrided by applying output power: 90W, scanning speed: 300mm/min, nitrogen flow rate: 20L/min and beam diameter: 0.4mm. Laser tracks were fabricated on the NiTi substrate forming longitudinal and transverse pattern. After wearing test, wearing tracks were formed on sample surface. The wear track went across laser tracks and untreated regions. The cross sectional profile of the track was measured. Figure 4.26i to 4.26v present the typical wearing track of each sample.

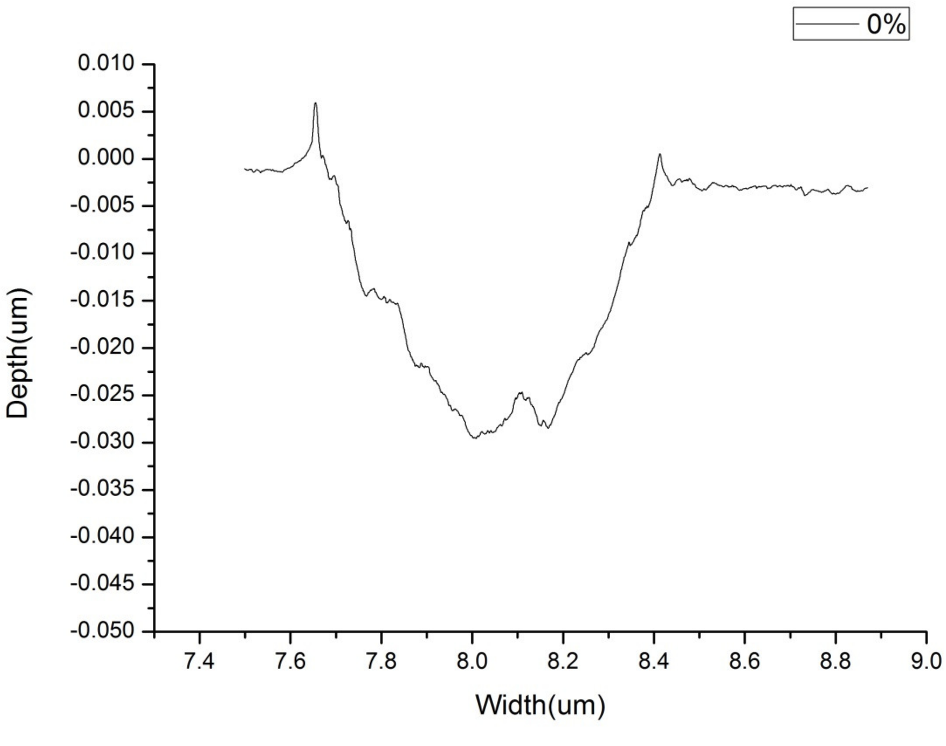

Figure 4.26i – Surface profile of Sample W0 (untreated sample)

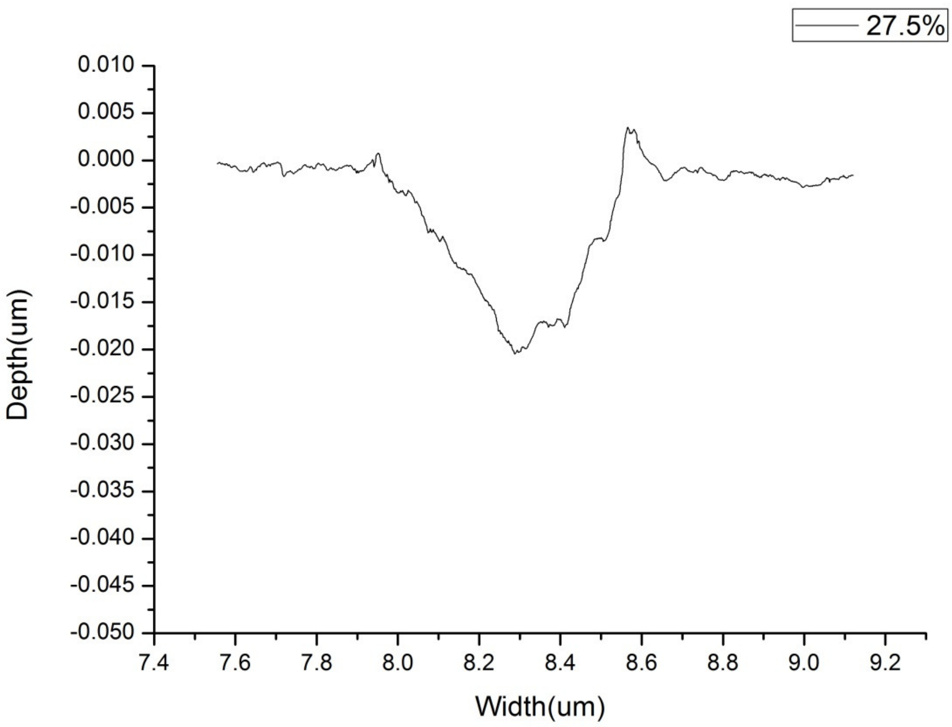

Figure 4.26ii – Surface profile of Sample W1 (27.5% TiN coverage)

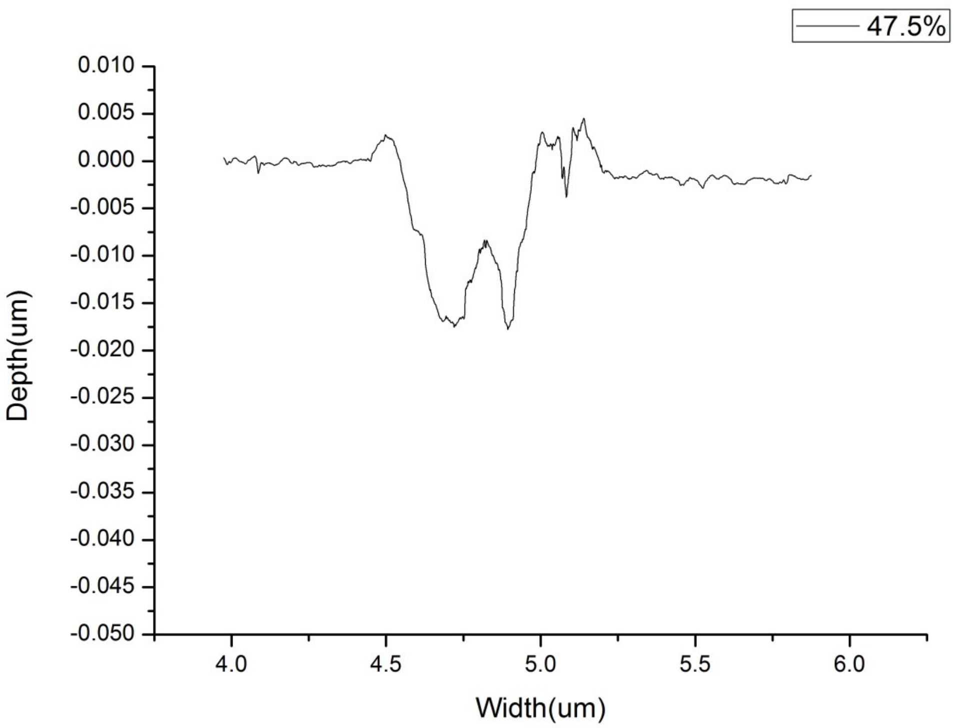

Figure 4.26iii – Surface profile of Sample W2 (47.5% TiN coverage)

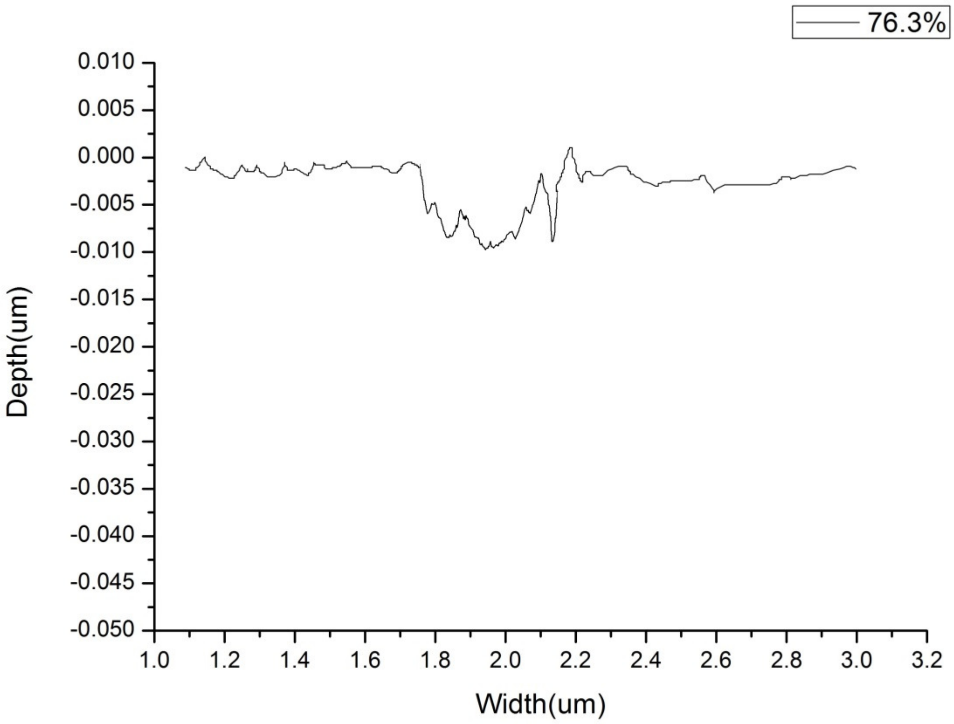

Figure 4.26iv – Surface profile of Sample W3 (76.3% TiN coverage)

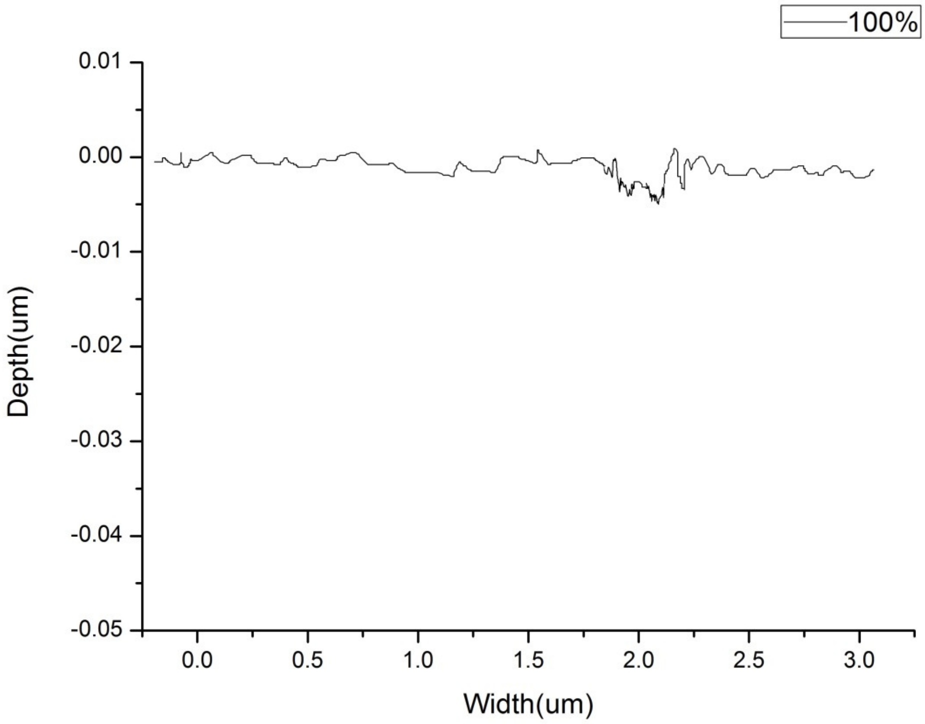

Figure 4.26v – Surface profile of Sample W4 (100% TiN coverage)

The average wearing volume of each sample was computed and is shown in Figure 4.27.

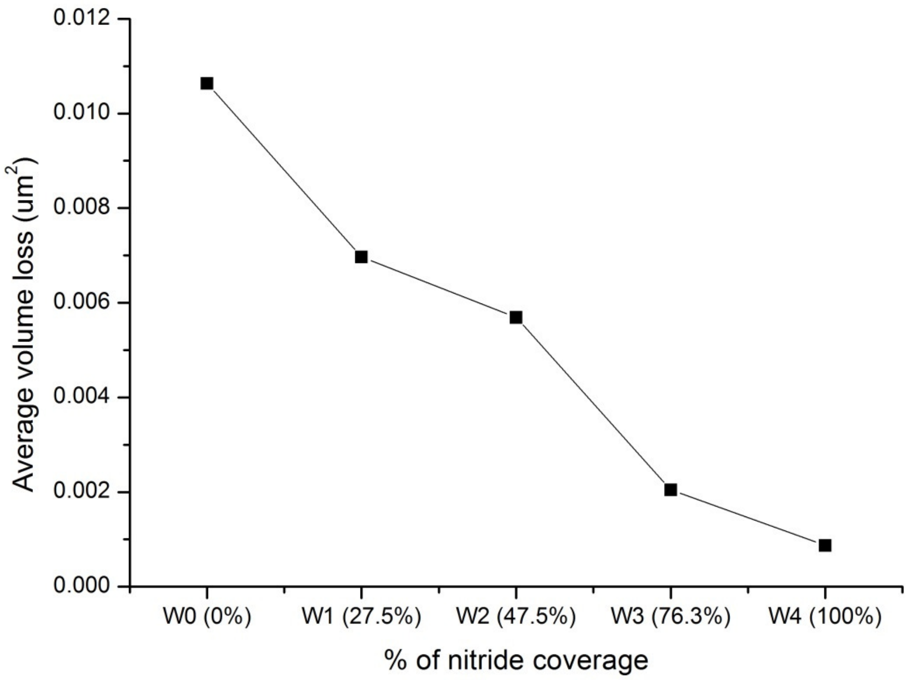

Figure 4.27 – Change of average volume loss to percentage coverage of TiN

The results show that the average volume loss of material decreases with increasing percentage coverage of TiN. It may suggest that wear resistance of NiTi could be improved by laser gas nitriding. The higher the percentage coverage of TiN, the higher the wear resistance of the surface. The increase of wear resistance should be probably related to the reinforcement network of TiN on the surface. The result from this wearing test is consistent to other previous research concerning improvement of material by TiN surface coating. The improvement of wear resistance could be related to the relatively higher hardness of TiN compared with NiTi. According to hardness test, the hardness of laser TiN track could reach 700HV. But that of NiTi without treatment could only reach about 350HV. There is about two times higher hardness for TiN to NiTi. The relatively high hardness of surface TiN coverage could act as protective agent to prevent material from wear away during the test. As discussed in previous chapter, TiN could be fabricated on alloy surface by laser gas nitriding and the tracks are metallurgically bonded to the alloy matrix. This bonding is very strong. Therefore, during wearing, TiN reinforcement network could provide a great protection to NiTi without shedding easily.

4.8 Nano-indentation Hardness Analysis

Load-displacement curves were obtained and are presented in Figure 4.28. The hardness H_N and reduced Young's modulus E_r are shown in Table 4.11.

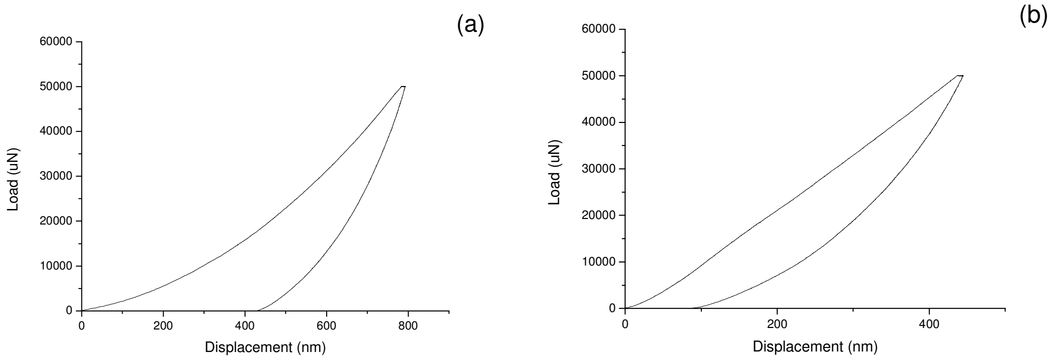

Figure 4.28 – Nano-indentation curves of (a) untreated NiTi (b) TiN

Table 4.11 – Results of nano-indentation hardness test

Sample	**Hardness (H_N)**	**Reduced Young's modulus (E_r)**	**H_N / E_r ratio**
Untreated NiTi	3.69 GPa	62.51 GPa	0.059
TiN track	13.7 GPa	123.67 GPa	0.111

According to the results, it is found that TiN coating exhibited much higher hardness and reduced Young's modulus than that of untreated NiTi. Smaller indentation depths at the same indentation load were observed on TiN when compared with that on the untreated NiTi. This may show that laser gas nitriding hardened the sample surface. Hardness-to-reduced Young modulus ratio (H_N/E_r) could be useful to determine wear resistance of coatings. According to Wangyang Ni et al. (2004), a higher value of H_N/E_r

ratio represents higher wearing resistance. From the result, the ratio for untreated NiTi is about half that of TiN. This indicates that TiN has higher wear resistance than that of the untreated NiTi.

Chapter 5 Conclusions and Further Work

5.1 Conclusions

NiTi has various advantages including excellent mechanical properties, formability and stability. All these advantages make it a favorable material for components used in different industries. To further improve the wear resistance, corrosion resistance and tensile stiffness of NiTi, laser gas nitriding is applied.

Surface texturing of NiTi by laser gas nitriding to create a grid of TiN on the surface was conducted in this project. Taguchi method was applied so that it is possible to investigation of the whole parameter range of laser parameters with a limited number of trial experiments. Optimum parameter set was obtained by the Taguchi analysis successfully. The surface hardness, morphologies, corrosion behavior and stiffness of NiTi after and before laser gas nitriding with network grid reinforcement was investigated. The results could be concluded as follows:

- The optimum parameter set for laser gas nitriding within the investigated parameters range is:

  Output power: 90W

  Scanning speed: 300mm/min

  Beam diameter: 0.4mm

  Nitrogen flow rate: 20L/min

  By the laser parameters concluded above, the resulting hardness after laser gas nitriding could reach more than 700HV.

- According to ANOVA analysis, the most significant parameters that affect the resulting hardness are scanning speed and beam diameter in this project.

- Longitudinal parallel tracks of TiN could improve the stiffness of NiTi. However, the increase in stiffness of samples is not proportional to the percentage coverage of TiN. TiN may act as reinforcing elements when force is applied on the sample during tensile test, so that stiffness increases. Sample with 40% TiN surface coverage has the highest stiffness, which is even higher than sample with 60% TiN surface coverage. This may due to the fact that laser gas nitriding induces two opposing effects on the tensile properties of the NiTi samples, namely, strengthening due to the formation of TiN tracks and annealing due to heat input.

- The network grid of TiN could improve the corrosion behavior of NiTi. The higher the percentage coverage of TiN could result in a lower corrosion current density and higher pitting potential. Number of pits is reduced when percentage coverage of TiN increase. TiN reinforcement network could successfully protect NiTi from corrosion in 0.9% w.t. sodium chloride solution under the temperature of 37°C.

- Wear resistance of NiTi could be successfully improved by the surface reinforcement TiN network. The higher the percentage coverage of TiN, the less the volume loss during wearing condition. This should be related to the strongly fabricated TiN on sample surface. Also, the high hardness of TiN could reduce wearing of sample.

- Laser parameters could be converted to laser energy density. It is highly related to the surface hardness of sample after laser gas nitriding. The higher laser density could lead to higher resulting hardness on sample surface. XRD measurement has shown the relative content of TiN on sample surface. The higher the laser density could lead to the higher concentration of TiN fabricated on sample surface.

- TiN coating exhibited much higher hardness and reduced Young's modulus than that of untreated NiTi. Laser gas nitriding could harden the sample surface.

- The stiffness, corrosion resistance and wear resistance of NiTi could be effectively improved by laser gas nitriding with TiN reinforcement tracks or network. It is believed that this kind of nitriding method could improve the properties of NiTi in an economical manner.

5.2 Further Work

Investigating laser gas nitriding with new patterns

In this study, transverse and longitudinal laser tracks were fabricated on NiTi. Those tracks were perpendicular or parallel to the pulling force during tensile test. This study has demonstrated that different surface coverage of TiN on NiTi could affect the tensile stiffness of NiTi. Therefore in the next step of investigation, it is suggested to further study laser patterning with laser gas nitriding with other patterns. The laser tracks could be in different directions or even could combine laser dots with laser tracks as new pattern.

Investigating influence new patterns to the wear behavior of NiTi

The current research has briefly studied the effects of surface texturing on wear. Detail study could be conducted to investigate the effect of different pattern of laser tracks to the wearing behavior of the material. Different surface texturing may alter the wear or even the mechanical properties of NiTi alloy.

Conducting corrosion analysis with other electrolytes

To further know about the corrosion behavior in body fluid, it is suggested to use other electrolyte for potentiodynamic polarization measurement such as Hank's solution and Ringer solution. Such kind of solution contains ingredients similar to body fluid. Therefore, the measurement result may be more representative.

Conducting immersion test for analyzing galvanic corrosion

For corrosion analysis, since the two phases on the sample are NiTi and TiN. A galvanic cell may form between these two phases at the interface and galvanic corrosion occurs. Galvanic corrosion occurs when two phases or material having different potentials are electrically connected. To further study galvanic corrosion of the laser treated sample, long term corrosion test such as immersion test is suggested to be conducted.

Investigating laser gas nitriding without surface melting

After laser gas nitriding, surface melting would occur along laser tracks. Post-polishing may be required. Previous research has studied laser gas nitriding on titanium alloy without melting the sample surface (Man, Bai, and Cheng 2011). It is suggested to study the effect for combining such scanning method with laser patterning.

References

Abboud, J. H., Fidel, A. F., & Benyounis, K. Y. (2008). Surface nitriding of Ti–6Al–4V alloy with a high power CO2 laser. *Optics & Laser Technology*, *40*(2), 405–414. doi:10.1016/j.optlastec.2007.07.005

Asua. E, Feuchtwanger J., Etxebarria V., and Garcia-Arribas A. (2009), Shape Memory Alloys In Micropositioning Applications, *Shape Memory Alloys: Manufacture, Properties and Applications*, New York: Nova Science Publishers Inc., 441-485

Bayat, N., Sanjabi, S., & Barber, Z. H. (2011). Improvement of corrosion resistance of NiTi sputtered thin films by anodization. *Applied Surface Science*, *257*(20), 8493–8499. doi:10.1016/j.apsusc.2011.05.001

Chan, C. W., & Man, H. C. (2011). Laser welding of thin foil nickel–titanium shape memory alloy. *Optics and Lasers in Engineering*, *49*(1), 121–126. doi:10.1016/j.optlaseng.2010.08.007

Chan, C. W., Man, H. C., & Yue, T. M. (2012). Effect of post-weld heat-treatment on the oxide film and corrosion behaviour of laser-welded shape memory NiTi wires. *Corrosion Science*, *56*, 158–167. doi:10.1016/j.corsci.2011.11.020

Chen, K. C., & Jaung, G. J. (1997). D.c. diode ion nitriding behavior of titanium and Ti-6Al-4V. *Thin Solid Films*, *303*(1–2), 226–231. doi:10.1016/S0040-6090(97)00075-8

Cheng, Y., and Y.F. Zheng. (2006) "Formation of TiN Films on Biomedical NiTi Shape Memory Alloy by PIIID." *Materials Science and Engineering: A* 434 (1–2) (October 25): 99–104. doi:10.1016/j.msea.2006.07.027.

Cui, Z.D., H.C. Man, and X.J. Yang. (2003). "Characterization of the Laser Gas Nitrided Surface of NiTi Shape Memory Alloy." *Applied Surface Science* 208–209 (March 15): 388–393. doi:10.1016/S0169-4332(02)01414-9.

Duerig, T., Pelton, A., & Stöckel, D. (1999). An overview of nitinol medical applications. *Materials Science and Engineering: A*, *273–275*, 149–160. doi:10.1016/S0921-5093(99)00294-4

Frohlich, F., Grau P., Grellmann, W. (1977), Performance and Analysis of Recording Microhardness Tests, *Physic Status Solidi (a)*, 42, 79-89

Gorji, M.R., and S. Sanjabi. (2012). "Corrosion Behavior of Ion Implanted NiTi Shape Memory Alloy Thin Films." *Materials Letters* 73 (April): 179–82. doi:10.1016/j.matlet.2011.12.075.

Hicks, C. R. (1999). *Fundamental concepts in the design of experiments* (5th ed.). New York: Oxford University Press.

Huang, W. (2002). On the selection of shape memory alloys for actuators. *Materials & Design*, *23*(1), 11–19. doi:10.1016/S0261-3069(01)00039-5

Kannatey-Asibu, E. (2009). *Principles of laser materials processing*. Hoboken, N.J.: Wiley.

Kauffman, G. B., & Mayo, I. (1997). The Story of Nitinol: The Serendipitous Discovery of the Memory Metal and Its Applications. *The Chemical Educator*, *2*(2), 1–21. doi:10.1007/s00897970111a

Kim, K.-H. (2010). *Surface modification of titanium for biomaterial applications.* S.l.: s.n.].

Kumar, A., & Kaur, D. (2009). Nanoindentation and corrosion studies of TiN/NiTi thin films for biomedical applications. *Surface and Coatings Technology*, *204*(6–7), 1132–1136. doi:10.1016/j.surfcoat.2009.06.002

Liu, X. (2009). *Sheng wu yi yong tai cai liao ji qi biao mian gai xing = Biomedical titanium alloys and surface modification*. Beijing Shi: Hua xue gong ye chu ban she.

Lomax, R. G. (2007). *Statistical concepts: a second course* (3rd ed.). Mahwah, N.J: Lawrence Erlbaum Associates.

Malinov S., Zhecheva A., Sha W. (2003), Proceedings of the 1st International,Surface Engineering Congress and the 13th IFHTSE Congress,ASM International, Materials Park, OH, 344.

Mändl, S., & Rauschenbach, B. (2002). Improving the biocompatibility of medical implants with plasma immersion ion implantation. *Surface and Coatings Technology*, *156*(1–3), 276–283. doi:10.1016/S0257-8972(02)00085-3

Man, H. C., Bai, M., & Cheng, F. T. (2011). Laser diffusion nitriding of Ti–6Al–4V for improving hardness and wear resistance. *Applied Surface Science*, *258*(1), 436–441. doi:10.1016/j.apsusc.2011.08.114

Man, H. C., Cui, Z. D., Yue, T. M., & Cheng, F. T. (2003). Cavitation erosion behavior of laser gas nitrided Ti and Ti6Al4V alloy. *Materials Science and Engineering: A*, *355*(1–2), 167–173. doi:10.1016/S0921-5093(03)00062-5

Man, H.C., and N.Q. Zhao. (2006). "Phase Transformation Characteristics of Laser Gas Nitrided NiTi Shape Memory Alloy." *Surface and Coatings Technology* 200 (18–19) (May 8): 5598–5605. doi:10.1016/j.surfcoat.2005.07.079.

Mccafferty E. (2010), Kinetics of Corrosion, *Introduction to Corrosion Science*,, New

York: Springer New York, 168

Milošev, I., and B. Navinšek. (1994). “A Corrosion Study of TiN (physical Vapour Deposition) Hard Coatings Deposited on Various Substrates.” *Surface and Coatings Technology* 63 (3) (March): 173–180. doi:10.1016/0257-8972(94)90095-7.

Miyamoto, I. (2005). Applications of High Power Single-Mode Fiber Lasers to Novel Microwelding and Micromachning. *Review of Laser Engineering, 33* (4), 249-253.

Miyazaki S. (1998), *Shape memory materials*. Cambridge ; New York: Cambridge University Press. 267-281

Peter, S. (2002). Laser nitriding of metals. *Progress in Materials Science*, *47*(1), 1–161. doi:10.1016/S0079-6425(00)00003-7

Pierson, H. O. (1996). *Handbook of refractory carbides and nitrides : properties, characteristics, processing, and applications*. Park Ridge, N.J.: Noyes Publications.

Rie, K.-T., & Broszeit, E. (1995). Plasma diffusion treatment and duplex treatment — recent development and new applications. *Surface and Coatings Technology*, *76–77, Part 2*, 425–436. doi:10.1016/0257-8972(95)02513-8

Rolinski, E., & Sharp, G. (2004). Ion Nitriding and Nitrocarburizing of Sintered PM Parts. *Industrial Heating*, *71*(10), 33–35.

Rondelli, G. (1996). Corrosion resistance tests on NiTi shape memory alloy. *Biomaterials*, *17*(20), 2003–2008. doi:10.1016/0142-9612(95)00352-5

Ross, P. J. (1996). *Taguchi techniques for quality engineering : loss function, orthogonal experiments, parameter and tolerance design*, New York: McGraw-Hill.

Roy, R. K. (2001). *Design of experiments using the Taguchi approach: 16 steps to product and process improvement*. New York: Wiley.

Ryhänen, J. (1999). Biocompatibility evaluation of nickel-titanium shape memory metal alloy. Retrieved February 1, 2013, from http://herkules.oulu.fi/isbn9514252217/html/index.html/x1004.html

Shape Memory Materials. (1998). Cambridge ; New York: Cambridge University Press.

Starosvetsky, D., & Gotman, I. (2001). TiN coating improves the corrosion behavior of superelastic NiTi surgical alloy. *Surface and Coatings Technology*, *148*(2–3), 268–276. doi:10.1016/S0257-8972(01)01356-1

Steen, W. M. (2003). *Laser material processing* (3rd ed.). London ; New York: Springer.

Taguchi, G. (1993). *Taguchi methods: design of experiments* (Vol. 4). ASI Press.

Trépanier, C, M Tabrizian, L H Yahia, L Bilodeau, and D L Piron. (1998). “Effect of Modification of Oxide Layer on NiTi Stent Corrosion Resistance.” *Journal of Biomedical Materials Research* 43 (4): 433–440.

Wangyang Ni, Yang-Tse Cheng, Lukitsch, M. J., Weiner, A. M., Lev, L. C., & Grummon, D. S. (2004). Effects of the ratio of hardness to Young’s modulus on the friction and wear behavior of bilayer coatings. *Applied Physics Letters*, *85*(18), 4028–4030. doi:10.1063/1.1811377

Williams, D. F. (1999). *The Williams dictionary of biomaterials*. Liverpool: Liverpool University Press.

Williams, D. F. (2008). On the mechanisms of biocompatibility. *Biomaterials*, *29*(20), 2941–2953. doi:10.1016/j.biomaterials.2008.04.023

Yasmin, A., & Bowen, P. (2003). Fatigue crack growth behavior of off-axis Ti–6Al–4V/SCS-6 metal matrix composites. *Materials Science and Engineering: A*, *356*(1–2), 54–68. doi:10.1016/S0921-5093(03)00004-2

Yoneyama, T., & Miyazaki, S. (2009). *Shape memory alloys for biomedical applications*. Cambridge, England; Boca Raton: Woodhead Pub. ; CRC Press.

Yu, H., Sun, F., & Zhang, J. (2009). Laser and plasma nitriding of titanium using CW-CO2 laser in the atmosphere. *Current Applied Physics*, *9*(1), 227–233. doi:10.1016/j.cap.2008.01.013

Zhang, S., Tang, H. J., Hu, F., Zhang, C. H., Man, H. C., & Zhang, Q. Q. (2011). Electrochemical Corrosion Behavior of Laser Gas Nitrided Layer on the NiTi Shape Memory Alloy in Hank's Solution. *Advanced Materials Research*, *299-300*, 179–182. doi:10.4028/www.scientific.net/AMR.299-300.179

Zhao, N.Q., H.C. Man, Z.D. Cui, and X.J. Yang. (2006). "Structure and Wear Properties of Laser Gas Nitrided NiTi Surface." *Surface and Coatings Technology* 200 (16–17): 4879–84. doi:10.1016/j.surfcoat.2005.04.043.

Zhecheva, A., Sha, W., Malinov, S., & Long, A. (2005). Enhancing the microstructure and properties of titanium alloys through nitriding and other surface engineering methods. *Surface and Coatings Technology*, *200*(7), 2192–2207. doi:10.1016/j.surfcoat.2004.07.115